RETINAL CONTOUR AND PERIPHERAL ABERRATIONS: THE EFFECTS OF ACCOMMODATION IN DIFFERENT REFRACTIVE ERROR GROUPS

A thesis submitted to the graduate faculty of

The New England College of Optometry

in partial fulfillment of the requirements for the degree of

Master of Science

by

Lee Johnson

May, 2010

©Lee Johnson
All Rights Reserved

The author hereby grants The New England College of Optometry permission to reproduce and to distribute publicly paper and electronic copies of the thesis document in whole or in part.

RETINAL CONTOUR AND PERIPHERAL ABERRATIONS:
THE EFFECTS OF ACCOMMODATION IN DIFFERENT
REFRACTIVE ERROR GROUPS

Lee Johnson

This manuscript has been read and accepted by the Thesis Committee
in satisfaction of the thesis requirement for the degree of Master of Science.

5-12-10
Date

Nancy Coletta, OD, PhD
Graduate Faculty Advisor

Frank Thorn, OD, PhD

Nathan Doble, PhD

David Troilo, PhD

5-25-10
Date

Nancy Coletta, OD, PhD
Director of Graduate Studies

Abstract

Purpose: Both accommodation and peripheral refraction have been implicated as factors in myopia development. Recent studies have investigated the relationship between peripheral aberrations and accommodation[1,2] and the effect that such optical triggers may have on myopia development. Numerous studies rely on assessment of retinal contour to study the growth of the eye during emmetropization and myopia development. Dunne has shown that the contour of the peripheral retina can be estimated from peripheral refractions calculated from measurements of peripheral aberrations[3]. Since retinal contour itself can directly affect the aberration profile, peripheral retinal contour and peripheral aberrations are inherently linked.

We calculated retinal contours using peripheral aberrations measured with varying accommodation and pupil diameter. We then compared the calculated contours to examine the performance of the algorithm in a group of subjects with a wide range of refractive errors. We also compared these contours to those measured using a newly proposed technique emploing partial coherence interferometry[4]. We then examined peripheral aberrations directly to study how they were affected by accommodation. All of these effects were examined in different refractive error groups.

Methods: Aberrations were measured with a COAS aberrometer on forty young adult subjects whose mean Spherical Equivalent (SE) refraction ranged from -12.00 D to +2.00 D. Subjects fixated a high contrast letter reflected through a beam splitter, which was mounted between the eye and the COAS. The beamsplitter was rotated to alter gaze position. A Badal lens and a translational stage were used to both correct the eye's refractive error and to control the accommodative stimulus. Measurements were taken in 10° steps out to 50° on the horizontal meridian and out to 40° on the vertical meridian, at 0.00 D and 4.00 D accommodative demands, in natural pupil conditions and with administration of 1 drop 2.5% phenylephrine. Measures were also taken at 0.00 D with administration of 1.0% tropicamide. Zernike coefficients up to 7th order were corrected for elliptical pupils in eccentric gaze positions. Changes in coefficients were analyzed for differences between emmetropes (EM, less than -1.00 D), low myopes (LM, between -1.00 D and -6.00 D), and high myopes (HM, greater than -6.00 D). Meridian directions are specified for the retinal position.

Corneal topography, anterior chamber depth and lens thickness were measured in accommodative and non-accommodative states with an Oculus Pentacam. Biometry and refractions were used to compute retinal contours with the Dunne scheme. Following ad-

ministration of tropicamide, central axial length and peripheral ocular dimensions were measured with a Zeiss IOL Master. A card was mounted to the IOL Master with fixation marks at the various gaze positions to measure peripheral axial length. Retinal surface coordinates were calculated from the peripheral axial lengths, adjusted for differences in optical path length for different gaze angles.

Results: In general we found that in the unaccommodated state, myopes had relatively less total RMS aberration in the periphery relative to their fovea, while emmetropes had relatively more aberration in the periphery. All subjects showed an increase in relative peripheral total aberration with accommodation. However, myopes showed a larger increase in total peripheral RMS with accommodation than emmetropes.

We found several differences in how the individual coefficients changed with accommodation for the different refractive groups. Compared to the other groups, HM showed a smaller increase in Z_2^0 and Z_2^2 with accommodation across the horizontal meridian. These effects were significant temporally from 10° to 50° ($p < 0.015$) and nasally from 10-50° ($p < 0.001$), respectively. LM and HM showed a larger increase in Z_3^1 nasally than EM ($p = 0.015$). On the inferior vertical meridian, LM and HM showed a larger increase in Z_3^1 ($p < 0.001$) and a larger decrease in Z_5^1 ($p < 0.001$) compared to EM. Near the fovea, inferiorly, LM and HM both showed a larger negative shift in Z_4^0 than EM ($p = 0.022$) and a positive shift in Z_6^0 ($p < 0.001$) relative to EM.

The measured contours in high myopia are consistent with a prolate eye shape found in numerous previous studies. Asphericity coefficients were seen to vary significantly with refractive error in both the nasal and temporal retinas, but no such correlation was found in the vertical meridian. Retinal contours calculated from the Dunne model using data taken with tropicamide administered and contours from the IOL Master showed agreement within ± 0.7 mm. The Dunne algorithm generally showed a posterior shift in calculated peripheral retinal contour with accommodation which was minimal at the fovea and varied from the tropicamide contour by as much as 0.8 mm in the far periphery. Contours calculated from data taken with different pupil states showed less discrepancy from the tropicamide data (± 0.4 mm), and contour was not predominantly seen to shift in one direction. The algorithm was found to be very robust to inaccurate measures of anterior chamber depth and lens thickness.

Conclusions: Peripheral aberrations changed differently with accommodation in myopic and emmetropic eyes. These effects may be associated with differences between the groups in the crystalline lens optics, optical alignment, or the peripheral retinal contour.

Partial coherence interferometry is a fast method of estimating retinal contour, but it shows more variation than calculation from peripheral refraction. The Dunne algorithm is fairly robust to computation of retinal contour in the presence of pupil diameter variation and inaccurate measures of anterior segment parameters, but retinal contour may be altered in the presence of accommodation.

Acknowledgments

I would like to acknowledge the subjects who participated in this study, without which none of this data could have been collected.

I also wish to thank Beta Sigma Kappa for the grant we received, which enabled us to recruit additional subjects and to purchase equipment to aid in data acquisition.

I would like to thank my advisor, Dr. Nancy Coletta, for the time she has spent helping design, set up, and troubleshoot this experiment from its initial stages to its final completion, and for the help she has put into this final report.

Finally, I would like to thank my wife, Kristin, for her tireless support waiting up through many long days and late nights, watching children alone, reviewing drafts, and offering insightful suggestions.

Contents

Abstract iii

Acknowledgments v

Table of Contents vi

List of Figures viii

List of Tables xi

1 Background 1
- 1.1 Peripheral Retinal Contour and Myopia . . . 1
  - 1.1.1 Theories of Myopic Growth . . . 2
  - 1.1.2 Effect of Accommodation on Retinal Contour Measurements . . . 3
  - 1.1.3 Methods of Measuring Retinal Contour . . . 5
- 1.2 Peripheral Aberrations and Myopia . . . 8
  - 1.2.1 Peripheral Aberrations of the Human Eye . . . 8
  - 1.2.2 Effect of Accommodation on Peripheral Aberrations . . . 11

2 Methods 15
- 2.1 Subjects and Initial Measurements . . . 15
- 2.2 Measurement of Peripheral Aberrations and Ocular dimensions . . . 17
- 2.3 Comparison of Peripheral Aberrations . . . 25
  - 2.3.1 Pupil correction . . . 25
  - 2.3.2 Subject Grouping and Statistical Analysis . . . 27
- 2.4 Calculation of Peripheral Retinal Contour . . . 31

3 Results and Discussion: Peripheral Aberrations 38
- 3.1 Analysis of Power Vectors . . . 39
  - 3.1.1 Non-Accommodative Power Vector Measurements . . . 39
  - 3.1.2 Power Vector differences with accommodation . . . 44
- 3.2 Analysis of Zernike Coefficients . . . 48
  - 3.2.1 Non-Accommodative Zernike Coefficients . . . 49
  - 3.2.2 Non-accommodative RMS wavefront error in Zernike orders . . . 57

3.2.3 Zernike Coefficient differences with accommodation 61
3.2.4 Change in RMS wavefront error in Zernike orders with accommodation 69

4 Results and Discussion: Retinal Contour 72
4.1 Analysis of Retinal Contours 73
4.2 Comparison of Retinal Contour Measurement Methods 78
4.2.1 Comparison of Dunne and IOL Master Measurement 79
4.2.2 The Effect of Accommodation on Retinal Contour Calculation . . . 83
4.2.3 The Effect of Pupil Size on Retinal Contour Calculation 86
4.2.4 The Effect of Anterior Chamber Dimension Variation on Retinal Contour Calculation 91

5 Summary and Conclusion 101

A Consent form 103

B Questionnaire 108

C Bootstrap Method for Analysis of Significance 112

D Retinal Curve Fitting Process 117

E Supplemental Plots 120
E.1 Non-accommodative Zernike Supplemental Plots 120
E.1.1 Foveally normalized non-accommodative Zernike plots 120
E.1.2 Low Significance non-accommodative Zernike Plots 120
E.2 Low Significance Accommodative Difference Zernike Plots 122
E.3 Retinal Contour plots for Refractive Groups 125

Bibliography 128

Index 139

List of Figures

1.1 Myopia Growth Models 2

2.1 Fixation target presented to subjects 18
2.2 Diagram of COAS setup. 20
2.3 Subject refractive error and axial length characteristics. 27
2.4 Regression plots of accommodative response, pupil diameter, and pupil constriction against refractive error and axial length. 28
2.5 Discrepancy between measured anterior segment parameters and regression predicted values. 33
2.6 Plotting conventions for contour calculation and curve fitting. 36

3.1 Results of ANOVA analysis of Non-accommodative power vectors across refractive error groups. 39
3.2 Non-accommodative M relative to fovea. 40
3.3 Non-accommodative J_{45} relative to fovea. 42
3.4 Non-accommodative J_{180} relative to fovea. 43
3.5 Results of ANOVA analysis of accommodative differences of power vectors across refractive error groups. 44
3.6 Accommodative change in M 45
3.7 Accommodative change in J_{45} 46
3.8 Accommodative change in J_{180} 47
3.9 Results of ANOVA analysis of horizontal and vertical meridian non-accommodative Zernike Coefficients across refractive error groups. 50
3.10 Non-accommodative 2nd order Zernike coefficients across gaze angle. . . . 51
3.11 Non-accommodative 3rd order trefoil terms, Z_3^{-3} and Z_3^3 52
3.12 Non-accommodative 3rd order vertical and horizontal coma terms, Z_3^{-1} and Z_3^1 53
3.13 Non-accommodative 4th and 6th order oblique astigmatism, Z_4^{-2} and Z_6^{-2} . . 55
3.14 Non-accommodative spherical aberration and 6th order defocus, Z_4^0 and Z_6^0 . 57
3.15 Non-accommodative RMS aberrations 2nd order and above. 58
3.16 Non-accommodative RMS aberrations 3rd order and above. 59
3.17 ANOVA comparison of accommodative differences of Zernike Coefficients across refractive error groups. 61

3.18 Changes in 2nd order Zernike coefficients with accommodation across gaze angle. . . . 62
3.19 Changes in 3rd, 5th and 7th order horizontal coma terms (Z_3^1, Z_5^1, and Z_7^1) with accommodation. . . . 64
3.20 Regression lines of refractive error and axial length against change in Z_3^1 with accommodation over inferior retina. . . . 65
3.21 Changes in Z_4^0 and Z_6^0 with accommodation. . . . 68
3.22 Changes in RMS aberrations with accommodation, 2nd order and above. . . . 69
3.23 Changes in RMS aberrations with accommodation, 3rd order and above. . . . 70

4.1 Retinal contours for groups plotted by gaze angle. . . . 73
4.2 Retinal contours for groups plotted in cartesian coordinate system. . . . 74
4.3 Change in retinal curvature (Q) with refractive error. . . . 75
4.4 Change in retinal radius with refractive error. . . . 77
4.5 Group retinal contours from IOL Master and Dunne tropicamide data. . . . 80
4.6 Group retinal contours from IOL Master data calculated using 1-surface and 3-surface model eyes. . . . 80
4.7 Pooled discrepancies in retinal contour between IOL Master and Dunne tropicamide data sets. . . . 81
4.8 Grouped discrepancies in retinal contour between IOL Master and Dunne tropicamide data sets. . . . 82
4.9 Pooled discrepancies between accommodative contours and tropicamide contour. . . . 83
4.10 Grouped discrepancies between accommodative contours and tropicamide contour. . . . 84
4.11 Pooled discrepancies in retinal contour between tropicamide data and other non-accommodative data. . . . 87
4.12 Discrepancies in retinal contour between non-accommodative data sets of varying pupil diameters. . . . 88
4.13 Discrepancies in retinal contour between tropicamide scan with normal and 3mm corrected pupils for each refractive group. . . . 89
4.14 Changes in M and J_{180} between tropicamide scan with normal and 3mm corrected pupils. . . . 90
4.15 Discrepancies in retinal contour between tropicamide scan with normal and 3mm corrected pupils for each refractive group without incorporation of 4th order Zernike terms. . . . 91
4.16 Effect of anterior chamber depth variation on calculated retinal contour in emmetropes. . . . 93
4.17 Effect of anterior chamber depth variation on calculated retinal contour in low and high myopes. . . . 94
4.18 Effect of lens thickness variation on calculated retinal contour in emmetropes. 95
4.19 Effect of lens thickness variation on calculated retinal contour in low and high myopes. . . . 96

4.20 Combined effect of AC depth and lens thickness variation on calculated retinal contour in emmetropes. 97
4.21 Combined effect of AC depth and lens thickness variation on calculated retinal contour in low and high myopes. 98
4.22 Effect of axial length variation on calculated retinal contour. 99
4.23 Effect of axial length variation on calculated retinal contour in low and high myopes. 99

C.1 Illustration of statistical approach for analysis of significance of trends. . . . 113
C.2 Illustration of relative position neglect error inherent in numerical method. . 115

E.1 Non-accommodative 2nd order Zernike coefficients across gaze angle. . . . 121
E.2 Non-accommodative 3rd order vertical and horizontal coma terms, Z_3^{-1} and Z_3^1 121
E.3 Non-accommodative 7rd order plots 122
E.4 Changes in Z_3^{-3}, Z_3^3, and Z_3^{-1} with accommodation. 123
E.5 Changes in Z_4^{-4} and Z_6^{-4} with accommodation. 123
E.6 Changes in Z_5^{-5}, Z_5^{-3}, and Z_7^7 with accommodation. 124
E.7 Group retinal contours, with and without accommodation. 125
E.8 Group retinal contours, with and without accommodation. 126
E.9 Group retinal contours from non-accommodative scans of varying pupil diameter. 126
E.10 Group retinal contours from non-accommodative scans of varying pupil diameter. 127

List of Tables

2.1 Regression results of retinal curvature (Q) vs refractive error. 29

3.1 Regression results of refractive error and axial length against accommodative change in Z_3^1 over inferior retina. 66

4.1 Regression results of retinal curvature (Q) vs refractive error. 75
4.2 Regression results of retinal radius (R) vs refractive error. 77

Chapter 1

Background

1.1 Peripheral Retinal Contour and Myopia

The mechanism by which eyes grow myopic, or ”emmetropization”, has been the subject of research for decades. Most myopia is generally recognized as axial in nature, indicating that the eye grows such that the retina falls behind the focal plane of the optics of the anterior segment. This definition of myopia depends implicitly on the position of the retina with respect to the anterior optics of the eye, and therefore indirectly on the shape of the eye as a whole. For this reason, knowledge about retinal position and contour, in some form, is inherently important to almost any investigation of myopia development.

In recent years considerable excitement has arisen in myopia research regarding how the peripheral retina and peripheral optical properties of the eye might play a role in the development of myopia. Numerous studies have compared peripheral refractions across refractive error in human subjects to investigate, among other things, any predictive effect that peripheral refraction may have on the development of myopia[5–9]. Measurements of peripheral refraction depend implicitly on the relationship between the optics of the eye and retinal position, and as such retinal contour is important in these studies as well. Ev-

idence also suggests that peripheral refraction can influence retinal contour development. Animal studies in chicks using hemifield defocus have demonstrated local control of emmetropization[10,11], and experiments using macaques have shown that retinal contour can be locally changed in response to a peripheral growth stimulus despite the lack of a central stimulus[12,13]. Other studies have directly investigated the differences in peripheral retinal contour between human myopic and emmetropic subjects. For studies regarding the development of myopia and corresponding changes in retinal contour, an accurate and easily accessible method of measuring retinal contour during refractive development would be extremely valuable.

1.1.1 Theories of Myopic Growth

Retinal contour measurement can also be applied to investigate how the eye elongates during myopic progression. Three general models for ocular growth in myopia have been proposed (see figure 1.1)[14], which are by no means mutually exclusive. The first is that the eye could elongate only axially – along the visual axis, thus forming an ellipsoid which becomes more prolate with increasing myopia. This type of expansion would predict that myopic eyes would become relatively hyperopic (or at least less myopic) in the periphery. The second possible model would be a global expansion, causing the eye to increase in size in all dimensions. This model would predict less relative peripheral hyperopia than axial

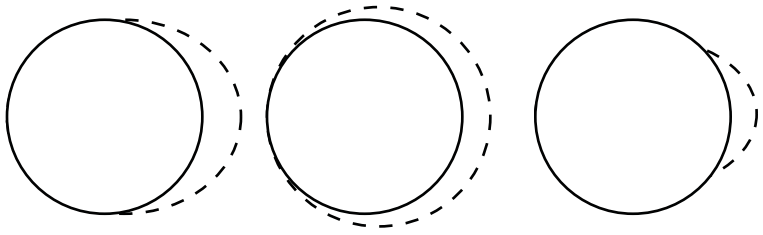

Figure 1.1 Three models explaining the growth of the eye in Myopia.

expansion. The third possible model is a local expansion in the posterior pole. This model would predict less peripheral myopia, and hence greater relative peripheral hyperopia, than either the axial or global expansion models.

Evidence has been presented by various groups that myopic elongation of the globe proceeds primarily axially, leading to a relatively prolate (or less oblate) retinal contour in myopic subjects as compared to emmetropic and hyperopic subjects[6,7,15,16]. Recent studies of acuity in myopic subjects support this by indicating that acuity falls off with increasing axial length at a faster rate than predicted by the global expansion model[17,18].

1.1.2 Effect of Accommodation on Retinal Contour Measurements

Another important application of retinal contour measurement is to investigate the effect of accommodation on myopia development. Accommodation has long been linked to the development of refractive error, though the exact nature of this relationship remains poorly understood. It is well known that the presence of accommodative lag or accommodative facility disorders correlates with the presence of myopia[19,20] or its progression[21,22]. Numerous studies have investigated whether attempting to reduce accommodative lag as a factor could slow or stop myopic progression. Studies investigating the effect of bifocal correction on the progression of myopia found a small effect which was statistically significant but too small to be clinically significant (only about 0.25 D less myopia progression with correction)[23]. An initial study investigating progressive lenses found a larger effect (about 0.50 D)[24], but a larger multi-center study found the effect to be similar in magnitude to that of the previous bifocal study[25]. Further studies are still underway to examine if there is an effect in subjects with different accommodative lags or near esophorias. These findings suggests that reduction of accommodation does little to slow the progression of myopia.

In studying the relationship between accommodation and the development of myopia, it is important to have an accurate retinal contour. This is primarily in order to examine

the change in retinal contour produced by the development of axial refractive error, but also to investigate any transient effect that accommodation itself might have on retinal contour. Accommodation may create a blur stimulus to induce axial elongation. Few studies have directly investigated the effect of accommodation on retinal contour. One particular study measured axial lengths of emmetropic and myopic eyes using a Zeiss IOL Master and found that myopic eyes elongated slightly more than emmetropic eyes during accommodation[26]. However, this study was limited in that it only examined axial elongation and did not investigate peripheral retinal contour changes.

Another study measured relative peripheral refractive error (RPRE), or the spherical equivalent refractive error in the periphery relative to the central refractive error, and found an immediate hyperopic shift in RPRE upon onset of accommodation, which decreased with sustained nearwork[27]. They concluded that this hyperopic shift was due to the retina becoming prolate during accommodation, but that this effect decreased with time. However, their study only measured RPRE at one point, 30° temporal in one eye, so it could be reasonably questioned if this is an accurate profile of the change in RPRE induced by accommodation throughout the eye. Moreover, this study assumed that the hyperopic shift in RPRE with accommodation was due to movement of the retina, when such effects could easily be caused by changes in the anterior ocular media such as the crystalline lens or the cornea. The crystalline lens has a gradient index whose profile deforms during accommodation[28], and the cornea has also been found to change shape during accommodation[29]. Both of these factors could account for the hyperopic shift in RPRE that was noted in this study. No information has been collected on whether sustained accommodation induces a change in the optical behavior of the cornea or lens, but this could also account for the reduced effect over time.

To the best of our knowledge at the time of this publication, a thorough study investigating the change in retinal contour with accommodation across refractive error groups

has not been conducted. Such a study would likewise require an accurate measurement of retinal contour in order to make meaningful comparisons.

1.1.3 Methods of Measuring Retinal Contour

Numerous methods have been proposed for the in vivo measurement of retinal topography. The standard for measuring on-axis ocular dimensions (axial length) is ultrasound biometry. A-scan ultrasound has not been extensively investigated for measurement of off-axis retinal dimensions, and therefore its accuracy in such a setting is unknown. B-scan ultrasonography has been used to compare axial lengths to equatorial widths in myopic eyes, and as lengths increased at almost three times the rate of widths, the results supported a primarily (though not exclusively) axial model of elongation[30]. However, only axial lengths and equatorial diameters were measured - B-scan ultrasonography was not used to give an actual retinal contour. Moreover, no information was reported with regards to the precision or accuracy of this technique, nor did the authors compare this method of measurement with any other.

Some studies have used radiographic imaging techniques such as X-ray[31], Computed Topography (CT)[32,33], or Magnetic Resonance Imaging (MRI)[15,16,34–38]. These techniques all carry the advantage of being able to provide direct cross-sectional images of the globe, from which retinal contour can be calculated. In the case of MRI, it is possible to obtain a three-dimensional image of soft tissue structure, which would be ideal for analysis of eye shape and ocular growth in myopia. However, due to involuntary eye movements, short scans must generally be taken to avoid distortion. These scans are therefore limited in resolution capabilities. Accuracy of MRI measurements of ocular dimensions has been estimated at around 0.3 mm[15], which is comparable to the accuracy of A-scan ultrasonography for axial measurements. Furthermore, the equipment required to take these measurements is not readily available in many clinic or research settings due to prohibitive

cost. It is also large and cumbersome and not well suited to quick measurements[3].

Another method that has recently been used to investigate ocular growth in myopia relies on psychophysical methods. In one study, spatial misperceptions were measured in the peripheral visual field and used to determine the likely manner in which ganglion receptive fields were stretched[39]. The investigators could thus infer the most likely manner of ocular expansion. This study supported an axial stretch model, but the results don't lend themselves to precise quantitative interpretation. As a result, this technique would not be ideal for measurement of retinal contour with the purpose of direct comparison throughout growth.

One of the main methods used in current studies is to calculate retinal contour from peripheral refractive data. This is often done simply by assuming that the eye's image shell is spherical and using the spherical equivalent refractive error to compute position as a deviation from that surface[40]. However, this basic approach introduces numerous inaccuracies. This method relies on the weak assumption that the optics of the eye produce a spherical image shell, which has not been validated. The optics of the eye represent a complex combination of aspheric surfaces, relative decentration and misalignment, and a gradient index lens. These optical characteristics make it unlikely that the eye would produce a spherical image shell; therefore, they must be accounted for in any calculations undertaken to derive an accurate retinal contour from optical measurements.

M. C. Dunne developed an algorithm which compensated for the complex optical properties of the eye when computing retinal contour from peripheral refraction measurements[3]. Using this method, a three surface model eye is constructed based on measured parameters of axial length, central corneal curvature, and central refraction. Refraction is then measured at each peripheral gaze position and the corneal asphericity in the model is adjusted to match the measured peripheral astigmatism. This presumably compensates for the complex optical characteristics of the eye. Retinal contour can then be adjusted rela-

tive to the sagittal and tangential image shells of the model eye to reproduce the complete spherocylindrical refraction at that point.

The accuracy of this computational scheme was directly assessed by Dunne. Rotationally symmetric test eyes with varying surface asphericities and gradient index profiles were modeled and retinal contours were calculated out to $60°$. The calculated contours were found to be within the error margin of axial A-scan ultrasound out to $50°$, and in most instances was much more accurate than either ultrasound or MRI[3]. A subsequent study used this algorithm to derive retinal contours of an anisomyope[41]. Five separate measurements of peripheral refraction were taken and five retinal contours calculated. The spread of the calculated retinal contours was large, likely due to variability in their measurements of peripheral refraction. While this spread was considerably larger than the inherent error in the computing scheme noted from the model eye simulations, its accuracy was sufficient to note the differences in retinal contours between the two eyes of the anisomyope. This algorithm has also been used in a recent study to investigate differences in myopic growth patterns between white and Asian myopes[42], which found that Asian myopes tended to show a larger and more symmetrical growth pattern than white myopes, who showed a more pronounced temporal-nasal asymmetry in retinal contour. These studies suggest that the algorithm is reasonably accurate and may be suited to measure retinal contour in research settings, although it's accuracy in living subjects has not been thoroughly investigated.

Finally, a recently proposed method of peripheral retinal contour measurement is the use of optical low coherence techniques. Optical low coherence reflectometry has been found to accurately measure retinal contour out to $15°$, but it has not been used for more eccentric retinal positions[7,43,44]. Partial coherence interferometry has recently been suggested by Mallen and Kashyap as a method to measure peripheral retinal contour, but the accuracy of this method has not been thoroughly investigated[4]. One study has indicated that gaze position can significantly affect the measurement of retinal contour with this method[45].

Both the algorithm developed by Dunne and the use of partial coherence interferometry show promise in that they are much more accessible, less expensive, less time consuming, and less invasive than radiographic measurements such as CT or MRI. They are less invasive than ultrasound measurements and may show better accuracy in measurement of peripheral dimensions. The primary purpose of our study was to examine the robustness of retinal contours calculated from the Dunne algorithm in the presence of controlled changes in accommodative state and pupil diameter and to compare the results across different refractive groups. Furthermore, these calculated contours will be compared to measurements of retinal contour taken directly using a Zeiss IOL Master, as described by Mallen and Kashyap[4].

1.2 Peripheral Aberrations and Myopia

Intimately related to the measurement of retinal contour and the development of myopia is the study of the optical behavior of the human eye in the peripheral retina. Although the study of peripheral refractive error and aberrations is not new, it has drawn considerable attention in recent years due to numerous studies investigating possible roles that peripheral refraction might serve as a stimulus to myopia development.

1.2.1 Peripheral Aberrations of the Human Eye

It is well known that the human eye, like any optical system, shows induced astigmatism in the peripheral visual field, seen as sagittal and tangential image shells that typically show increasing separation with higher eccentricities. This peripheral astigmatism is not corrected by central refractive error[46–49]. It has been suggested that the peripheral aberrations of the eye could serve as a stimulus for axial elongation regardless of the focus centrally[8].

Numerous experiments have shown that emmetropization is locally controlled. Locally

imposed form deprivation in one hemisphere has been shown to induce eye growth only in that hemisphere[10]. Locally imposed defocus has been shown to have the same effect, even when accommodation is still present[11]. Peripheral form deprivation has been shown to induce myopia in rhesus monkeys despite unrestricted central vision, and subsequent foveal ablation did not inhibit emmetropization upon removal of the peripheral form deprivation[12]. It has also been shown that foveal ablation fails to inhibit subsequent form-deprivation-induced myopia in rhesus monkeys[13]. These studies strongly suggest that certain peripheral optical stimuli might contribute to myopic growth regardless of the central optical profile. Peripheral astigmatism could be a contributing factor, since sagittal and tangential image shells could provide a natural cue to the retina in determining the sign of defocus and thus the direction the retina should grow to emmetropize.

Differences in the optical elements of myopic and emmetropic eyes could create different optical behavior in the periphery. It has already been found that the myopic lens could differ from the emmetropic lens in various characteristics, such as back focal length[50], lens capsule thickness[6,51], and in the manner in which the myopic lens fails to thin over time when compared to the emmetropic lens[52]. It has not been determined whether myopic growth might be stimulated by blur generated by differing focusing properties of the myopic optical elements, or instead due to some as yet undetermined difference between refractive error groups in the mechanisms of local blur interpretation in the retina which drive emmetropization.

In investigating peripheral refractions directly, numerous differences have been found between emmetropic and myopic eyes. Although some recent studies look at higher order Zernike aberration coefficients, most studies of peripheral optics have focused primarily on the three 2nd order optical aberrations expressed as power vectors[53,54] - spherical equivalent (M), horizontal astigmatism (J_{180}), and oblique astigmatism (J_{45}). These power vectors may incorporate weighted contributions from corresponding higher order coefficients, rather

than only 2nd order terms.

One generally common finding has been that the RPRE of myopic eyes tends to be hyperopic or less myopic when compared to emmetropic or hyperopic eyes[6,7,9,16,42,55–58], and that hyperopic RPRE can be predictive of myopia development[5,9]. Other studies have investigated the change in RPRE with age. One retrospective study found a relative hyperopic central shift and a myopic peripheral shift in subjects over a thirty year time period[59]. Another study investigated groups of differently aged subjects and found no meaningful difference between subjects of different age groups[60].

Numerous studies have also noted temporal-nasal asymmetries that differed in myopic eyes compared to emmetropic eyes. The most commonly found trend is that J_{180} reaches a minimum in the nasal retina rather than at the fovea and tends to increase temporally more than nasally[55–57,61,62]. This effect is smaller in myopic eyes[57,61]. No asymmetry was found on the vertical meridian[56,57], although J_{45} was found to increase with eccentricity three times faster in myopes than in emmetropes.

Despite the differences that have been found between the peripheral refractive profiles of different refractive groups, it is impossible to infer that these differences are causative of myopic development because it is equally possible that they are a result of axial enlargement. It has been recently shown that form deprived rhesus monkeys, which would presumably have neither a central or peripheral optical stimulus for myopia development, still develop a retinal contour that yields a hyperopic RPRE[63]. Moreover, although peripheral form deprivation has been shown to induce myopic growth despite unrestricted central vision, imposed local blur in the periphery has failed to generate the same response[64]. Both of these findings present strong evidence against the hypothesis that peripheral blur is a causative stimulus for myopic development.

1.2.2 Effect of Accommodation on Peripheral Aberrations

Much attention has been focused on the peripheral refractive profile as a possible stimulus for myopic development, but if there is indeed a link between myopia and near work that has yet to be understood, it could be more informative to examine how the peripheral retinal image behaves with changes in accommodation.

Changes in peripheral refraction with accommodation have been examined in several studies. One of the first studies was done by Smith et al.[65] They measured spherocylindrical refractions with and without accommodation and found significant changes in astigmatism with accommodation in the far periphery ($\geq 50^\circ$), as well as an increase in field curvature in the periphery ($> 30^\circ$). They also found that accommodation affected sagittal foci more than tangential – effectively suggesting that accommodation will affect the interval of Sturm in the periphery and not just the spherical equivalent or RPRE.

Little follow-up was done to the study by Smith et al. until very recently. Calver et al. looked at vector components of peripheral refractions out to 30° horizontally with and without accommodation in emmetropes and myopes. They found that overall there was little difference in the effect of accommodation on peripheral refraction between refractive error groups except at 30° temporal, where J_{180} changed with accommodation more in emmetropes than in myopes[61]. Whatham looked at peripheral refractive error in myopes under three different accommodative demands: 0.00 D, 2.50 D, and 3.33 D[66]. They noted that RPRE became more hyperopic with increasing accommodation but that this decreased with increasing eccentricity. They also noted the same significant increase in J_{180} with accommodation for large retinal eccentricities ($> 30^\circ$ temporal and $> 40^\circ$ nasal), but they could not compare this effect across different refractive groups since they only examined myopes. Davies et al. similarly measured peripheral refractive error in emmetropes and myopes out to $\pm 30^\circ$ on the horizontal meridian at four different accommodation levels[58]. They reported that accommodative level had no significant effect on RPRE in emmetropes

or myopes. They found accommodation did effect J_{180} significantly in the temporal visual field, but they found no effect of refractive error on this finding.

The above studies suffer from two limitations in that none of them examined the effect of accommodation on peripheral refraction in the vertical meridian and none examined aberrations higher than 2nd order (defocus and astigmatism). One study did examine changes in higher order aberrations with accommodation, but only in the central visual field[67]. They found significant changes in defocus (Z_2^0), astigmatism (Z_2^{-2}, Z_2^2), and horizontal and vertical coma (Z_3^1, Z_3^{-1}). They suggested that these might be accounted for by some form of lens tilt induced by accommodation.

Two groups have recently published results examining peripheral higher order aberrations with and without accommodation in both vertical and horizontal meridians. Mathur et al. recently published an article examining higher order aberrations in 38 points throughout the central $30^\circ \times 40^\circ$ visual field (out to $\pm 21^\circ$ horizontally and $\pm 16^\circ$ vertically) in emmetropes and myopes[68]. Surprisingly, they found myopic RPREs in both groups, with no hyperopic peripheral trend among the myopes as had been noticed in most other studies. They stated that this may have been due to the relatively small field that they examined. Furthermore, when examining individual Zernike coefficients they found that Z_4^0 (spherical aberration) decreased with myopia, Z_3^{-3} was lower in emmetropes, and radial coma (Z_3^1 horizontally and Z_3^{-1} vertically) varied more rapidly across the visual field in myopes than in emmetropes. In this study they did not look at any effect of accommodation.

The same group subsequently published another study in which they examined the effect of accommodation on higher order aberrations in the same field among emmetropes[2]. They found that the myopic RPRE they observed in emmetropes shifted slightly hyperopic (though not significantly) with accommodation in agreement with earlier findings[27,66]. Also surprising was that they found very little change with accommodation in astigmatic coefficients Z_2^{-2} and Z_2^2. They did find significant changes in spherical aberration Z_4^0 and

horizontal coma Z_3^1 with accommodation, in that Z_4^0 became more negative throughout the field and Z_3^1 became more positive in the nasal field. In this study they only examined emmetropes and thus could not perform comparisons to make inferences across refractive groups. Furthermore, as noted above, the visual field area they examined was small compared to other studies, and since significant trends have typically been noted only for farther eccentricities, this could account for the discrepancies between their results and previous studies.

The most comprehensive study that has been performed to date in this area was performed by Lundström et al[1]. They examined higher order aberrations with and without accommodation in emmetropes and myopes out to $\pm 40^\circ$ on the horizontal axis and $\pm 20^\circ$ on the vertical axis. Similar to previous studies, they found a relatively hyperopic RPRE in myopes which was greater in the temporal retina. They also noted a relative hyperopia among myopes in the superior retina, which had not been previously noted. They found no interaction between accommodation and gaze angle, indicating that accommodation affected aberrations similarly across the retina. They found that emmetropes became more myopic in the periphery with accommodation whereas myopes showed no change or became slightly hyperopic. Their discussion focused primarily on 2nd order coefficients, and although they collected and showed data on some higher order coefficients, they did not discuss them in depth.

In order to calculate retinal contour, we gathered peripheral aberration data for various refractive error groups and in different states of accommodation. This was done to examine if accommodative state affected the calculation of retinal contour from peripheral refraction. Having this data, we were subsequently able to examine the changes in higher order aberrations with accommodation farther out in the periphery than any study to date ($\pm 50^\circ$ horizontally and $\pm 40^\circ$ vertically)) and compare those changes between subjects in three different refractive error groups. Furthermore, this allowed comparison to see if any

differences in peripheral aberrations correlated with different retinal contours between the groups.

Chapter 2

Methods

Prior to initiation of this study, the procedure was approved by the Institutional Review Board at the New England College of Optometry. Informed consent was obtained from all subjects prior to enrollment in the study, and all participants were given the opportunity to ask any questions before any measurements were taken.

2.1 Subjects and Initial Measurements

At the time this study was initiated, there was no published data examining either the robustness of the Dunne algorithm in calculating retinal contour for human subjects or the comparison of higher order aberrations across refractive groups with accommodation. Because of this, we initially recruited 20 subjects, following which we performed a power analysis on the preliminary data. We then recruited an additional 20 subjects to ensure statistical power.

A total of 40 subjects were recruited primarily from the students at the New England College of Optometry, ranging in age from 21-29 years of age (mean 24.5 ± 1.98). All subjects were given a consent form (Appendix A), the purpose and procedures of the study

were explained to them, and they were given an opportunity to ask any questions. Inclusion criteria for subject selection required that all subjects have adequate hearing, language skills and mental ability to understand the consent process and the instructions during the experiment. Soft contact lens wearers were eligible to participate in the study; however, for each of the two visits, they could not wear contact lenses within 12 hours of the study procedures. Contact lenses were not worn during the study procedures in the measured eye. Subject selection was also determined by prior set exclusion criteria including:

- visual acuity not correctable to at least 20/25 in each eye after a refraction performed during the lab procedure
- use of extended wear, multifocal or rigid contact lenses
- cataract or other media opacity
- fixational instability (e.g., nystagmus) or restricted movement of either eye
- narrow anterior chamber angles (angle less than 1:3 by von Herrick method)
- intraocular pressure above 18mm Hg
- any history of acute angle closure
- any history of ocular disease, surgery, or orthokeratology
- any present ocular medications
- central astigmatism greater than 1.50 diopters
- age under 18 years

After reading and signing the informed consent, subjects filled out a questionnaire (Appendix B). Visual Acuity was then taken using a 100% contrast logMAR letter chart

(Bailey-Lovie). Best acuity was established by performing a trial frame refraction over the subject's current glasses prescription. In the event that the subject's habitual correction was contact lenses only, a subjective trial frame refraction was performed to establish best correction.

Intraocular pressure was measured using a Topcon CT-80 Air-Puff Tonometer. Pressure greater than 18 mm Hg prohibited participation in the study, as stated in the exclusion criteria above. Anterior chamber angles were measured by the Von-Herrick technique. These precautions were taken due to the known risk of increased IOP and angle closure that can take place following dilation[69,70]. We also checked corneal integrity while measuring angles at the slit lamp. Any subjects showing signs of corneal opacities, corneal dystrophy or abrasions were excluded from the study.

2.2 Measurement of Peripheral Aberrations and Ocular dimensions

Measurements of peripheral aberrations were taken in two separate visits. The first visit involved pupil dilation and generally took about 2.5 hours. The subject was administered two drops of 2.5% phenylephrine accompanied by punctal occlusion and separated by five minutes. They were then asked to wait 40 minutes while the pupil dilated. The majority of subjects were given drops only in the left eye, although a small number requested to receive drops in both eyes. Phenylephrine was administered to dilate the subject's pupils while still preserving the ability to accommodate. Aberrations were then measured with the Wavefront Sciences Complete Ophthalmic Analysis System (COAS, Wavefront Sciences, Albuquerque, NM, USA), which uses the Hartmann-Shack wavefront sensing technique, and expressed as OSA standard Zernike coefficients up to 7th order. Subjects were seated at a chinrest and forehead restraint and asked to fixate a target. The target used to control

fixation and accommodation was viewed through a Badal lens located one focal length from the corneal plane. The target consisted of a random array of letters whose size was approximately 30 minutes of arc (about $\frac{20}{120}$). The size was chosen well above the acuity limit in order to better stimulate accommodation, yet the letters contained textures and details sufficient that the subject could report if they were sharply focused (see figure 2.1). Measurements were performed under dim room illumination with the Badal target back-illuminated to a low photopic light level. The target was located on a translational stage which could be adjusted to change the accommodative demand.

For measurements on the horizontal meridian, the target was viewed reflected through a partially reflecting beam splitter mounted on a rotating stage. The mirror was rotated by half the angle of gaze that we wished to elicit, so that the reflected image would approach the subject's eye at the appropriate trajectory. Due to slight differences in facial structures between subjects, we performed an initial calibration with each subject to ensure the proper gaze position throughout the horizontal scans. The rotating mirror was placed at 0° and each subject was asked to view the chart with their left eye while their right eye

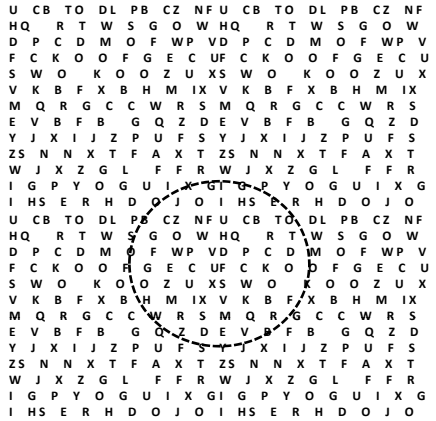

Figure 2.1 The fixation target presented to the subject. The dashed circle represents the approximate area of the target visible through the Badal lens. The target was back-illuminated using an LED with a rheostat to adjust illumination. Letters were displayed reversed so as to appear in the proper orientation when reflected in the beam splitter.

was patched. The COAS camera was centered on the subject's pupil viewed through the beamsplitter, at which time the letter target was seen by the subject to overlie the fixation light in the COAS. Rather than have one letter on the target which all subjects would be told to fixate, the subject was asked to report whichever letter on the target overlaid the central fixation light of the COAS. This letter became their fixation target throughout that scan. In this way we ensured that at the 0° setting of the rotational mirror, the subject's gaze was directed straight at the COAS camera. The subject was then instructed to follow that same letter and attend to it as the mirror was rotated to adjust gaze position. The subject was instructed to translate their head laterally on the chin rest as necessary to follow the target as the mirror was rotated to stimulate extreme gaze positions; they were told to keep their brow and cheek opposed to the beamsplitter throughout the procedure to avoid large fluctuations in vertex distance. The chin cup of the COAS was removed to facilitate lateral translation of the head during this process. Calibration was repeated after any adjustment of the target on the translational stage to stimulate accommodation, but since the target was viewed monocularly and accommodative convergence was therefore not a factor, we found this was largely unnecessary. The same letter was almost always found by the subject to overlie the COAS fixation target after adjustments were made to stimulate accommodation.

Some concern may be raised over whether it is valid to measure peripheral aberrations when the eye is in a secondary gaze position, rather than in primary gaze. Early studies found that peripheral refractions changed significantly with sustained eccentric gaze positions[71,72]. More recent studies have investigated the influence of gaze position on measurements of higher order peripheral aberrations. Aside from the aforementioned study by Macfadden et al., which found that gaze position can significantly affect measurements of retinal contour with the IOL Master[45], the majority of studies have found that any effect that gaze position may have on measurements of peripheral aberrations is generally less than the variability of the coefficients themselves[1,73–75]. Since any change in retinal

contour should manifest directly as altering the aberration profile of the eye, the fact that no significant changes in peripheral aberrations have been noted with changing gaze angle suggests that the reliability of the IOL Master technique to measure retinal contour may be questionable.

For measurements on the vertical axis, the beamsplitter was removed and the subject viewed a separate Badal system which had a screen mounted on a vertical translational stage. This Badal system was set up to be viewed by the right eye, though measurements were still taken on the left eye. A translational stage was once again used to adjust the accommodative demand. The target was focused through a Badal lens and reflected off a mirror to be seen by the right eye. The entire setup is shown in figure 2.2.

This setup of separate Badal systems was chosen to make it quicker to switch between horizontal and vertical meridians and to make the setup less cluttered, since it eliminated the necessity of mounting two translational stages near the left eye. Nevertheless, since the

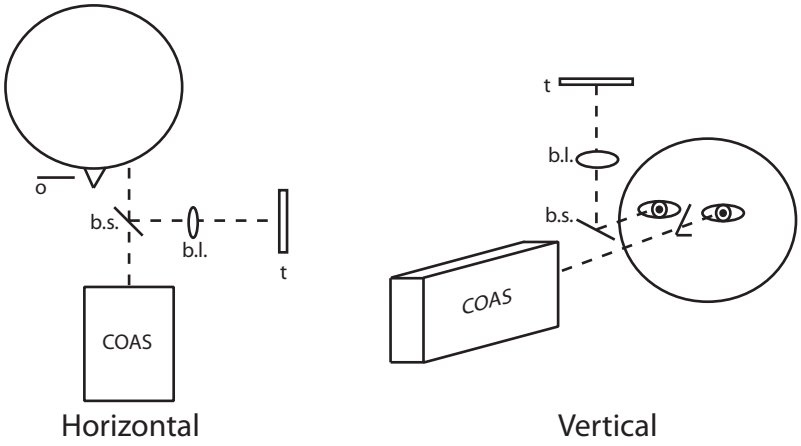

Figure 2.2 Illustration of our COAS setup in the Horizontal and Vertical meridians. The accommodative target was placed on a translating stage (t) and viewed through a badal lens (b.l.) reflected in a beamsplitter (b.s.) which was mounted on a rotating stage. In the horizontal meridian, the right eye was occluded (o) while measurements were taken of the left eye through the beam splitter. In the vertical meridian the badal system was viewed by the right eye while measurements were taken of the left eye.

interaction between the subject, target, and COAS was no longer monocular for measurements along the vertical meridian, it introduced accommodative convergence as a factor that had to be controlled in order to ensure that measurements were taken at the correct gaze position. To achieve this, the same alignment procedure was followed as described above, except that the letter target was seen by the right eye and the COAS fixation light was seen by the left. The COAS central fixation light seen by the left eye consisted of a red LED, which generally provided a sufficient stimulus to be perceived despite the subject concentrating on the image of the right eye. Care was then taken to instruct the patient to note which letter overlaid the fixation light *while the letters were clear*. The importance of this was that we wanted to ensure that the subject was not under-accommodating due to the distraction posed by the COAS fixation light.

When the subject reported a letter, the alignment was repeated, this time asking the subject to concentrate on that particular letter and focus on keeping it clear, and to note if the light remained stationary or moved to the left. A movement to the left corresponded to an increase in convergence, indicating that that the effort to clear the letter had produced more accommodation. The subject was then asked to report the new letter that overlaid the fixation light, and the process was repeated until the light no longer moved to the left and the subject reported that the letters were clear. The final letter was chosen to be the subject's fixation target, and the subject was instructed to fixate it and to concentrate on keeping it clear and sharp while the mirror was rotated to adjust the vertical gaze angle. It was assumed that as accommodative demand was kept constant, little change in accommodative vergence would be introduced by rotation of the mirror.

An important alteration made to the procedure for measurements along the vertical axis was that highly myopic subjects (> 6.00 D) viewed the target with a soft contact lens on the right eye (all subjects in this group had contacts). This was done because adjustment of the Badal system for high myopes required placing the translational stage near the end of

its translational range. In this position, the target interfered with the vertical translation of the COAS camera and would have made it difficult to follow the subject's pupil during the vertical translations necessary for gaze positions in the far inferior field. No contact lens was placed in the measured (left) eye, and when a contact lens was used in the right eye it was put in place well before the alignment procedure was carried out.

Two sets of measurements were taken starting 30 minutes after administration of 2.5% phenylephrine: in the first set, the Badal lens was set for optical infinity to relax accommodation. The stage position was determined according to the subject's refractive error, such that the vergence of the light at the cornea was zero. Five measurements were taken at each gaze position, first with central fixation and then at each of 20 positions of gaze: from 50° nasal to 50° temporal and from 40° superior to 40° inferior, in 10° increments. Central fixation was measured twice - once using the horizontal Badal system and again using the vertical Badal system. Throughout the procedure, the COAS was translated so that aberration measurements were made through the center of the pupil. The entire procedure was then repeated with the translational stage placed at the appropriate distance to present -4.00 D of vergence at the corneal plane of the right eye, thus stimulating 4.00 D of accommodation. This allowed wavefront aberrations to be obtained with the dilated pupil for both accommodative and non-accommodative states.

Following data collection on the COAS, the dimensions of the optical elements of the anterior segment were measured using a Pentacam (Oculus Optikgeräte GmbH, Wetzlar, Germany). These measurements were taken to better model corneal curvature and the positions of the anterior and posterior surfaces of the crystalline lens, which were used to construct each subject's 3-surface model eye required for the Dunne algorithm. Measurements were taken of the left eye in primary gaze. A 4.00 D accommodative target, reflected in a mirror, was presented to the distance-corrected fellow (right) eye. Alignment was undertaken similarly to the procedure noted above. The subject viewed the Pentacam fixation

target with their left eye while viewing the accommodative target with the right eye. The subject was asked to report which letter in the accommodative target overlaid the Pentacam fixation light, then to concentrate on keeping that letter clear and report if the fixation target remained stationary or moved to the left. This process was repeated until we were confident that the subject was accommodating fully while simultaneously directing the gaze of their left eye into the camera. Three measurements were then taken with the Pentacam.

Following these measurements, the subjects were administered 1 gtt 1.0% tropicamide. (This was occasionally done on a separate visit, but the majority of subjects received tropicamide directly following the measurements with phenylephrine.) Once again subjects were permitted to receive drops in the left eye only or in both eyes, as they preferred. Thirty minutes after dilation with tropicamide, aberration measurements along the horizontal and vertical meridians were taken with the COAS as described above, with the Badal system set again to optical infinity. The purpose of the tropicamide scan was to minimize accommodation as much as possible. Following measurements with the COAS, images were taken with the Pentacam as described above, but this time with no accommodative target and with the subject simply asked to fixate on the central fixation target within the device. Three measurements were taken.

Following measurements with the COAS and Pentacam with 1.0% tropicamide administered, retinal contour was measured using a Zeiss IOL Master. A marked fixation card was mounted on the device to direct the subject's gaze while measurements were taken. Measurements were taken centrally and peripherally in 10° increments out to 40° nasally, temporally, inferiorly, and superiorly. We were unable to precisely match the horizontal scan range with the COAS data ($\pm 50^\circ$) because in such far eccentric positions the IOL Master measurement beam fell outside of the dilated entrance pupil and the instrument could not obtain data. Measurements were often difficult to obtain at 40°, but generally possible with repeated trials. For this same reason IOL Master measurements were not

taken with the subjects in an accommodative state. Dilation of the pupil with phenylephrine alone resulted in a smaller entrance pupil than with tropicamide, and the ability to obtain data in eccentric positions of gaze was limited. The first visit generally concluded following measurements with the IOL Master.

The second visit was without dilation, and generally took about one hour. Measurements were once again taken with the COAS as described above, in both accommodative and non-accommodative states, but this time with a natural pupil which had not been administered any drops. This allowed us to analyze any effect that the dilating drops may have had on our measurements. Following measurements of aberrations with the COAS, corneal shape was measured with a Humphrey Atlas 995 corneal topographer. Measurements were taken with no accommodative stimulus, and were repeated until four measurements were obtained with stable image integrity over the whole corneal surface.

The final results of this procedure yielded the following data sets for each subject:

- two natural pupil aberration data sets, one accommodating and one non-accommodating
- two phenylephrine aberration data sets, one accommodating and one non-accommodating
- one tropicamide aberration data set, non-accommodating
- one IOL Master data set, taken dilated with tropicamide
- six scans of anterior segment dimensions using the Pentacam, three accommodating (phenylephrine) and three non-accommodating (tropicamide)
- four scans of corneal topography, non-accommodating

Thus we ended up with a total of five sets of Zernike coefficients, two of which were with accommodation (natural and phenylephrine) and three of which were without accom-

modation (natural, phenylephrine, and tropicamide). Each data set contained horizontal and vertical meridians which could be analyzed entirely independently of each other, due to the fact that central refractions were taken separately for each meridian to account for different Badal systems being used to control accommodation and gaze position. Thus the end result was effectively ten data sets which could be analyzed for comparisons.

2.3 Comparison of Peripheral Aberrations

2.3.1 Pupil correction

In order to compare Zernike coefficients across subjects, all pupils had to be normalized to a common diameter. The Zernike coefficients from the five data sets for each subject were exported from the COAS as an Excel spreadsheet and imported into Matlab (R2008b, MathWorks, Natick, Massachusetts, USA). For elliptical pupils encountered in peripheral gaze positions, pupil diameter was considered as the minor axis of the ellipse. We wrote a Matlab code to proceed through all acquired scans from all subjects and find the minimum pupil size, then to progress again through each scan and re-calculate the Zernike coefficients for each subject at the new minimum diameter. Zernike coefficients were scaled to the new pupil diameter using the Matlab algorithm outlined by Lundström[76]. This algorithm was checked for accuracy and found to yield a more faithful representation of the original wavefront over the scaled pupil than if the pupil was manually scaled down in the COAS software prior to data export. Scaling the pupil within the COAS software removes sampling points outside of the shrunken pupil which help calculate the original wavefront. Removal of these points leads to extrapolation near the borders of the new pupil when the wavefront is re-calculated by the COAS software. This does not happen if the original wavefront is kept and the pupil simply shrunken mathematically. In our analysis we also imposed cutoffs such that subjects were excluded from analysis in a given meridian

if their minimum pupil diameter in that meridian was less than 3.0 mm or if their central accommodative response in that meridian was < 3.00 D or > 5.00 D.

In working with elliptical pupils, some controversy has arisen as to how to represent these wavefronts with Zernike coefficients, which require circular pupils. The three methods of addressing this issue, as discussed by Lundström[77], are to stretch the wavefront along the pupil's minor axis, to extrapolate the wavefront out to a circle enclosing the entire pupil with a diameter equal to the major axis, or to truncate the edges of wavefront with by imposing a small circlar window of diameter equal to the minor axis of the ellipse. Of the two main groups that have recently examined effects of accommodation on higher order aberrations in the peripheral visual field, Mathur et al. has used the method of stretching the wavefront along its minor axis out to a diameter equal to the major axis[2,68], whereas Lundström has used the method of extrapolating the wavefront out to this same diameter[1].

As Lundström describes[77], stretching the wavefront to form a circle requires imposing a transformation on the Zernike coefficients which is unique to each gaze position. This therefore makes it much more difficult to directly compare Zernike coefficients for different peripheral gaze angles. Lundström notes that extrapolation allows expression of the wavefront in Zernike coefficients and direct comparison across gaze positions without sacrificing information in the original wavefront. Upon consideration, we chose the most conservative approach: truncating the wavefronts to circular apertures corresponding to the minor ellipse of the pupil. While this meant sacrificing data on the wavefront at the edges of the pupil along the major axis, we felt that extrapolation would produce coefficients which we didn't feel confident in using for comparisons and inferences, especially for gaze positions in the far periphery. Generally as the range of extrapolation increases, less confidence can be placed in the accuracy of the extrapolated representation. Earlier studies suggest that changes in peripheral refraction with accommodation are seen primarily in the far peripheral field ($> \pm 40^{\circ}$)[65], and that those positions have the greatest difference between major

and minor axes and thus would be exposed to the largest degree of extrapolation. As such, we felt accurate comparison of those points required as reliable of a representation of the wavefront within the pupil as possible.

2.3.2 Subject Grouping and Statistical Analysis

We originally had one highly hyperopic subject whose refraction was +7.00 D, but this subject's data was removed from this analysis due to failure to recruit additional subjects of similar refractive error. We also eliminated one emmetrope due to an unusually large spread in the subject's data. For the remaining 38 subjects, refractive error was calculated from the central COAS measurement in the tropicamide data set, and ranged from -11.75 D to +1.50 D. Axial lengths ranged from 29.17 mm to 21.83 mm (see figure 2.3). The criteria for pupil size mentioned above was applied to all subjects, which resulted in the removal of one emmetrope, one low myope, and one high myope from analysis. Following this, the

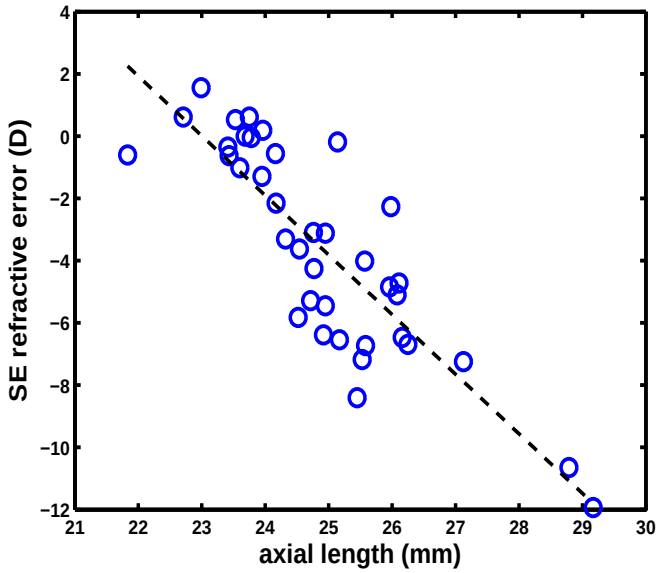

Figure 2.3 Graph showing regression of subjects' refractive errors against axial lengths. The two variables showed a strong relationship, as expected ($y = -1.9748 * x + 44.0494$, $r^2 = 0.7112$, $p < 10^{-10}$).

criteria for accommodative response was applied separately to the vertical and horizontal meridians, resulting in one additional low myope being removed from analysis along the vertical meridian. Then, to eliminate possible confounding variables, we checked to ensure that there was no significant correlation between refractive error and the accommodative response. Since retinal contours were calculated from Zernikes which weren't globally scaled in pupil diameter, we also checked for correlations with non-accommodative pupil diameter and the change in pupil size with accommodation. Regression plots are shown in figure 2.4, and statistics are given in table 2.1.

In none of the regressions was any significant correlation found. Accommodative response was taken as the difference between the phenylephrine accommodative and tropi-

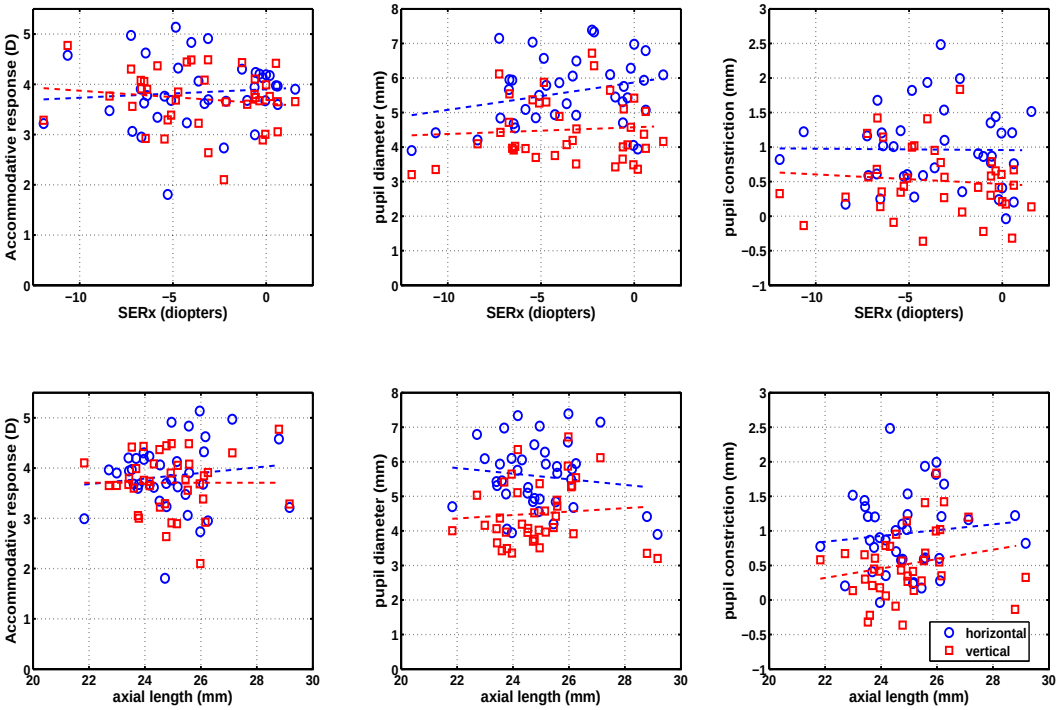

Figure 2.4 Regressions of accommodative response (1st column), non-accommodative pupil diameter (2nd column), and accommodative pupil constriction (3rd column) against refractive error (1st row) and axial length (2nd row). Pupils were scaled as discussed in section 2.3.1 prior to calculation of accommodative response.

y-variable	x-variable	Horizontal Meridian		Vertical Meridian	
		p	r^2	p	r^2
Acc Resp	SERx	0.21	0.049	0.34	0.03
	Axial Length	0.96	< 0.001	0.43	0.021
Pup Diam	SERx	0.09	0.078	0.65	0.006
	Axial Length	0.45	0.016	0.63	0.007
Pup Co	SERx	0.95	< 0.001	0.096	< 0.001
	Axial Length	0.52	0.012	0.51	0.012

Table 2.1 Statistical results from linear regressions of the central spherical equivalent refractive error (SERx) and axial length against accommodative response (Acc Resp), pupil diameter (Pup Diam), and pupil constriction (Pup Constr). Regressions were performed independently for the data taken in the horizontal and vertical meridians.

camide central refractions, since these were the two primary data sets we compared. However, comparison of natural pupil data was similar in that no significant correlations were found. Pupil diameter and constriction were taken from the natural pupil data. We also performed regressions for pupil diameter and constriction comparing tropicamide and phenylephrine accommodative data, and no significant correlations were found.

Subjects were subsequently divided into three groups based on spherical equivalent refractive error (SERx):

- emmetropes, SERx< -1.00 (horizontal meridian $n = 12$, mean SERx=0.09 ± 0.19; vertical $n = 11$, mean SERx=0.09 ± 0.21)
- low myopes, -1.00 <SERx< -6.00 (horizontal meridian $n = 15$, mean SERx=-3.61 ± 0.38; vertical $n = 14$, mean SERx=-3.86 ± 0.41)
- high myopes, SERx> -6.00 (horizontal meridian $n = 9$, mean SERx=-7.51 ± 0.59; vertical $n = 10$, mean SERx=-7.82 ± 0.62)

The differing number of subjects between horizontal and vertical meridians in the low myope group was due to the fact that accommodative response exclusion criteria were applied separately within each meridian. Thus a subject could be excluded in one meridian but still be included in the other if they met the criteria described above in section 2.3.1. This only affected one -2.27 D myope, who was within the allowable accommodative response range in the scan of the horizontal meridian but was not in the scan of the vertical meridian.

Unless noted otherwise, the tropicamide data set was used as the baseline condition whenever comparing non-accommodative aberrations with accommodative aberrations. Differences were examined between the natural non-accommodative data and the tropicamide data and the few trends found were either non-significant or were extremely small in magnitude. Similar analysis was performed between the data obtained with natural accommodation and the data obtained during accommodation with phenylephrine administered, and no significant differences were noted. Because of this, we chose to use the phenylephrine data set for the accommodative comparison. While the larger pupils obtained with phenylephrine may not perfectly represent natural conditions, we felt it would give a better picture of what was happening optically in the periphery with accommodation.

Following normalization of the Zernike coefficients for pupil diameter, we looked for trends by running one-way ANOVA tests between the three groups to look for differences in each Zernike coefficient with and without accommodation at each position of gaze. Since there were 11 gaze positions on the horizontal meridian, 9 gaze positions for the vertical meridian, and 35 Zernike coefficients (eliminating the Z_0^0 piston coefficient from analysis), this analysis generated a table of 11×35 p-values for the horizontal meridian and table of 9×35 p-values for the vertical meridian. These p-values were viewed graphically as heat maps, which we examined for trends. Examples of these are seen in figures 3.1, 3.5, 3.9(a), 3.9(b), 3.17(a), and 3.17(b).

We evaluated the heat maps for significant separations between the groups spanning multiple consecutive positions of gaze using a numerical bootstrap method[78,79]. Precise details of this method are outlined in Appendix C. This method examined the relative spreads of data between the groups at each point in a suspected trend and determined the probability of achieving similar spreads consecutively by chance alone. However, since the ANOVA test is a non-directionally sensitive assessment of spread, our method of analysis only calculated the probability of consecutive spreads lying next to each other and didn't take into consideration if the three groups consistently held the same relative positions to one another. Because of this, our method yielded p-values which were more conservative (higher) than the true significance had it been possible to incorporate relative group position into this method. A simple adjustment by Bonferroni correction of the p-value required to mark significance would have been much too conservative, as it would have required $p < 0.05/700$ to reach significance, which was unlikely given our small sample size. Nevertheless, it was sufficient in most cases to mark notable trends as significant. In our analysis, the few instances where a notable trend was observed on visual inspection and yet our numerical method failed to find significance will be mentioned specifically.

2.4 Calculation of Peripheral Retinal Contour

Calculation of retinal contour using the algorithm outlined by Dunne required first that we create a model eye for each subject using measurements of corneal power, central refraction, anterior chamber depth, lens thickness, and axial length[3]. Axial length was taken from the central IOL Master reading. Numerous studies have shown the IOL Master to give reliable and accurate readings of central axial length[80–83]. Central refraction was calculated from the Zernike coefficients obtained from the COAS data sets corresponding to the retinal contour being calculated.

Central corneal power and anterior chamber depth were obtained from the Pentacam measurements. Studies investigating the effectiveness of measuring corneal curvature and anterior chamber depth with the Pentacam have found it comparable to other methods[84–86], generally reporting small discrepancies of 0.05 mm or less in anterior chamber depth when compared to ultrasound and IOL Master methods of measurement. At the time the study was initiated, we had originally planned to obtain anterior chamber depth and lens thickness values for construction of the initial model eye. However, a recent study has shown that the Pentacam may produce distortions which can confound quantitative measurements of anterior chamber depth and lens thickness[87]. We attempted to compare our measurements of anterior chamber depth and lens thickness to age regressions performed previously by Dubbelman et al.[28,88], which were also obtained using a similar Schiempflug imaging system but were corrected manually for distortions. Our regressions differed dramatically in slope from their data and were highly non-significant. Nevertheless, this was likely due to the fact that our subjects spanned a much smaller age range than the sample studied by Dubbelman et al. We examined the percent difference between our values and those predicted by Dubbelman, performing regressions with axial length and refractive error on the supposition that the myopic eye might possibly cause different distortions within the Pentacam optical system, thereby altering measured parameters differently than in emmetropes. No significant correlation was found between axial length or refractive error and the percent deviation from predicted values for either anterior chamber depth (SERx: $p = 0.62$, AxLngth $p = 0.43$) or lens thickness (SERx: $p = 0.29$, AxLngth $p = 0.95$), but we did discover that our measured values of non-accommodative anterior chamber depth and lens thickness were consistently larger predicted in all but five cases (see figure 2.5). This was highly suspicious, since any normal subject variation would have likewise been present in the regression by Dubbelman and therefore would be expected to distribute itself evenly around the predicted values.

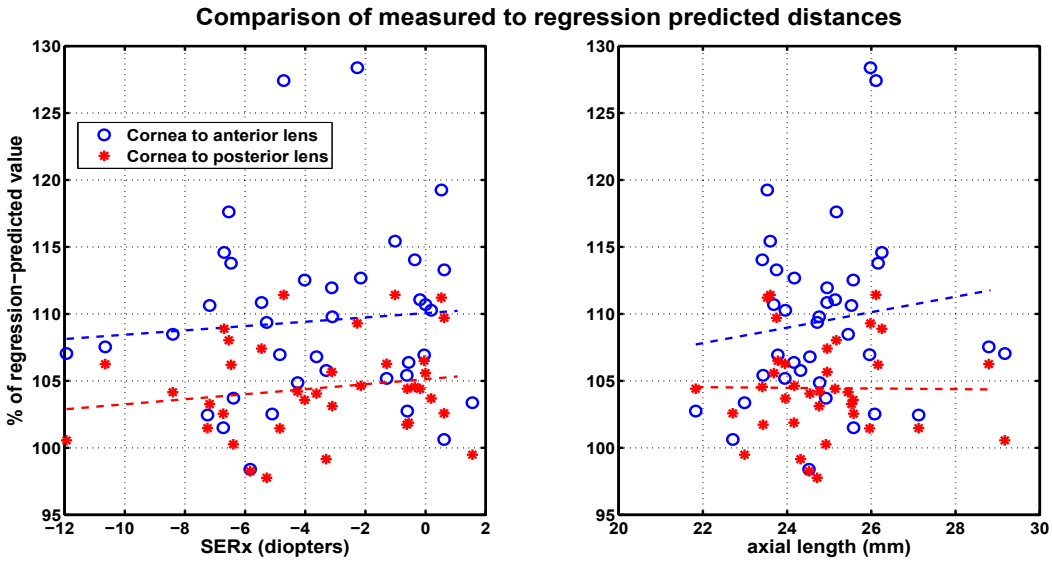

Figure 2.5 Plot of non-accommodative anterior segment parameters, measured with tropicamide administered, as a percentage of the regression predicted values. In almost all cases the Pentacam gave higher values than the regression predicted. Note that the paper by Dubbelman et al. provides regression data for lens thickness indirectly as the cornea to posterior lens surface distance.

Because of the possibility of error in measurement of anterior chamber depth and lens thickness, we decided to construct model eyes for subjects based on anterior chamber depth and lens thickness calculated from regression statistics. Regression data has shown that lens thickness is not correlated to the eye's refractive error[89]. Although it has recently been suggested that the myopic lens fails to thin in the same manner as the emmetropic lens at the onset of myopia[52], this appears to be a developmental phenomenon and shouldn't effect the regression. Using regressions of previously presented data by Dubbelman et al. on lens thickness changes with accommodation[88], we calculated the anterior chamber depth and lens thickness in both the accommodative and non-accommodative states for each subject using the subject's age and accommodative response. The accommodative response was taken as the difference between the central spherical equivalent refractions calculated from aberrations measured in whichever state was being analyzed and the tropicamide state.

We retained information from the Pentacam measurements about anterior chamber di-

mensions, and after calculation of retinal contours we examined the effect that discrepancies in these measurements might cause. For the tropicamide Pentacam measurements, subjects' pupils were generally large enough to provide an adequate image of the posterior lens surface and thus allow measurement of both anterior chamber depth and lens thickness. This was not the case during the accommodative Pentacam scans, however, and only anterior chamber depth was measured directly in these states. To obtain a value for accommodative lens thickness to use in our model, the non-accommodative lens thickness measured with the Pentacam was adjusted using the regression statistics mentioned above.

Following construction of each subject's model eye, peripheral refractions were calculated from measured peripheral aberrations at each gaze position for each of the COAS scans. The Zernike coefficients from the five measurements at each gaze position of the scan in question were normalized by scaling the pupils to match whichever of the five measurements had the smallest pupil diameter[77] and then averaged for that gaze position. Refractions in vector component form were then calculated from the corrected zernikes using 2nd and some 4th order coefficients by equations 2.1[90]:

$$\begin{aligned} M &= \frac{-4\sqrt{3}}{r^2} Z_2^0 + \frac{12\sqrt{5}}{r^2} Z_4^0 \\ J_{45} &= \frac{-2\sqrt{6}}{r^2} Z_2^{-2} + \frac{6\sqrt{10}}{r^2} Z_4^{-2} \\ J_{180} &= \frac{-2\sqrt{6}}{r^2} Z_2^2 + \frac{6\sqrt{10}}{r^2} Z_4^2. \end{aligned} \tag{2.1}$$

Calculation of vector component refractions from Zernike coefficients in this form is described in numerous sources[53,54,91]. In the above equations, r_0 is the pupil radius and the Z terms are Zernike coefficients of 2nd and 4th order. Higher order terms may also be incorporated[91], but were not included in this study. Following calculation of the above vector refractions, spherocylindrical refractions were then calculated and used as input for the Dunne algorithm. This was performed with the following equations[54]:

$$\begin{aligned} \text{Cyl} &= -2\sqrt{J_{45}^2 + J_{180}^2} \\ \text{Sph} &= \text{M} - \frac{\text{Cyl}}{2} \\ \text{Axis} &= \frac{1}{2}\tan^{-1}\left(\frac{J_{45}}{J_{180}}\right). \end{aligned} \tag{2.2}$$

Numerous studies have examined using the COAS in this manner to derive spherocylindrical refractions in the central and peripheral visual fields and have found it repeatable and either comparable or superior to most autorefractors[54,62,92–94]. Matlab R2008b was used to perform these calculations and to automate them for all subjects across all gaze positions in each scan. The details of the algorithm for calculation of retinal contour have been described elsewhere and will not be described further here[3].

Retinal contour from the IOL Master was calculated by tracing a ray through the initial 3-surface eye constructed for the Dunne algorithm (prior to any adjustment of corneal asphericity) and using the measurement from the IOL Master to place the retina at the appropriate distance from the corneal intersection along the ray. We felt that this method was more accurate than that originally proposed by Mallen and Kashyap[4], since the original technical note makes no mention of accounting for refraction of the ray at any of the interfaces within the eye. Our simulations indicated that failure to account for this would create an artificially wide retinal profile. We used the corneal asphericity calculated from corneal topography to perform this raytrace.

Initial analysis consisted simply of comparison of the features of the retinal contours calculated with the Dunne algorithm for each group using the tropicamide data set. Contours were averaged for each group and plotted in terms of gaze angle and in direct cartesian coordinates calculated from the Dunne algorithm. We labeled the nasal and inferior retinas as negative angles on the horizontal and vertical meridians, respectively, as shown in figure 2.6(a). All retinal coordinates were calculated with the corneal vertex as the origin,

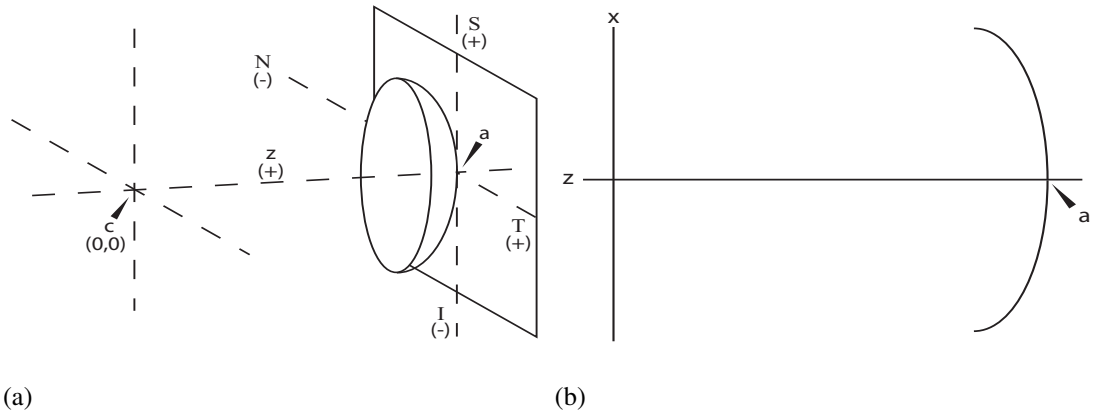

(a) (b)

Figure 2.6 : (a) – figure showing sign convention for calculation of retinal coordinates for the left eye. Corneal vertex (c) is the origin, z-axis corresponds to visual axis, x-axis to horizontal meridian, and y-axis to vertical meridian. Inferior and nasal retinas were marked as negative. Retinal curvature intersected the z-axis at (a), which was considered the eye's axial length. (b) – meridional cross section of (a), showing variable convention used in curve fitting in each meridian.

as shown. In some figures and analysis, however, we chose to view contour relative to the fovea, in which case the axial length was subtracted from the z-coordinate to translate the curve.

Following this, 2nd order polynomial curve fits were performed on the contour of each subject independently in each of the four semi-meridians (inferior, superior, nasal, and temporal retinas) to derive asphericity and central radius of curvature coefficients for each curve fit. The retina was modeled with the general conic section formula:

$$z = \frac{\left(\mathrm{r}_0 + \sqrt{\mathrm{r}_0^2 - px^2}\right)}{p} + a \tag{2.3}$$

Note that equation 2.3 has been modified slightly from that given by Dunne[3], in order to reverse the direction of the retinal curve and to account for its offset along the z-axis by the axial length (a). The details of the derivation of equation 2.3 are given in Appendix D. The asphericity of the conic section is given by p and the central radius of curvature by r_0. Also note that the radius of curvature r_0 is negative, since the center of curvature

of the surface lies to the left of the surface (see figure 2.6(b)). In our analysis, we viewed asphericity in terms of Q:

$$\mathrm{Q} = 1 - p. \tag{2.4}$$

We chose to discuss Q as it was easier to interpret – a negative Q corresponds to a prolate curve, whereas a positive Q corresponds to an oblate curve. A detailed discussion of how we calculated p and r_0 from the 2nd order polynomial curve fit is described in Appendix D. Asphericity and central radius were analyzed for any effect of refractive error or axial length.

Retinal contours calculated in different conditions were compared across all subjects to observe the effect of accommodation and pupil size on calculation. The dilated tropicamide data set from the Dunne algorithm was used as the baseline against which all other scans were compared. We began comparison of two contours by proceeding through a meridian point by point and computing the norm of the vector defined by the two measurements at that gaze position. This value was given a positive sign if the test contour point was farther from the corneal vertex than its corresponding tropicamide contour point. These norms were then averaged across all gaze positions within a meridian for the two scans in question. This gave a quantitative measure of the separation between the two scans in that meridian similar to the RMS. This value was then compared for different scans and across refractive error groups to observe for any significant differences. These plots are shown in chapter 4.

Chapter 3

Results and Discussion: Peripheral Aberrations

Since the principal peripheral aberration in the eye is astigmatism, we elected to first analyze power vector refraction components (Section 3.1) before proceeding to analyze Zernike coefficients directly (Section 3.2). We will first present non-accommodative vector and Zernike values for comparison with previous studies, after which we will discuss changes in these values with accommodation. Non-accommodative peripheral power vectors will be analyzed and discussed relative to their foveal values (section 3.1.1), but Zernike coefficients will be shown in absolute terms (section 3.2.1). Many published findings report relative foveal values, especially for second order terms, but we felt that by looking at both relative and absolute values we would be less likely to miss differences between the refractive groups. Foveally normalized plots for non-accommodative Zernike coefficients are presented in Appendix E.1.1. Accommodative differences were analyzed as absolute values for both power vectors and Zernike coefficients, in order to better note foveal discrepancies between the groups.

We will also mention a few conventions taken in this discussion for the sake of the

reader. In this discussion, "retinal angle" and "gaze angle" are used interchangeably to describe the position on the retina which we are examining (i.e. a nasal gaze angle would yield observation of the nasal retina and correspond to the temporal visual field). Also note that in our plots and discussion we label the nasal and inferior retinas as negative angles on the horizontal and vertical meridians, respectively, as shown in figure 2.6(a). This naturally had no bearing on the results, but it is repeated here simply to make comprehension of the graphs easier for the reader. Finally, for reference, all error bars in our plots represent the standard error of the mean (SEM).

3.1 Analysis of Power Vectors

3.1.1 Non-Accommodative Power Vector Measurements

In figure 3.1, we show the results of ANOVA analysis between the three refractive groups at each vector (M, J_{45}, and J_{180}) and gaze position (50° nasal to temporal on the horizontal meridian [left plot] and 40° superior to inferior on the vertical meridian [right plot]). The

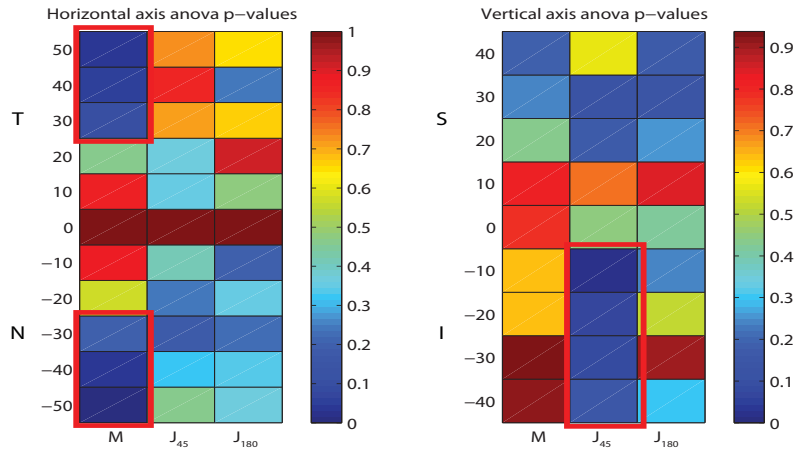

Figure 3.1 Heat map showing results of ANOVA analysis of non-accommodative power vector refraction components M, J_{45}, and J_{180} across refractive error groups (emmetropes, low myopes, and hyperopes).

results are shown as heat maps in figure 3.1. The color scale indicates the p-value found in ANOVA tests run. Numerical analysis showed significant differences between the groups in M in the far nasal retina ($p = 0.024$) and the far temporal retina ($p = 0.013$), and in J_{45} in the inferior retina ($p = 0.002$). These trends are outlined in red in the figure.

Figure 3.2 shows the non-accommodative variation in M for the three refractive groups across the horizontal and vertical meridians, equivalent to the RPRE analyzed in other studies. Negative values of M refer to peripheral myopia relative to the fovea, while positive values refer to relative peripheral hyperopia.

In the horizontal meridian, emmetropes show a relative hyperopic shift on the nasal retina and a slight relative myopic shift on the temporal retina, which becomes hyperopic in the far periphery (50°). We did not find a myopic RPRE over the entire retina in emmetropes, noted by Atchison et al.[57] This asymmetry has been noted previously by Berntsen[62] although it was not analyzed in that study for the effect of refractive error.

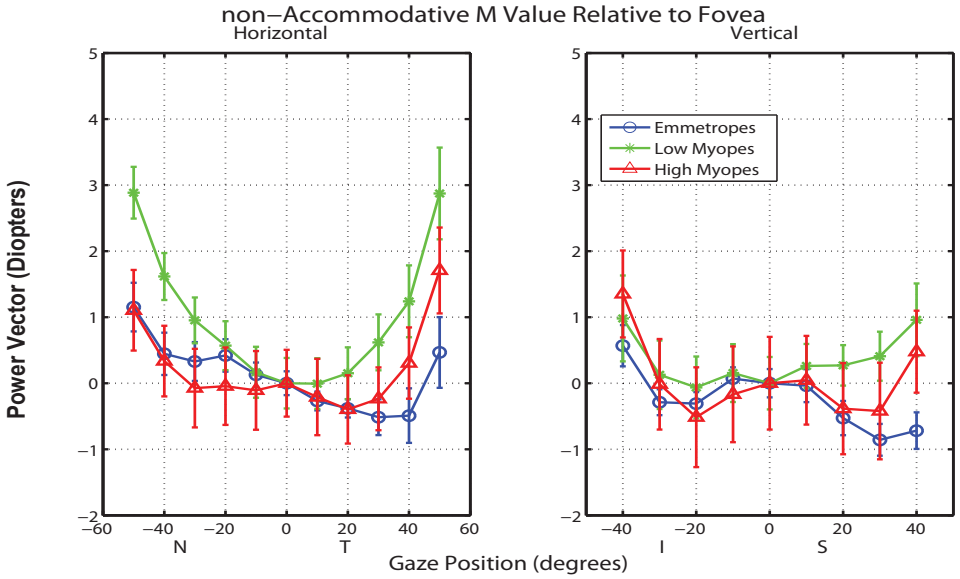

Figure 3.2 Variation in non-accommodative M across gaze position for the three refractive error groups. Negative values indicate relative myopia, positive values indicate relative hyperopia. Respective foveal mean values for the emmetropes, low myopes, and high myopes were 0.12, -3.54, and -7.46 D on the horizontal meridian scan and 0.05, -3.88, and -7.91 D on the vertical meridian.

The low myope group shows much less temporal-nasal asymmetry than either of the other groups, instead showing a pronounced peripheral hyperopia extending over the entire retina which is consistent with previous findings for myopes in general[6,7,9,16,42,55–58]. Interestingly, this peripheral hyperopia appears much less notable in the high myope group, though this group has a much steeper profile of increasing hyperopia in the far periphery. In the near temporal retina the high myope group actually shows a small myopic trend, an asymmetry similar to that of the emmetropic group. This is inconsistent with the general findings of hyperopic RPRE for all myopes. The fact that high myopes seem to have less relative peripheral hyperopia despite having more prolate retinas suggests the possibility of an optical difference which could be altering field curvature in this group alone.

The trends in M, highlighed in red on figure 3.1, are apparent on the extremes of the horizontal axis as a relative hyperopic separation of the low myopes from the other two groups over the nasal retina, and a relatively even separation of the three groups over the temporal retina, with the high myopic group falling between the two other groups.

No significant differences between the three groups were noted with ANOVA analysis of M on the vertical meridian. When first looking at the vertical meridian plot, it appears that there is less peripheral hyperopia on the vertical meridian than on the horizontal meridian, but this is deceiving since the vertical data only goes out to 40° rather than the 50° seen for the horizontal. If we look only out to 20° on the vertical as in the procedure performed by Lundström et al.[77], we note an asymmetry similar to that found by their group: emmetropes seem to have a symmetrically myopic RPRE over the vertical meridian (though much more pronounced at 20° than 10°, both inferiorly and superiorly) while the low myopes have a nearly emmetropic RPRE in the inferior retina and a hyperopic RPRE in the superior retina. Interestingly, this asymmetry is not noted in the high myope group, which seems to more closely parallel the emmetropic group. By extending our measurements out to 40° on the vertical meridian, we find that all groups become hyperopic on the inferior

retina, and at no point is there a significant separation between the groups. On the superior retina we do notice a marked separation of the groups, with the RPRE of the emmetropes remaining myopic, the RPRE of the low myopes remaining hyperopic, and the high myopes falling between. Our study indicates more asymmetry on the vertical meridian in emmetropes, rather than myopes, as reported by Lundström. It is interesting to note that there is considerably less hyperopia in the low myope group on the vertical meridian.

Non-accommodative variation in J_{45} (oblique astigmatism) for the three groups is shown in figure 3.3. No significant differences were found between the three groups in the horizontal meridian, but there is a notable negative trend for all groups in the temporal retina. This trend appears to be roughly linear, as has been noted previously by Atchison et al.[57]. We also note that while the rate of change of J_{45} appears constant in the temporal meridian, it does not appear so in the nasal meridian, where the trend appears to increase in the high myope group. In the vertical meridian, we found emmetropes to have significantly less J_{45}

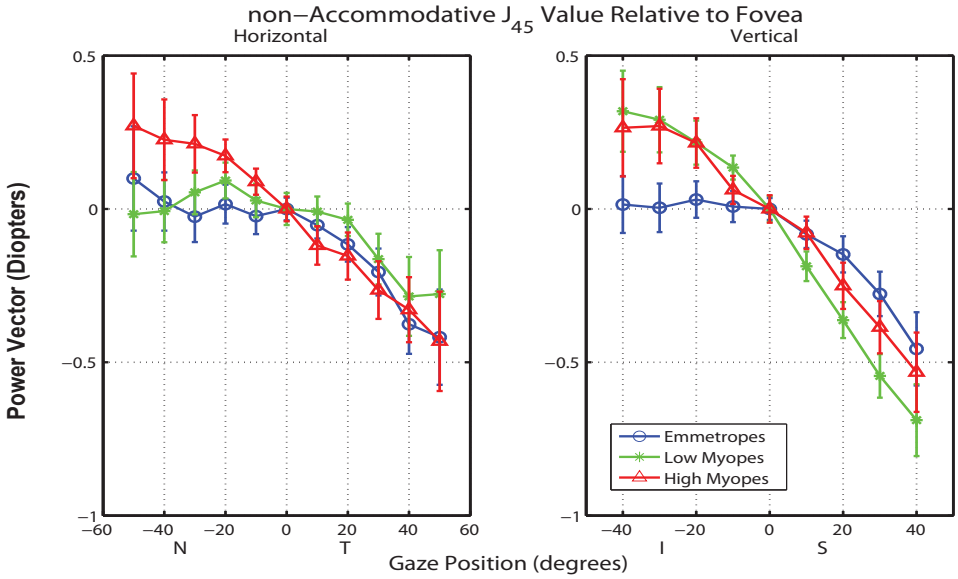

Figure 3.3 Non-accommodative J_{45} relative to fovea. One significant trend was found on the inferior retina ($p < 0.001$). Respective foveal mean values for the emmetropes, low myopes, and high myopes were 0.05, -0.05, and -0.02 D on the horizontal meridian scan and 0.09, 0.00, and -0.04 on the vertical meridian scan.

than myopes in the inferior retina ($p = 0.002$). Similar to the temporal retina, all three groups show a linear negative trend in the superior retina, and for the myopic groups this trend continues into the inferior retina. Unlike Atchison et al., we did not find a difference in the rate of change of J_{45} between the vertical and horizontal meridians.

Non-accommodative J_{180} variation for the three groups is shown in figure 3.4. Note that positive J_{180} corresponds to with-the-rule astigmatism and negative J_{180} corresponds to against-the-rule astigmatism. No significant differences were found between the groups. The temporal and superior retinas show faster rates of change than the nasal and inferior retinas, an asymmetry which has been noted previously[55,56,58,62]. Similar to Atchison et al.[57,61] we note that this trend decreases with myopia, though only notably on the temporal retina.

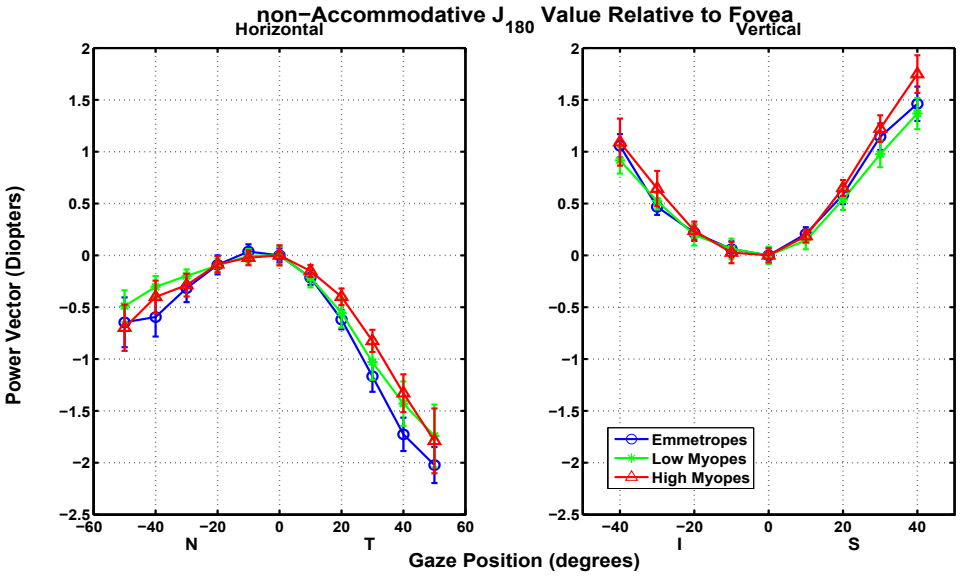

Figure 3.4 Non-accommodative J_{180} relative to fovea. Respective foveal mean values for the emmetropes, low myopes, and high myopes were 0.07, 0.12, and 0.28 D on the horizontal meridian scan and 0.03, 0.17, and 0.17 on the vertical meridian scan.

3.1.2 Power Vector differences with accommodation

We next examined the changes in power vectors with accommodation by comparing the tropicamide data to the phenylephrine accommodative data. Figure 3.5 shows a heat map for ANOVA analysis between refractive groups of accommodative changes in power vectors at each gaze position, similar to figure 3.1. Analysis showed significant differences between the groups in M in the temporal retina ($p < 0.001$) and in J_{180} in the nasal retina ($p < 0.001$). These areas are highlighted in the figure. An apparent trend is also visible in J_{45} in the superior retina, although it was not found to be significant through our numerical simulation ($p = 0.196$).

Figure 3.6 shows the change in M with accommodation. On the horizontal axis, we note a separation of the groups in the temporal meridian (p< 0.001), with high myopes having the least myopic change and low myopes the greatest. The temporal retina in high myope group actually shows a lag behind the fovea, which could presumably serve as a stimulus to myopic development. The high myope group consistently shows the smallest peripheral

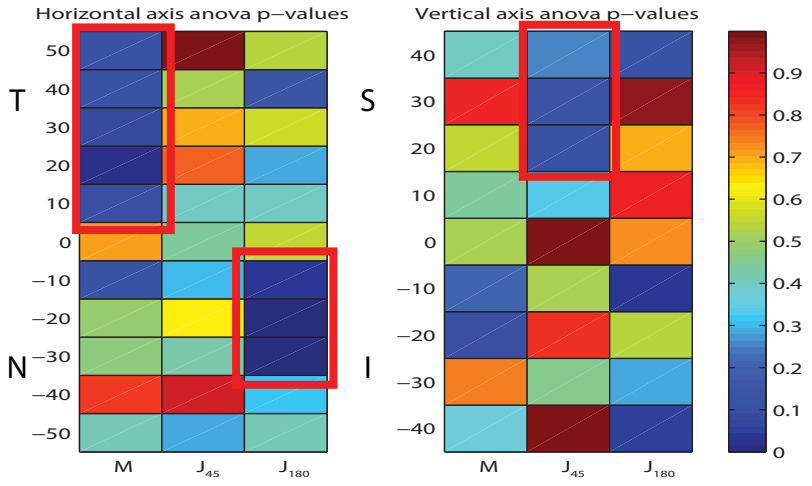

Figure 3.5 Heat map showing results of ANOVA analysis of accommodative differences of power vector refraction components M, J_{45}, and J_{180} across refractive error groups. Significant trends in M and J_{180} are highlighted in red on the horizontal meridian. A nonsignificant trend was was also found in J_{45} on the vertical meridian and is highlighted in red.

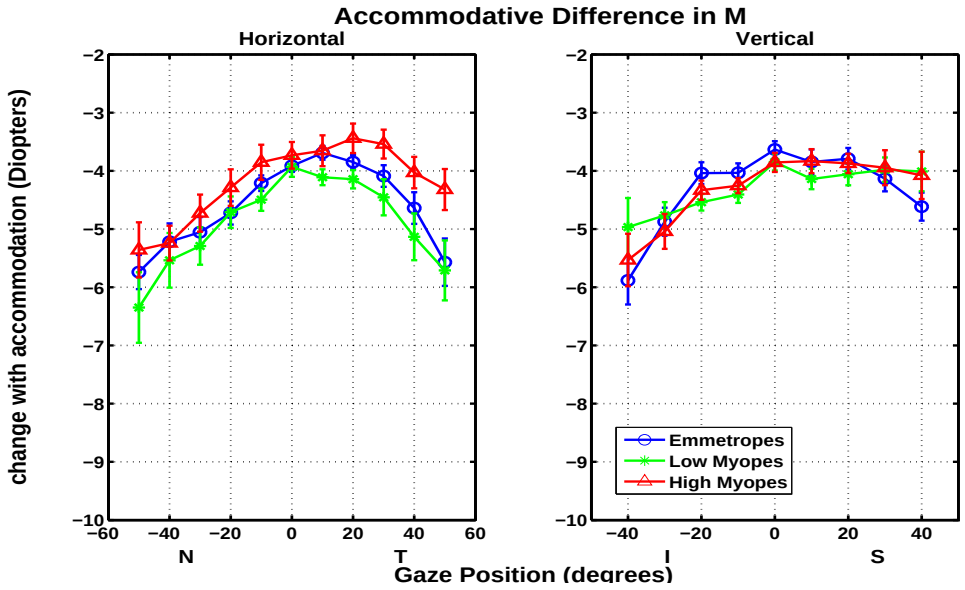

Figure 3.6 Change in M in response to 4.00 D accommodative stimulus across gaze position for the three refractive error groups.

myopic shift with accommodation and the low myopes a consistently higher. The myopes in this study should have had the same optical accommodative stimulus as the emmetropes, since vergence was calculated at the corneal plane and they were not viewing the target through spectacles. The vergence demand should therefore be the same across the three refractive error groups, and the observed differences cannot be explained by a difference in the vergence demand.

We also note a temporal-nasal asymmetry previously noted by Whatham et al.[66] in that the temporal retina has less of a myopic change during accommodation compared to the nasal retina. It is interesting that this asymmetry seems to oppose the asymmetry seen in the non-accommodative profile (see figure 3.2), particularly for the emmetropes and high myopes, in which the asymmetry was most pronounced. The relatively hyperopic nasal retina shows a greater myopic shift with accommodation than the relatively myopic temporal retina. We also note that this asymmetry is once again least pronounced for the low-myope group, although interestingly in this case the low myope group shows the greatest myopic

shift with accommodation over the entire retina, whereas in the non-accommodative state this group showed the greatest hyperopic RPRE (see figure 3.2). No significant separation was found on the nasal retina, although it is notable that the high myope group continues to have the lowest myopic change in RPRE and the low myopes the greatest.

No significant or notable differences were found between the groups for the change in M with accommodation on the vertical meridian. We noted that all groups showed a larger myopic shift in the far inferior retina ($\geq 30^{\circ}$) than in the superior retina, a finding which has not been noted previously.

The change in J_{45} with accommodation is shown in figure 3.7. In the horizontal meridian, no significant or notable difference was found between the three groups. All groups showed a small negative mean foveal change in J_{45} which remained negative on the near nasal retina and showed a positive increase along the temporal retina. It is interesting to observe that the zero for the function falls somewhere between 10° and 20° temporally, indicating that the retinal location where J_{45} remains constant with accommodation is not

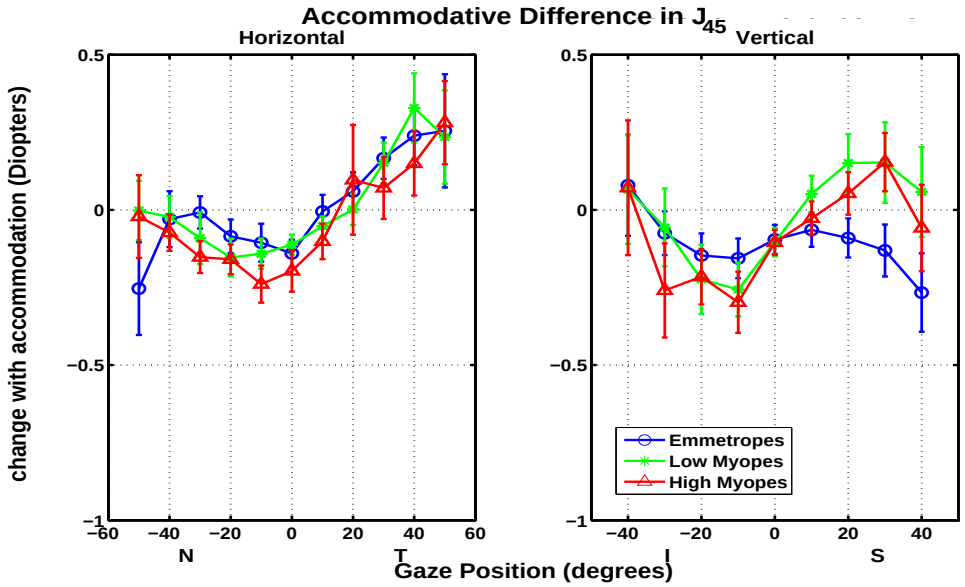

Figure 3.7 Change in J_{45} in response to 4.00 D accommodative stimulus across gaze position for the three refractive error groups.

foveal but slightly temporal for all groups. Changes in J_{45} are similarly small and negative on the inferior retina, but a notable separation is seen on the superior retina in that emmetropes continue to show a negative change while both myopic groups show a positive change. This trend is only present out to $30°$, and was not found to be significant in our numerical simulation.

Figure 3.8 shows the change in J_{180} with accommodation. J_{180} showed an increasingly negative change with accommodation as horizontal eccentricity increased, which can be interpreted as an progressive larger increase in against-the-rule (or decrease in with-the-rule) astigmatism with increasing horizontal eccentricity. A temporal-nasal asymmetry is once again visible in that J_{180} became more negative with accommodation in the nasal meridian than in the temporal meridian. Interestingly this asymmetry once again seems to oppose the asymmetry seen in the non-accommodative profile (see figure 3.4) The nasal retina, which has a less negative J_{180} in the non-accommodative state, seems to show a greater negative shift with accommodation. This asymmetry in the accommodative change seems

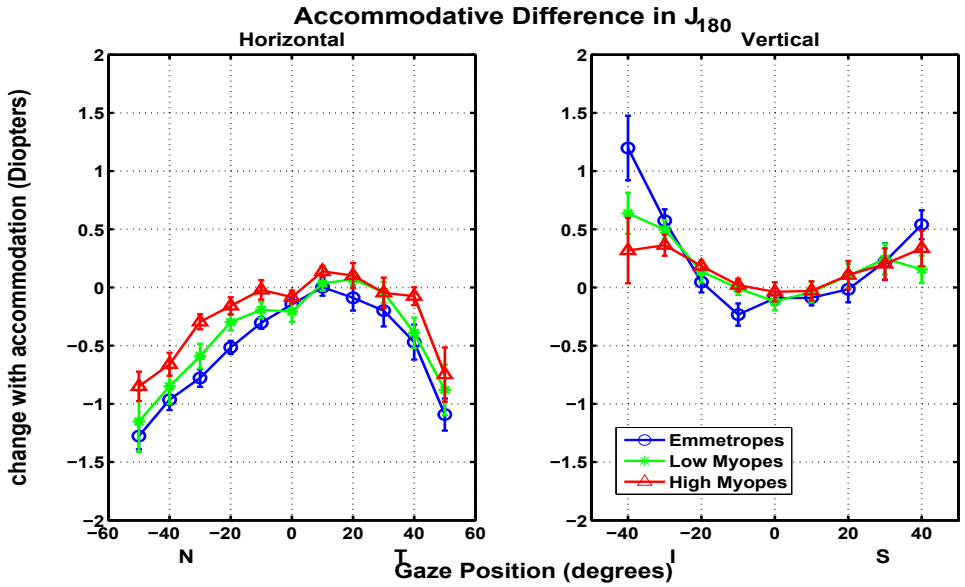

Figure 3.8 Change in J_{180} in response to 4.00 D accommodative stimulus across gaze position for the three refractive error groups.

to decrease with myopia, as the change in the nasal retina is successively less negative in the myopic groups ($p< 0.001$). Mathur et al. observed very little change in J_{180} with accommodation in emmetropes[2], but this may have been due to the fact that their range of measurements only extended out to $\pm 21^\circ$ horizontally and $\pm 16^\circ$ vertically, where the magnitude of the change is very small ($< 0.5D$ in the above graph). In the vertical meridian we saw a similar trend of increasing change in J_{180} with eccentricity except that the change was positive, indicating an increase in with-the-rule astigmatism. No obvious effects of refractive error were apparent through the ANOVA analysis or through visual inspection of the data. Although it is possible that there is a separation between the groups in the far inferior retina ($\geq 30^\circ$), the spread of the data was too great to be marked as significant by our numerical approach.

3.2 Analysis of Zernike Coefficients

In our analysis of higher order aberrations, we examined out to 7th order Zernike coefficients. As such, we had 35 variables in which to look for effects. All aberration values are given in microns (μm). In general, the magnitude of the coefficients as well as their changes with accommodation tended to decrease by approximately one order of magnitude with each order of terms compared to 2nd order terms (i.e. 2nd order terms were around 1 μm, 3rd order terms around 0.1 μm, etc), though this was by no means a firm rule. We did not exclude higher order terms from analysis due solely to a small amplitude. Nevertheless, we recognized the need to be judicious in presenting data which would be both useful and meaningful. We examined primarily to see if there were differences between refractive groups with increasing eccentricity and with accommodation. We included mention of trends which were visually notable even if they were not found to be significant, since our method of calculating significance was conservative and the true significance of

any trend was higher than our estimate. Furthermore, as will be shown, trends found in the higher order coefficients often showed similar behavior in lower order terms. In such cases the data for the two terms are discussed together. We will also only discuss trends that were flagged by our bootstrap method if they showed a notable or consistent pattern of separation between the plots for the different refractive groups. Any trends which failed to show any pattern are included in Appendix E.

3.2.1 Non-Accommodative Zernike Coefficients

Figures 3.9(a) and 3.9(b) show the results of ANOVA analysis of non-accommodative Zernike coefficients between the three groups at each gaze angle. ANOVA analysis of the horizontal meridian revealed significant differences between the groups in Z_3^3, Z_4^{-2} Z_6^{-2}, and Z_6^0. Significant trends were also flagged for Z_7^1, and Z_7^3, but on visual inspection of the data these trends either showed no consistent pattern of separation between the groups or were of negligible amplitude. Findings on the vertical axis revealed significant differences between the groups in Z_2^{-2}, Z_3^3, Z_4^0, and Z_6^{-6}.

Figure 3.10 shows the non-accommodative 2nd order Zernike coefficients in the horizontal and vertical meridians. Note that these are not plotted relative to the fovea, as the vector refraction components were – foveally normalized plots are included in Appendix E.1.1. Figure 3.10(a) shows the expected variation in defocus present between the three groups. The three curves contain more or less the same shapes as those for M shown in figure 3.2, save that they are reversed in sign and are no longer normalized by their foveal values. The curves for Z_2^0 and M don't correspond exactly, due to the small weighted contribution of spherical aberration (Z_4^0).

Zernike coefficient Z_2^{-2} is shown in figure 3.10(b), and corresponds with vector refraction component J_{45} shown in figure 3.3, save that in this instance the lack of foveal normalization enlarged the separations between the three groups in the nasal and superior

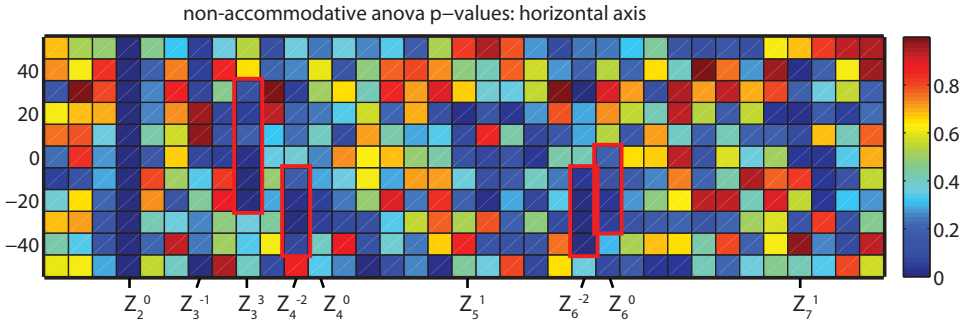

(a) Horizontal Meridian

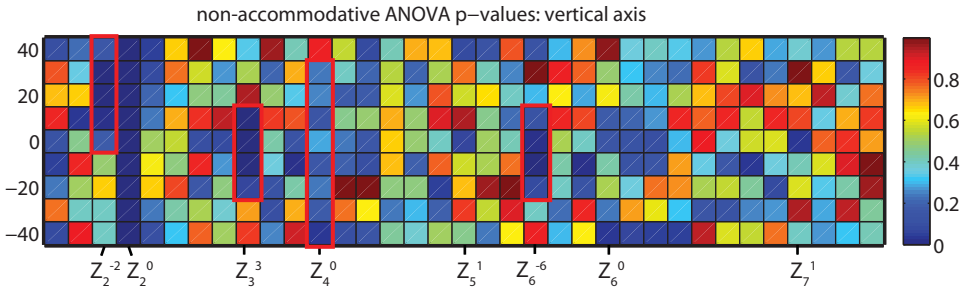

(b) Horizontal Meridian

Figure 3.9 ANOVA analysis of non-accommodative Zernike coefficients on horizontal (a) and vertical (a) meridians. Notable trends are highlighted in red.

retinas. The trend in the nasal retina shows the least oblique astigmatism in the low myope group and the most in the high myope group, with the emmetropes falling between. This trend was not found to be significant by our numerical method.

Zernike coefficient Z_2^2, shown in figure 3.10(c), corresponds to the J_{180} power vector viewed in figure 3.4. Note that the vertical and horizontal meridian plots have different scales on the y-axis, to better highlight the effects on each meridian. No significant differences were found between the three groups on initial analysis through our numerical method. However, when the three groups were normalized to foveal values (shown in figure E.1(c)), a significant separation was found in the nasal retina ($p < 0.001$) and a non-significant trend was found in the superior retina. In both cases, this was due to the relatively flatter profile of the low myope group's curve. This suggests that Z_2^2 changes less

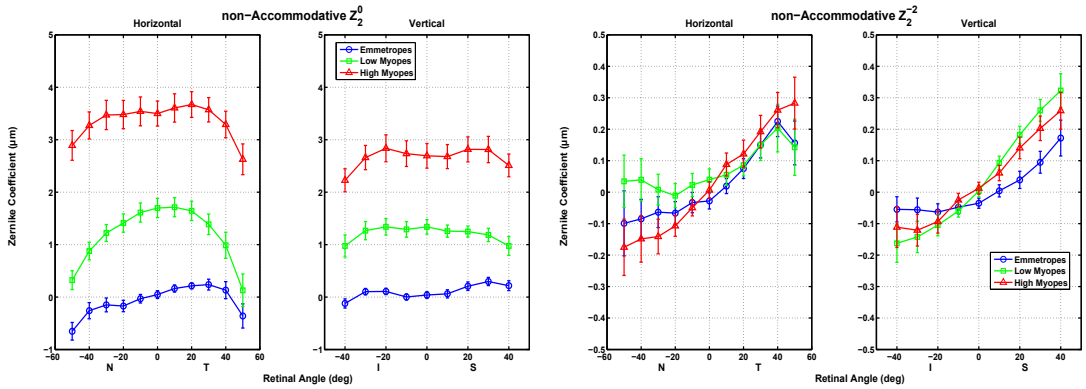

(a) Z_2^0

(b) Z_2^{-2}

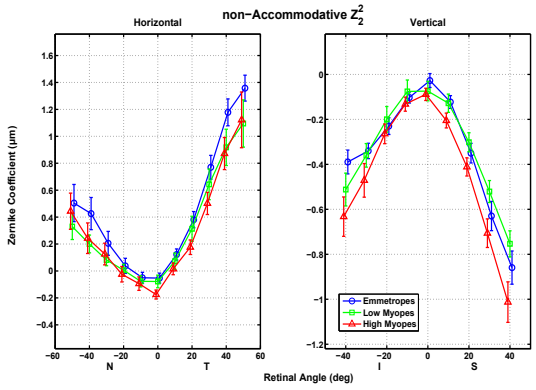

(c) Z_2^2

Figure 3.10 Plots of non-accommodative 2nd order Zernike coefficients Z_2^0 (a), Z_2^{-2} (b), and Z_2^2 (c). Note that the horizontal and vertical meridian plots for Z_2^2 do not have the same scale on the y-axis.

quickly with eccentricity in the superior and nasal retinas for this group.

Non-accommodative trefoil terms are shown in figure 3.11. Note that the horizontal and vertical meridian plots do not have the same scale on the y-axis. Coefficient Z_3^{-3} became more positive in the far nasal and temporal periphery for all groups (figure 3.11(a)). We did not note the trend that Mathur et al. noted[68] of emmetropes having a more positive Z_3^{-3}, although we did find a separate trend in that Z_3^3 showed a significant separation of the groups in the central regions of both the horizontal ($p< 0.001$) and vertical meridians ($p< 0.001$). This is seen only in the emmetropic group as a slightly negative Z_3^3 in the

central regions of both meridians. For both myopic groups Z_3^3 is essentially zero or slightly positive in these regions.

Figure 3.12 shows vertical and horizontal coma terms (Z_3^{-1} and Z_3^1) across the visual field. Note that the horizontal and vertical meridian plots do not have the same scale on the y-axis. As would be expected, vertical coma increases steadily from the inferior retina to

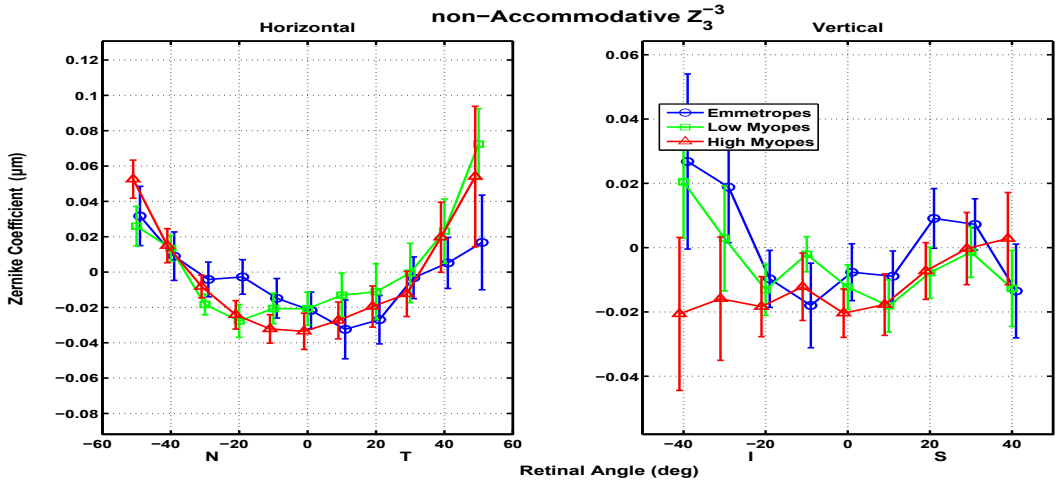

(a) Z_3^{-3}

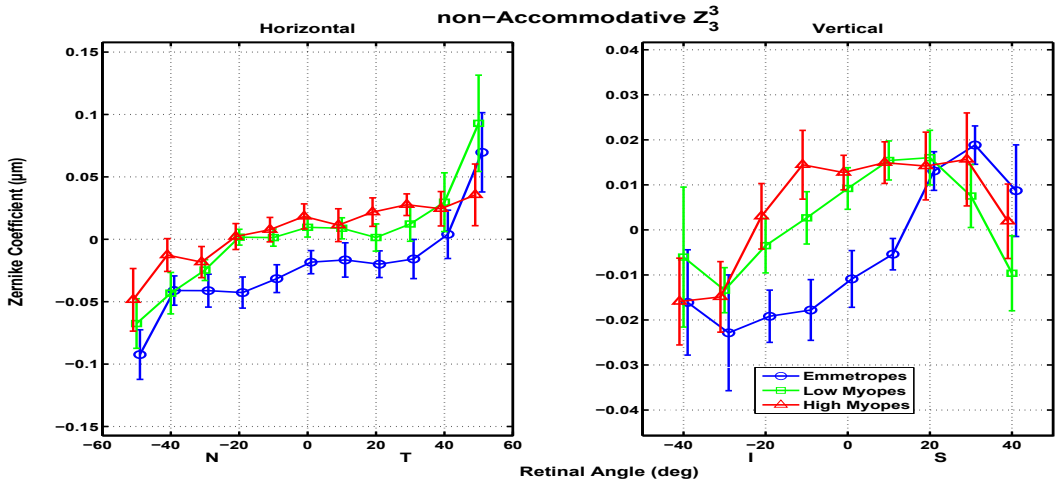

(b) Z_3^3

Figure 3.11 Non-accommodative 3rd order trefoil terms, Z_3^{-3} and Z_3^3. Note that the horizontal and vertical meridian plots do not have the same scale on the y-axis.

the superior retina. A similar increase is observed in horizontal coma from the nasal retina to the temporal retina. There is a small central increase in Z_3^1 for the emmetropic group which extends temporally and inferiorly; although not a significant separation in either meridian, this trend creates a significant separation in the superior meridian ($p< 0.001$) when the curves are foveally normalized (figure E.2(a)). This suggests that horizontal

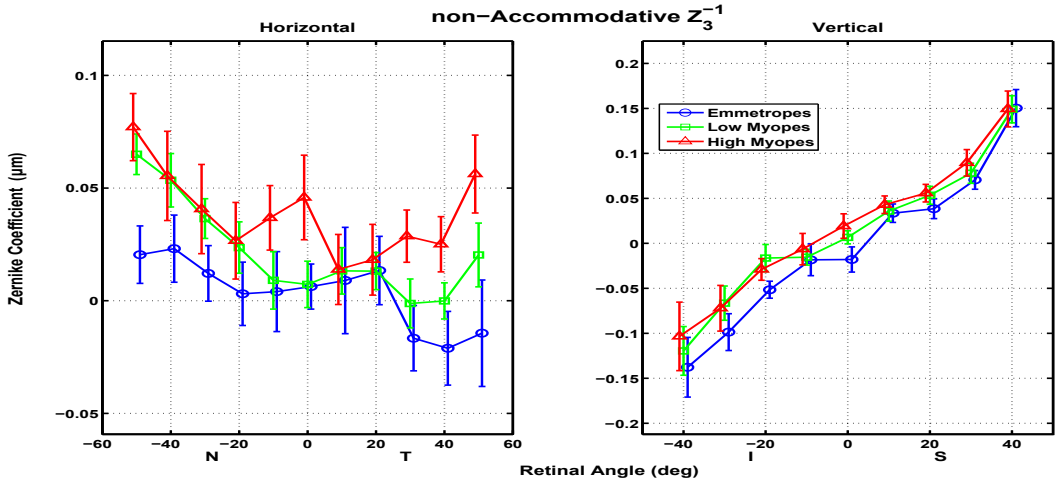

(a) Z_3^{-1}

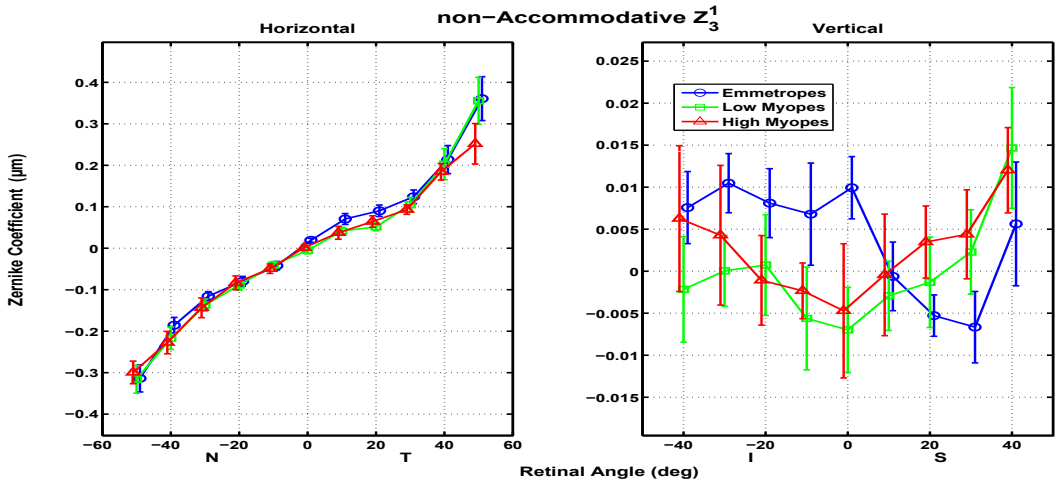

(b) Z_3^1

Figure 3.12 Non-accommodative 3rd order vertical (a) and horizontal (a) coma terms, Z_3^{-1} and Z_3^1. Note that the horizontal and vertical meridian plots do not have the same scale on the y-axis.

coma (Z_3^1) becomes negative with eccentricity faster for the emmetropic group than for the two myopic groups in the superior retina.

It is interesting to note that radial coma increases with eccentricity approximately twice as fast in the horizontal meridian than in the vertical, as noted by the differences in the slopes of the plots in the vertical meridian in figure 3.12(a) and the horizontal meridian in 3.12(b). This is consistent with data shown by Lundström[1], although they did not make note of or discuss it.

Charman and Atchison recently modeled the effect of decentration of the visual axis on aberrations[95]. Their modeling suggests that separation of the optic and visual axes will cause the appearance of horizontal coma along the vertical meridian and vertical coma along the horizontal meridian. Moreover, they show that such decentration would cause horizontal coma on the vertical axis to vary parabolically with eccentricity, which is similar to the form that the curves in figure 3.12(b) exhibit, especially for the myopic groups. Such decentration would also alter the rate of growth of the coefficient with eccentricity along the horizontal meridian, but we did not note an extremely large difference in slopes between the groups. However, we note a difference in Z_3^1 between the groups on the vertical meridian in that the curve for the emmetropic group appears to have negative curvature (curves down, from 30° superior to 40° inferior) and inferior decentration, while the curves for the myopic groups both appear to have positive curvature and little to no decentration. If the difference between groups in the horizontal and vertical coma terms were created only by decentration, we would expect it to cause a larger difference in the slopes of the plots on the horizontal meridian. Considering the magnitude of the inferior decentration of the emmetropic curve mentioned above and the fact that it has the opposite curvature from the myopic groups, we would expect a larger effect on the Z_3^1 coefficient in the horizontal meridian.

Fourth and sixth order oblique astigmatism terms are shown in figure 3.13. While small

in magnitude, there is a significant separation between the groups for the Z_4^{-2} term on the nasal retina (p$=0.035$). This separation is manifest as a slightly positive Z_4^{-2} value for the low myope group, a slightly negative Z_4^{-2} for the high myope group, and an even more negative value for the emmetropic group. The fact that this trend manifests significantly in the same retinal location and with the same relative location between groups in the higher

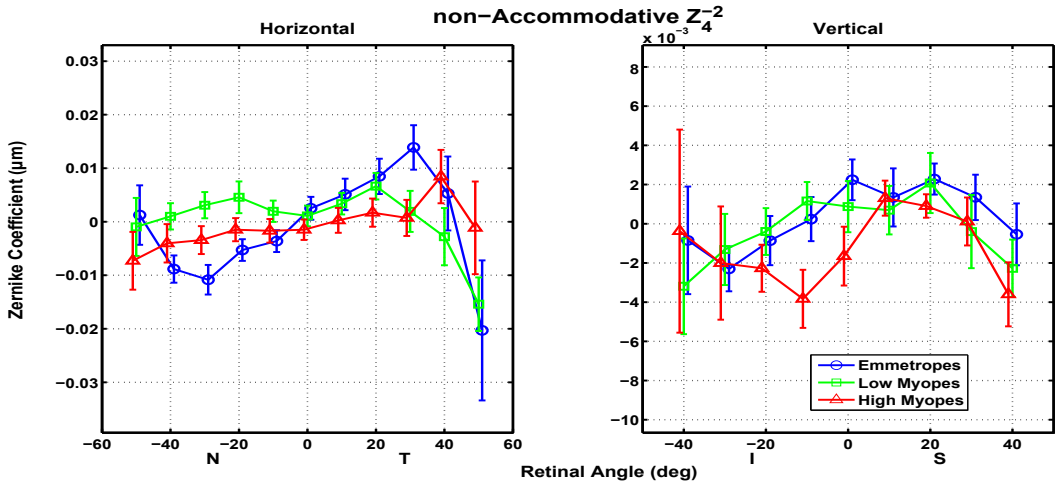

(a) Z_4^{-2}

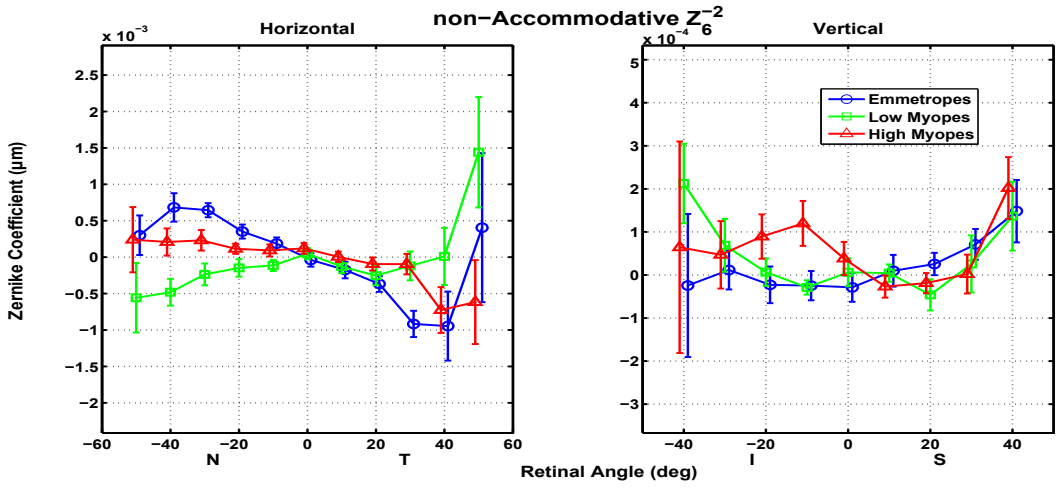

(b) Z_6^{-2}

Figure 3.13 Non-accommodative 4th (a) and 6th (b) order oblique astigmatism terms, Z_4^{-2} and Z_6^{-2}. Note that the y-axes do not hold the same scale in all plots.

order Z_6^{-2} term ($p< 0.001$) suggests that the trend is real and not just noise. Furthermore, this trend does not appear as simply a continuation of the trend seen in Z_2^{-2} (figure 3.10(b)), since the curves for the three groups are no longer in the same arrangement relative to each other or to the horizontal axis (the three groups here straddle the axis, which wasn't the case for Z_2^{-2}).

Plots for spherical aberration and 6th order defocus terms are shown in figures 3.14(a) and 3.14(b). Both terms appear to grow with eccentricity faster on the horizontal meridian than the vertical meridian, and the growth of Z_6^0 shows the expected reversed sign compared to the Z_4^0 term. We found the same trend that Mathur et al. found[68] in that emmetropes appear to have a more positive Z_4^0 which seems to decrease with myopia. This manifests as a separation between the groups which is significant on the nasal horizontal meridian ($p= 0.025$). We note also that this separation decreases with increasing retinal eccentricity, which was not noted by Mathur et al., probably due to their smaller range of eccentricities at which they measured. A similar significant separation is found in the same retinal location for Z_6^0 (p=0.015), except that in this case the separation between the groups seems to remain constant or increase with eccentricity. These two trends appear to be extensions of each other, since the three groups appear to hold the same relative positions for both. The two trends are likely related to Z_2^0 (see figures 3.2 and 3.10(a)), since some of the same temporal-nasal symmetries can be seen which were present for 2nd order defocus (although much less pronounced than they were for Z_2^0).

A significant separation of the three groups is also seen in Z_4^0 along the vertical meridian ($p= 0.018$), similar in nature to that observed along the horizontal meridian. It does not appear to have any related findings in the Z_2^0 or Z_6^0 terms.

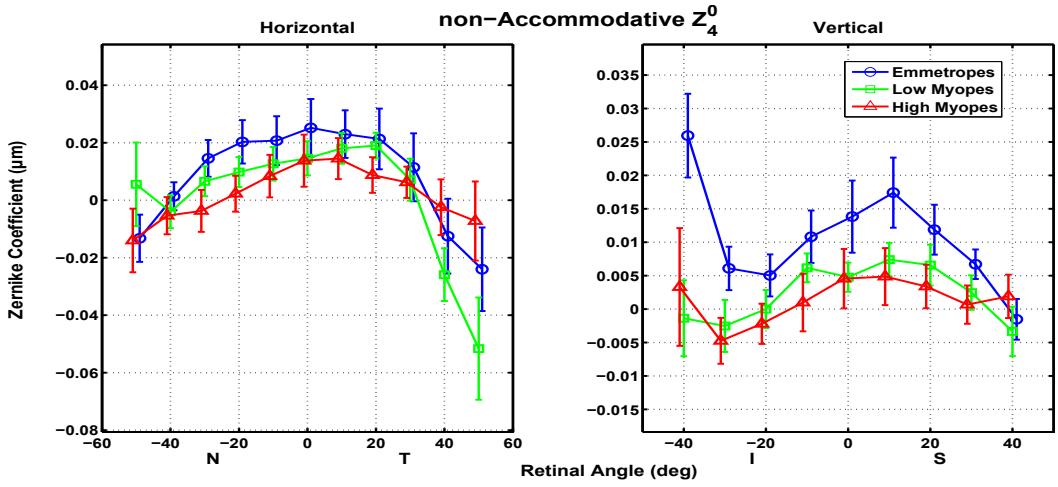

(a) Z_4^0

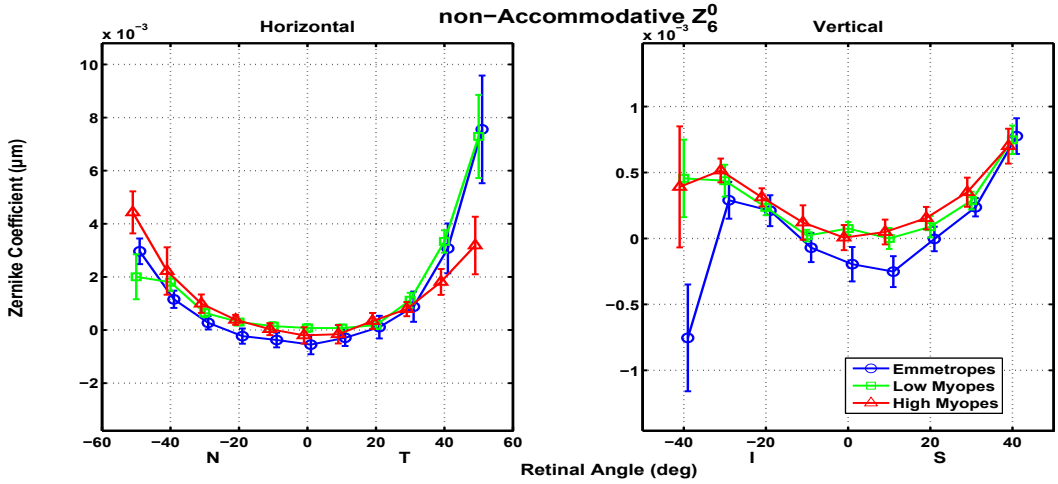

(b) Z_6^0

Figure 3.14 Non-accommodative 4th order defocus (spherical aberration) and 6th order defocus terms, Z_4^0 (a) and Z_6^0 (b). Note that the y-axes do not hold the same scale in all plots.

3.2.2 Non-accommodative RMS wavefront error in Zernike orders

Following analysis of individual Zernike coefficients, we looked at the RMS of all Zernike coefficients. The RMS of all coefficients 2nd order and above is shown in figure 3.15(a), and the RMS of all coefficients 3rd order and above in figure 3.16(a). Foveally normalized plots are shown in plots 3.15(b) and 3.16(b), and are also insightful. Examination of the absolute

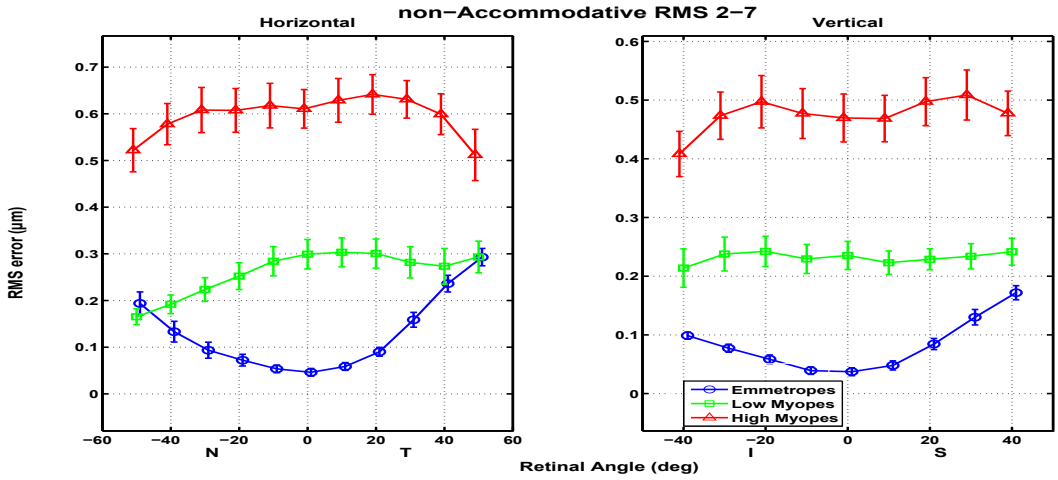

(a)

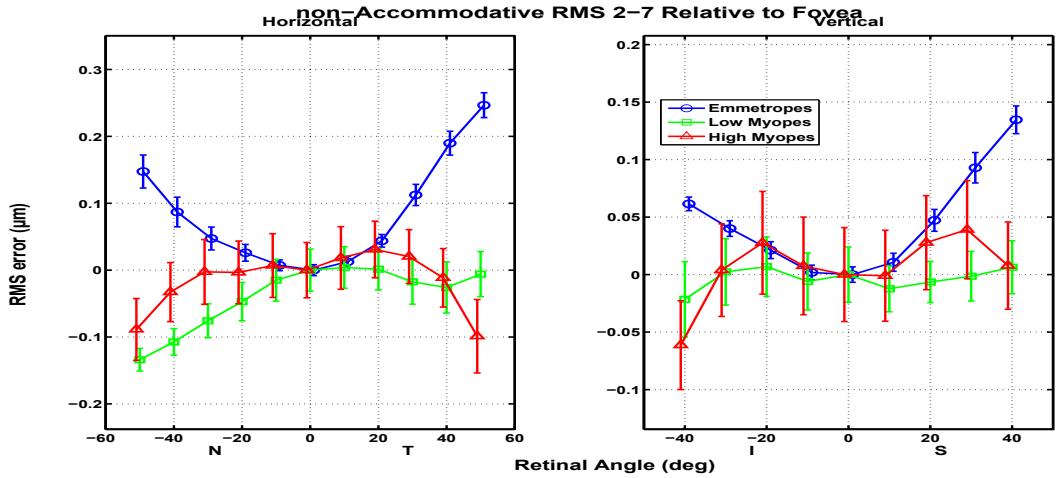

(b)

Figure 3.15 Non-accommodative RMS for all coefficients 2nd order and above plotted as absolute values (a) and relative to foveal values (b).

plots in figure 3.15(a) shows a vertical offset between the three curves which corresponds to the subjects' refractive error. This is determined principally by the 2nd order terms, which is best appreciated by comparison with the plots in figure 3.16(a)), in which 2nd order terms have been removed. Removal of 2nd order terms causes the the foveal discrepancies between the three groups to practically disappear.

Examination of the RMS aberrations relative to their foveal values in figure 3.15(b)

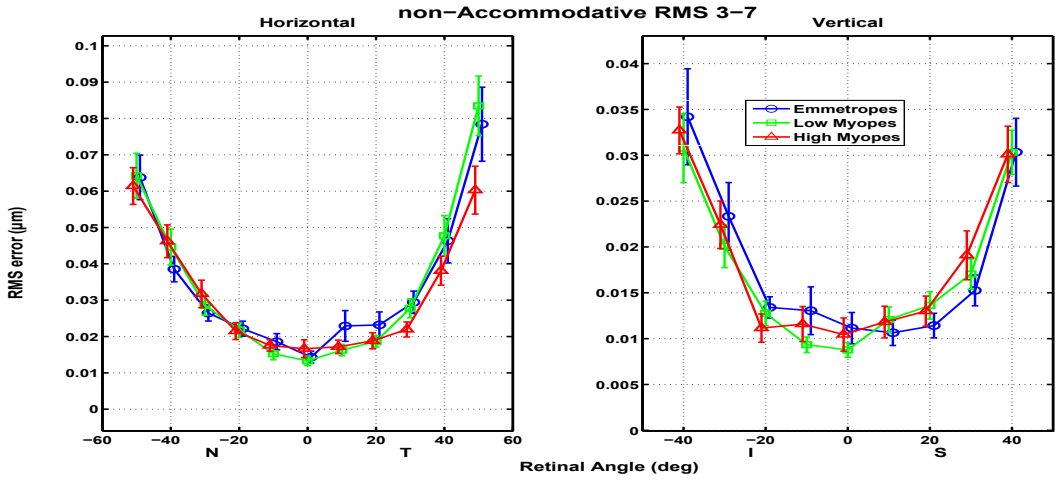

(a)

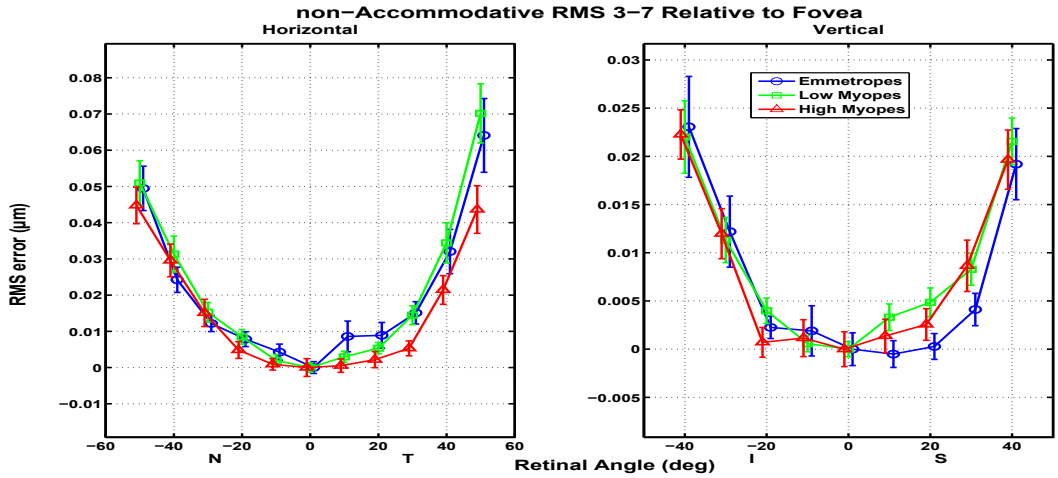

(b)

Figure 3.16 Non-accommodative RMS for all coefficients 3rd order and above plotted as absolute values (b) and relative to foveal values (a).

shows that emmetropes have increasing aberrations with eccentricity in both meridians, whereas both myopic groups show no change or a relatively small decrease in aberrations with eccentricity in both the horizontal and vertical meridians compared to foveal values. It is interesting that this trend doesn't progress steadily with myopia. Instead, the high myope curve falls between the emmetrope and low myope curves, only showing a steep relative decrease in aberrations in the far periphery of each meridian. Statistically significant sep-

arations of the three groups were found in the nasal ($\geq 10°$, p$< 10^{-4}$), temporal ($\geq 30°$, p$< 10^{-4}$), and superior retinas ($\geq 30°$, p$= 0.017$).

The finding that relative RMS increases in emmetropes and decreases in myopes was unexpected, but can be easily explained by examining the absolute 2nd order plots seen in figure 3.10. The Z_2^0 term is less in the periphery for all myopic subjects relative to their foveal term since they are less myopic in the periphery. The increase in astigmatism in the periphery is relatively a small contribution to the 2nd order in myopia since the Z_2^0 term is large (figure 3.10). In emmetropes, however, the Z_2^0 term is actually greater in absolute value in the periphery than it is in the fovea, and with the increase in peripheral astigmatism, there is an overall relative increase in 2nd order aberration in the periphery in emmetropia. Thus the pattern noted in figure 3.15(b) is due to the fact that the relative decrease in Z_2^0 dominates the RMS for myopes, but for emmetropes the Z_2^0 is small enough that the RMS shows an increase due to this term (due to the fact that RMS is insensitive to sign). The magnitude is also small enough that the Z_2^2 astigmatism term contributes notably.

The notion that the trend observed in figure 3.15(b) is caused primarily by 2nd order coefficients is supported by the fact that when these terms are omitted from the RMS calculation, not only is the vertical offset between the curves removed, but the separation between the groups is eliminate, as seen in figures 3.16(a) and 3.16(b). The curves for the three groups follow essentially the same course with no significant separation. These plots also show that the RMS due to higher order terms increases steadily with eccentricity in both meridians, though it may appear to grow slightly faster on the horizontal meridian (0.3 μm at $40°$ on the horizontal, compared to 0.2 μm at $40°$ on the vertical). It is notable also that higher order aberrations increase more slowly with eccentricity in the temporal retina for high myopes ($p = 0.004$) and in the superior retina for emmetropes ($p = 0.062$), as shown by the slightly lower curvature for these group in those respective areas of figure 3.16(b).

3.2.3 Zernike Coefficient differences with accommodation

Figures 3.17(a) and 3.17(b) show the results of ANOVA comparison of the three refractive groups for the changes in Zernike coefficients with accommodation at each gaze angle. ANOVA analysis of the horizontal meridian revealed significant differences between the groups in Z_2^0, Z_2^2, Z_3^1, Z_4^0, Z_5^1, and Z_6^0 (figure 3.17(a), outlined in red). Trends were also flagged in Z_3^{-3}, Z_3^{-1}, Z_5^{-5}, Z_5^{-3}, Z_6^{-4}, and Z_7^7 (figure 3.17(a), outlined in green), but on in-

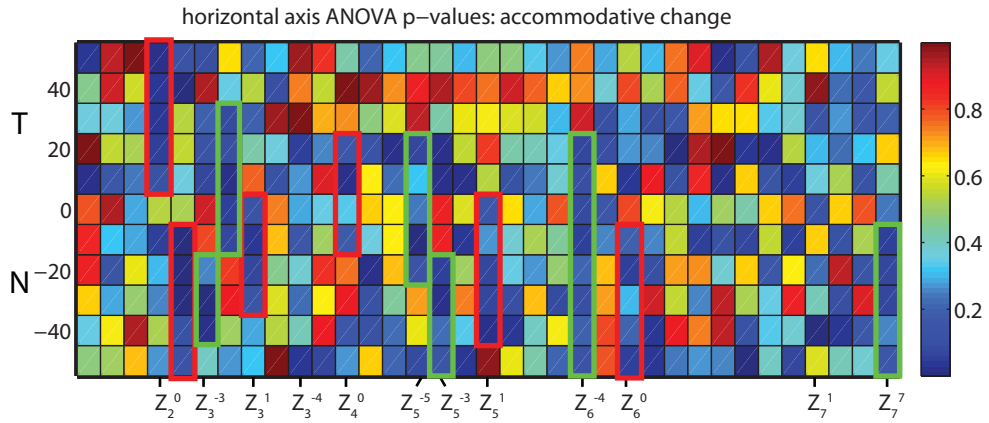

(a) Horizontal meridian

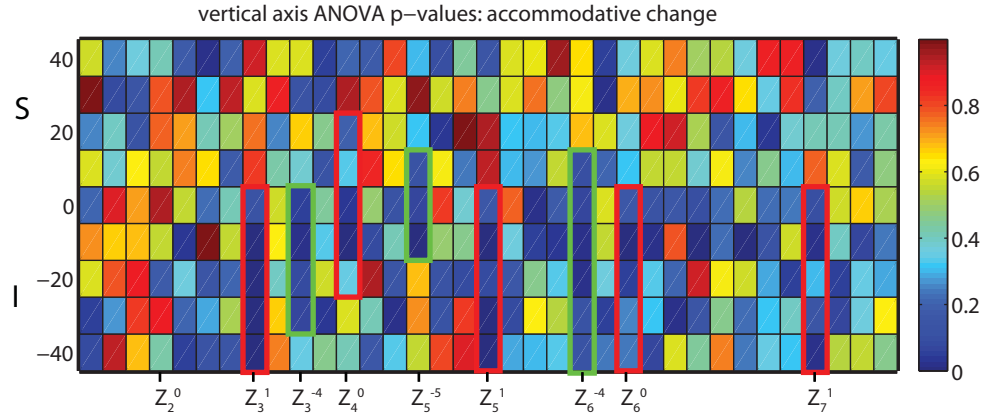

(b) Vertical Meridian

Figure 3.17 Results of ANOVA analysis of accommodative differences of Zernike Coefficients across refractive error groups on Horizontal (a) and vertical (b) axes.

spection of the data, these trends showed either no consistent pattern of separation between the groups or were of negligible amplitude. ANOVA analysis of the vertical meridian showed significant trends in Z_3^1, Z_4^0, Z_5^1, Z_6^0, and Z_7^1 (figure 3.17(b), outlined in red). Significant trends were also flagged in Z_4^{-4}, Z_5^{-5}, and Z_6^{-4} (figure 3.17(b), outlined in green), but they were of small amplitude, showed no consistent separation pattern between the three groups, or did not yield themselves to any meaningful interpretation.

Figure 3.18 shows accommodative differences in the 2nd order Zernike coefficients. They are extremely similar to the plots for the power vector changes with accommodation

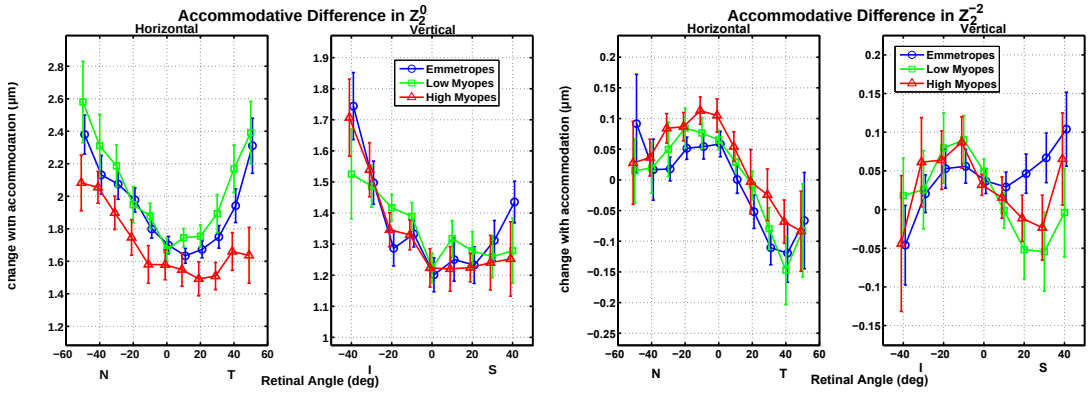

(a) Z_2^0

(b) Z_2^{-2}

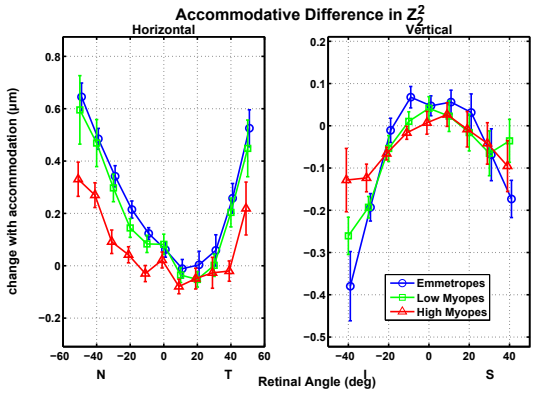

(c) Z_2^2

Figure 3.18 Plots of accommodative changes in 2nd order Zernike coefficients Z_2^0 (a), Z_2^{-2} (b), and Z_2^2 (c). Note that horizontal and vertical plots do not necessarily have the same scale on the y-axis.

(M, J_{45}, and J_{180} seen in figures 3.6, 3.7, and 3.8, respectively), and are included here for completeness. To avoid repetition, the reader is referred to section 3.1.2 for a detailed analysis. We will note, however, that the high myope group shows a larger discrepancy compared to the other groups when examining the change in the Z_2^0 term than was seen in the corresponding power vector term (M, seen in figure 3.6. We believe that this is due to the incorporation of 4th order spherical aberration term, Z_4^0, into the M term. As will be shown in figure 3.21(a), spherical aberration shows an opposing separation between the myope groups and the emmetrope group, which would serve to diminish this effect in the power vector term.

As mentioned above, the trends found in coefficients Z_3^{-3}, Z_3^{-1}, Z_4^{-4}, Z_5^{-5}, Z_5^{-3} Z_6^{-4}, and Z_7^7 were either small in magnitude, showed no consistent pattern of separation between the groups, or yielded no meaningful interpretation. They are mentioned here for completeness. Graphs are presented and discussed in Appendix E.3.

Analysis of horizontal coma terms proved interesting. Figures 3.19(a), (b), and (c) show changes in 3rd, 5th, and 7th order horizontal coma terms (Z_3^1, Z_5^1, and Z_7^1) with accommodation. In the horizontal meridian of the Z_3^1 plot we note that Z_3^1 shows a greater accommodative change with increasing eccentricity in both the nasal and temporal retinas. The emmetropic group shows an asymmetry in that this increase is faster in the temporal retina than in the nasal retina. This asymmetry seems to decrease with myopia, being less in the low myope group and completely absent or reversed in the high myope group. The separation of the three groups on the nasal retina was not found to be significant by our numerical method ($p = 0.0598$). A very similar trend is seen in the horizontal meridian of the Z_5^1 ($p = 0.025$), except that the sign is reversed (which is expected), the asymmetry is much more pronounced for all groups, and the curves for low myope and high myope groups have switched relative positions on the nasal retina, the high myopes now having intermediate values between the emmetropes and the low myopes. This trend was found

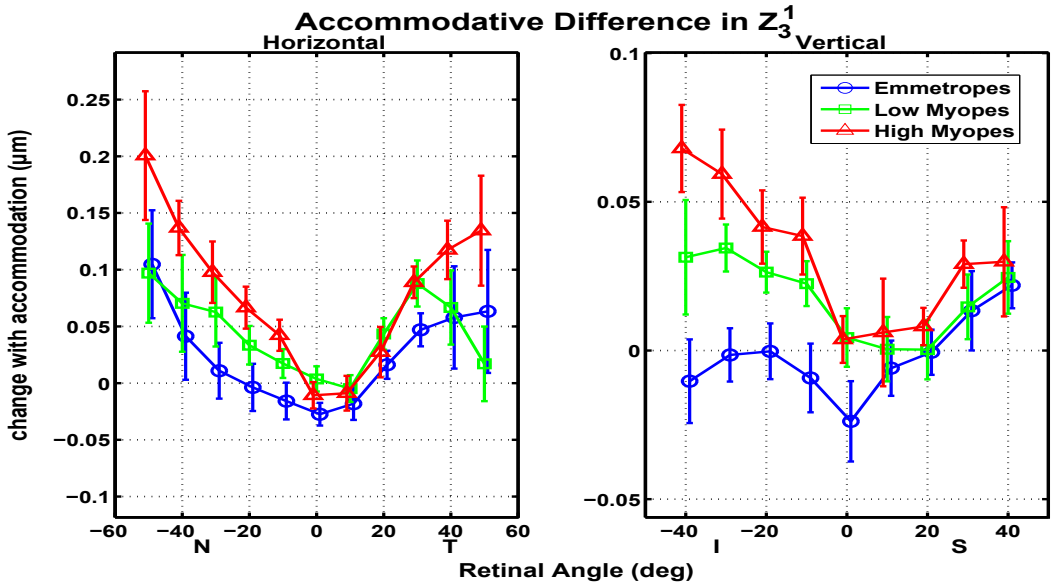

(a) Z_3^1

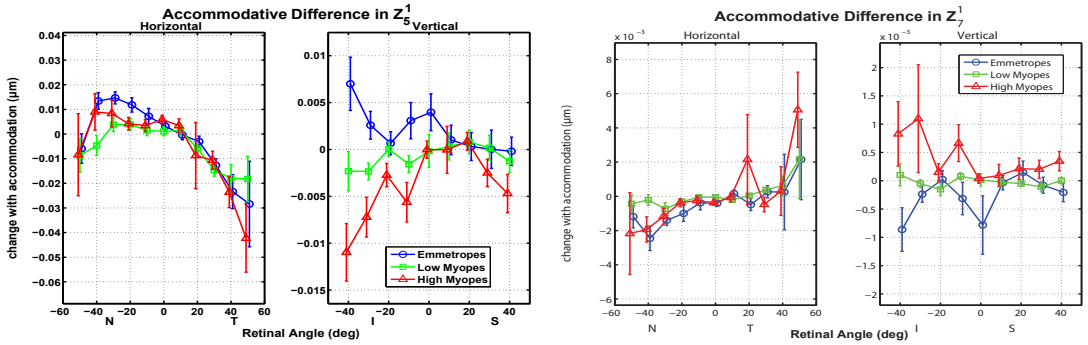

(b) Z_5^1

(c) Z_7^1

Figure 3.19 Changes in 3rd (a), 5th (b), and 7th (c) order horizontal coma terms (Z_3^1, Z_5^1, and Z_7^1) with accommodation. Note that horizontal and vertical plots do not necessarily have the same scale on the y-axis.

to be significant, although much lower in magnitude than when seen in Z_3^1. This trend is likewise seen to continue into the Z_7^1 term ($p = 0.008$).

The vertical meridian also showed interesting findings. The Z_3^1 coefficient is small for all three groups, but is positive for both myopic groups across the visual field. In all groups the coefficient seems to change more with accommodation as eccentricity increases, similar to the horizontal meridian. The plots for the three groups run close together on the superior

retina with no apparent or significant separation. At the fovea, the three groups split and show a significant separation over the inferior retina ($p< 10^{-4}$), as seen in figure 3.19(a). The nature of the separation suggests that over the inferior retina, horizontal coma shows a greater positive accommodative change with increasing myopia. This can also be seen as a superior-inferior asymmetry, manifesting as a lower accommodative change inferiorly in emmetropes which becomes higher for increasing myopia, until for high myopes the asymmetry is reversed. An extremely similar and likewise highly significant separation is viewed in the vertical meridian for Z_5^1 ($p< 10^{-4}$).

Figure 3.20 shows regression lines for the change in Z_3^1 over the five gaze positions marked in the trend. The data points for all subjects for each of the 5 plots are omitted to avoid cluttering the graph. Regressions were performed against SERx and axial length. Table 3.1 shows that regressions were highly significant at all points except 0°.

Mathur et al. noted that Z_3^1 was significantly affected by accommodation in emmetropes[2], though they were unable to compare the effect in different refractive groups. In observing

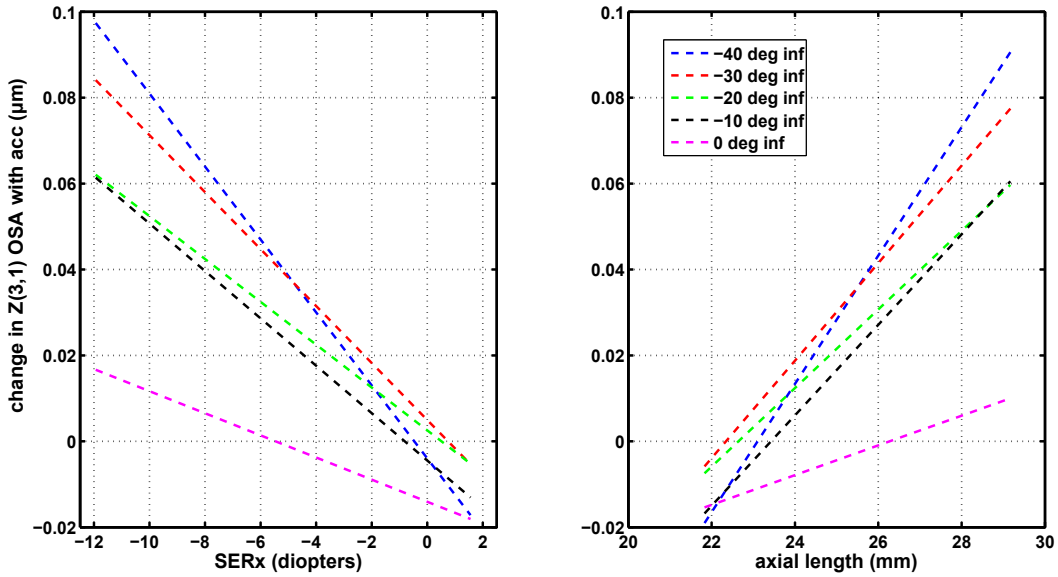

Figure 3.20 Regressions of refractive error (right plot) and axial length (left plot) against change in Z_3^1 with accommodation from 0° to 40° over the inferior retina.

	SERx				axial length			
	m	b	p	r^2	m	b	p	r^2
0° inf	-2.6e^{-3}	-1.4e^{-2}	0.160	0.057	3.3e^{-3}	-8.7e^{-2}	0.433	0.018
10° inf	-5.5e^{-3}	-4.3e^{-3}	0.003	0.233	1.0e^{-2}	-2.4e^{-1}	0.015	0.161
20° inf	-5.0e^{-3}	3.1e^{-3}	0.003	0.237	9.3e^{-3}	-2.1e^{-1}	0.015	0.161
30° inf	-6.7e^{-3}	4.3e^{-3}	0.001	0.290	1.1e^{-2}	-2.5e^{-1}	0.014	0.165
40° inf	-8.5e^{-3}	-3.6e^{-3}	0.005	0.208	1.5e^{-2}	-3.5e^{-1}	0.032	0.128

Table 3.1 Statistical results from linear regressions of the central spherical equivalent refractive error (SERx) and axial length against accommodative change in Z_3^1 from 0° to 40° over the inferior retina. Slope (m) and y-intercept (b) for each line are included.

their plots, no notable superior-inferior asymmetry is seen for the Z_3^1 coefficient, but this could be due to the relatively small field in which they took measurements ($\pm 16°$ vertically). Lundström compared changes in accommodation between emmetropes and myopes[1]. They did not mention any significant differences in Z_3^1 between groups of differing refractive errors on the vertical meridian, nor did they show a plot of such data with which we could compare our results. To the best of our knowledge, at the time of this publication this trend has not been noted before.

The differences observed in accommodative change for horizontal coma in the vertical meridian are likely too small to be perceived when compared to the peripheral changes in 2nd order terms seen in figure 3.18. However, these changes are much larger than the magnitude of the non-accommodative terms themselves. This suggests some optical change is taking place during accommodation which is inducing this change in horizontal coma over the inferior retina, and that this change differs in subjects of different refractive errors. We suggest three explanations as to what might be responsible for this change.

The first explanation is that this variation in accommodative change in Z_3^1 is experi-

mentally induced. Despite our best efforts at control, control of gaze during measurements along the vertical meridian was not separated from convergence. This introduces the possibility that some factor in our setup induced increasing convergence with increasing myopia during downgaze. While this explanation cannot be ruled out, we do not believe it explains this effect. This effect increases with myopia, which suggests that it is an optical effect, related to the subject's refractive error. As explained in section 2.2, subjects in the high myope group wore a contact lens in their right eye during the measurements on the vertical meridian. This means that during these measurements the right eye, which was responsible for accommodating and fixating, essentially had no refractive error. If some factor was inducing increasing convergence or accommodation (and thus accommodative convergence) with increasing myopia during downgaze, we would expect the high myope group to show results that more closely resembled the emmetropic group. Instead, the high myope group appears as an opposing extreme in the inferior retina.

Another possible explanation could be an alteration of retinal contour, since the Hartman-Shack technique of measuring aberrations relies on reflection of the measurement beam off the retinal surface. An alteration in retinal tilt along the vertical meridian could conceivably induce coma, but in this case it would have to be induced only during downgaze, which seems unlikely. It would also have to increase with myopia, which could conceivably be due to ocular growth.

A third possible explanation is that that the observed effect is caused by some change in lenticular or corneal shape, tilt, or decentration that is more pronounced during inferior gaze. While a change in lenticular shape or centration during accommodation could certainly affect levels of coma in the inferior retina, it seems unlikely that such a change would have such a localized effect. A local or asymmetric change to the cornea during accommodation likewise seems improbable, but seems a more reasonable explanation, since a change to the superior cornea could much more easily show a localized effect in the inferior

retina. He et al[29] have shown that the cornea can change shape during accommodation, but they note no such effects as the one mentioned above. However, their study had very few subjects and was limited primarily to emmetropes and low myopes ($n = 12$, SERx$\leq$ 3.00 D, mean$=$ 0.85 D), so an altered superior corneal profile cannot be ruled out.

Figure 3.21 shows the changes in spherical aberration (Z_4^0) with accommodation. Mathur et al.[68] found that non-accommodative spherical aberration was significantly more positive in emmetropes than in myopes. Our findings agree with this (3.21(a)), and further suggest that Z_4^0 shows less of a negative change with accommodation in emmetropes than in myopes in the near nasal and central vertical retinas. This trend is visible in both the vertical and horizontal meridians, though more pronounced in the vertical. Our numerical simulation did not find it significant in either meridian ($p = 0.38$ horizontal, $p = 0.14$ vertical). Figure 3.21(b) shows the changes in Z_6^0 with accommodation. A similar trend is visible on the vertical meridian, which was found to be significant ($p = 0.001$). The emmetrope and low myope curves appear separated across the inferior retina, whereas the high myope curve falls between the two. A separation of the high myope curve from the other two curves is visible on the nasal retina, but was not found significant by our method ($p = 0.106$).

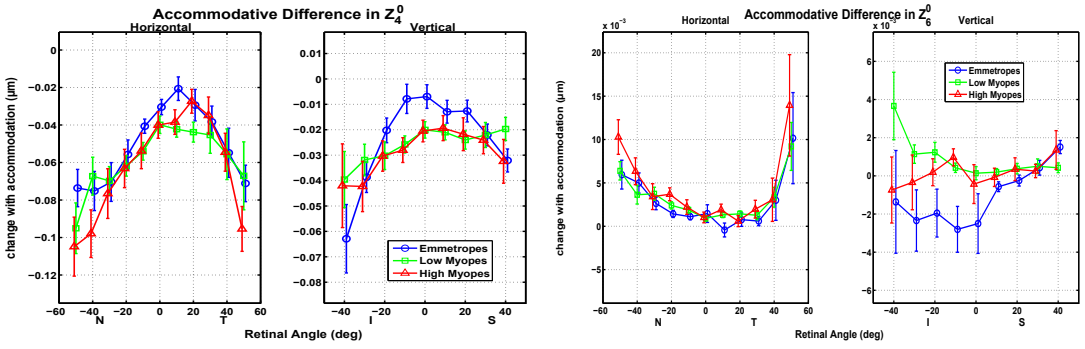

(a) Z_4^0 (b) Z_6^0

Figure 3.21 Changes in 4th (a) and 6th order (b) spherical aberration with accommodation (Z_4^0 and Z_6^0). Note that horizontal and vertical plots do not necessarily have the same scale on the y-axis.

3.2.4 Change in RMS wavefront error in Zernike orders with accommodation

The change in RMS of all Zernike coefficients 2nd order and above is presented as absolute and foveally normalized values in figures 3.22(a) and 3.22(b). The change in RMS of all coefficients 3rd order and above are similarly presented in figures 3.23(a) and 3.23(b). Ob-

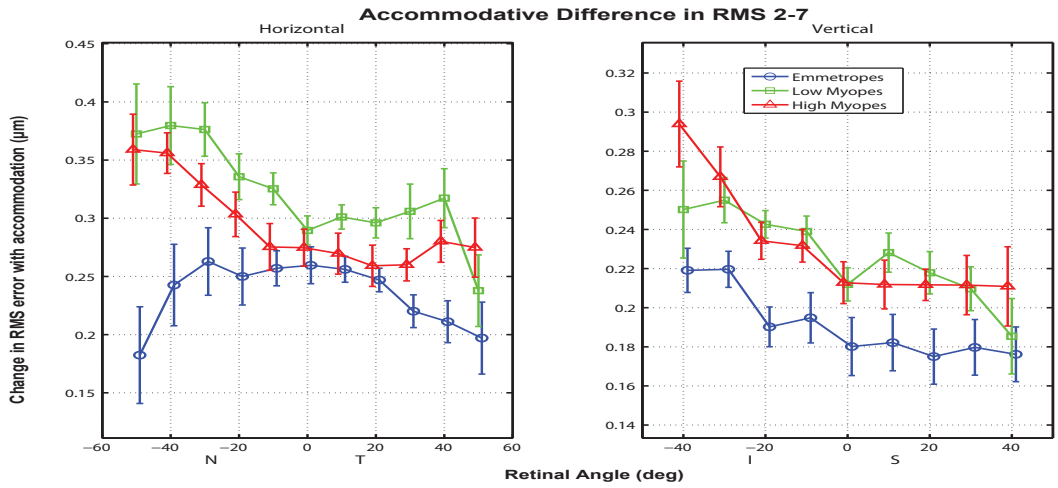

(a)

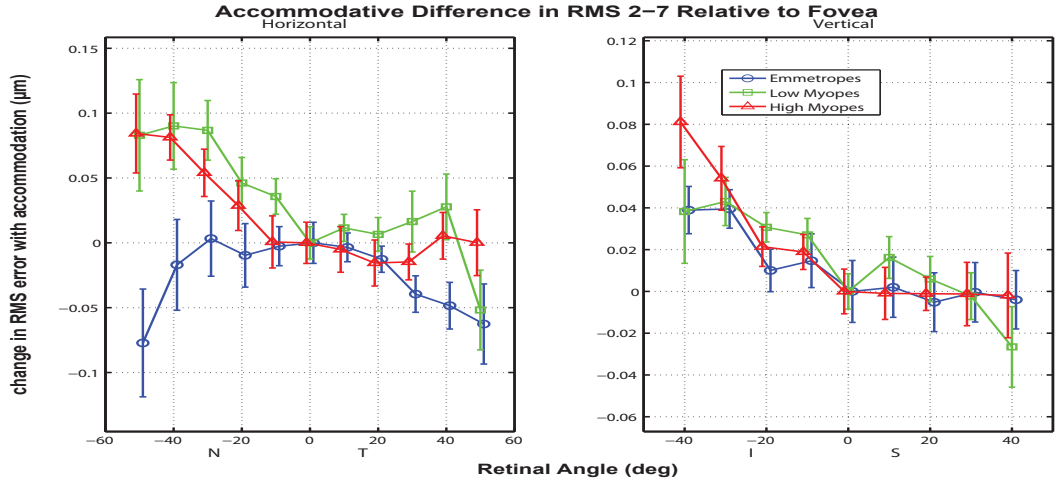

(b)

Figure 3.22 Accommodative changes in RMS for all coefficients 2nd order and above, plotted as absolute values (a) and relative to foveal values (b)..

servation of figure 3.22(b) shows interestingly that emmetropes show less of an increase in aberrations with accommodation in the periphery compared to both myopic groups. On the horizontal meridian, the low myopes appear to have an even higher increase than the high myopes, a finding which is highlighted more in the foveally normalized figure 3.22(b). Asymmetry is present in both meridians: the nasal and inferior retinas show more rapid and larger changes in aberrations than their respective counterparts. This is also well appreci-

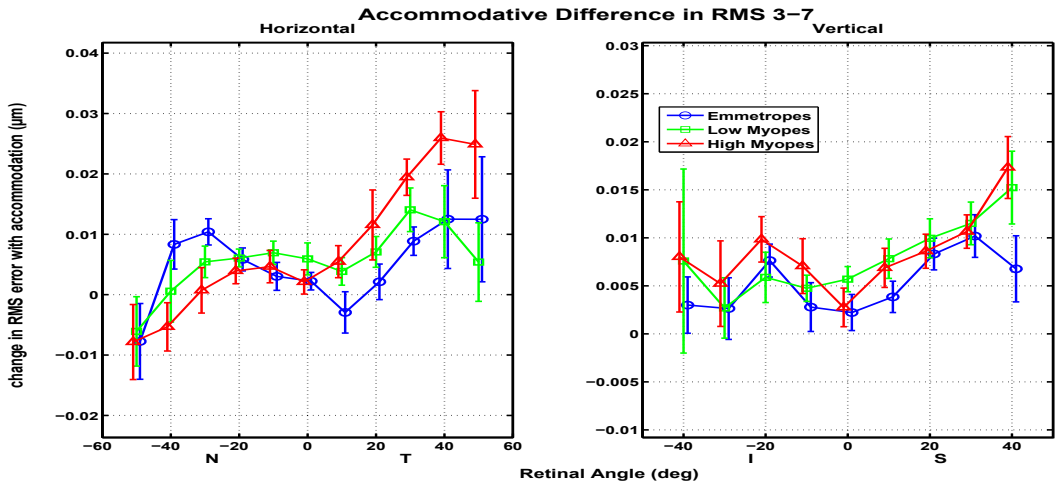

(a)

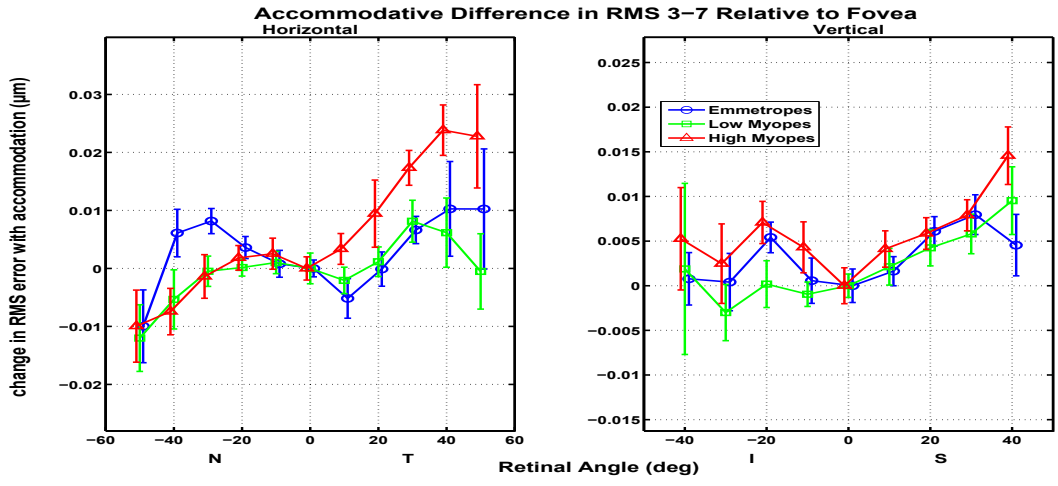

(b)

Figure 3.23 Accommodative changes in RMS for all coefficients 3rd order and above plotted as absolute values (a) and relative to foveal values (b).

ated in the foveally normalized plots.

Removal of the 2nd order terms, seen in figures 3.23(a) and (b), again causes a dramatic decrease in magnitude, but also causes the asymmetries in both meridians to reverse. This suggests that changes in higher order aberrations actually serve to counteract the asymmetric effect of second order aberrations on the RMS wavefront profile. The three curves in figure 3.23(a) are statistically inseparable over the vertical meridian, but show a separation in the temporal retina ($p = 0.052$), with the high myopes having a larger change in higher order RMS than the low myope or emmetropic groups. Foveal normalization accentuates this separation and increases its significance (figure 3.23(b), $p = 0.002$).

This finding of a larger increase in higher order RMS in the temporal retina of high myopes is difficult to explain other than to assume it is due to some inherent difference in the optical elements of the subjects' eyes, but the magnitude of the difference is small. Some asymmetry is visible in the Z_4^0 term, which may be more pronounced in the high myopes, and as such it is possible that this asymmetry is related to the accommodative lag noted among high myopes in the temporal retina (see discussion regarding figure 3.6). Observation of figure 3.22(a) shows that the 2nd order terms change asymmetrically with accommodation, which is also likely to account for the effects seen in the power vector analysis. Equation 2.1 shows that despite being of a much lower magnitude, the higher order terms receive a larger weight in the calculation of the power vector term, and as such the effect of these terms cannot be overlooked. However figure 3.22(a) does not show a marked separation between the low and high myope groups, as noted in the power vector plot, and as such it is hard to conclude definitively on the source of the accommodative lag in the temporal retina.

Chapter 4

Results and Discussion: Retinal Contour

We will first examine the differences in retinal contour between the subjects and between the refractive groups (section 4.1). Following this we will discuss the Dunne algorithm (section 4.2) and examine the effect on calculated retinal contour of accommodation (4.2.2) and pupil diameter (4.2.3). We will then compare retinal contour derived from the IOL Master with the Dunne algorithm (4.2.1). Finally, we will discuss the effect that inaccuracies in anterior segment measurements can produce on calculated retinal contour in the Dunne algorithm (4.2.4).

In our analysis, it was necessary to chose some convention with which to compare the various scenarios in which retinal contour was calculated. Unfortunately, no gold standard as yet exists for the measurement of peripheral retinal contour, and as such used our discretion to choose one of our scans as a baseline against which to compare the others. Since the Dunne algorithm has been tested for accuracy in simulated conditions and found to produce faithful representations of retinal contour (± 0.3 mm) out to 50°, we chose the retinal contour calculated through the Dunne algorithm from the tropicamide data set. We felt that since this set was least likely to possess errors due to accommodative and pupil size fluctuations, it was the most likely to approximate the true retinal contour.

4.1 Analysis of Retinal Contours

We first performed a rough comparison of retinal contours in each group. This was done by simply taking the mean of the x and z coordinates at each gaze position for all subjects in a group. The contours were calculated from the tropicamide data set. The results are shown in figures 4.1 and 4.2.

In reported literature, retinal contour is often examined in terms of retinal or gaze angle, rather than true cartesian coordinates, and as such we report both here. The most notable difference between the two plots is that when the z-coordinate is plotted by gaze angle, it artificially constrains measurements at a given gaze angle to have the same lateral separation (x-coordinate) for all subjects. This notably exaggerates the relative prolateness of the retinal contour with increasing axial length, particularly in the high myope group, since a longer eye will naturally present more lateral separation from the fovea at any given angle than a smaller eye. This is important to note because the only methods of retinal contour measurement that overcome this error are either those that bypass the optics of the eye completely (such as MRI and other radiographic techniques) or those which, like the

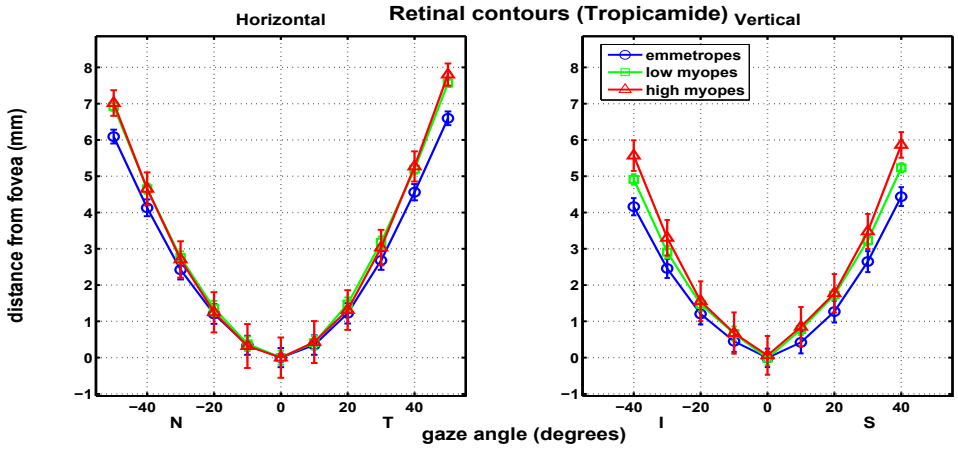

Figure 4.1 Grouped retinal contours plotted by gaze angle. Y-axis shows distance from x-y plane tangent to the fovea. Contours shown are calculated from the tropicamide data set.

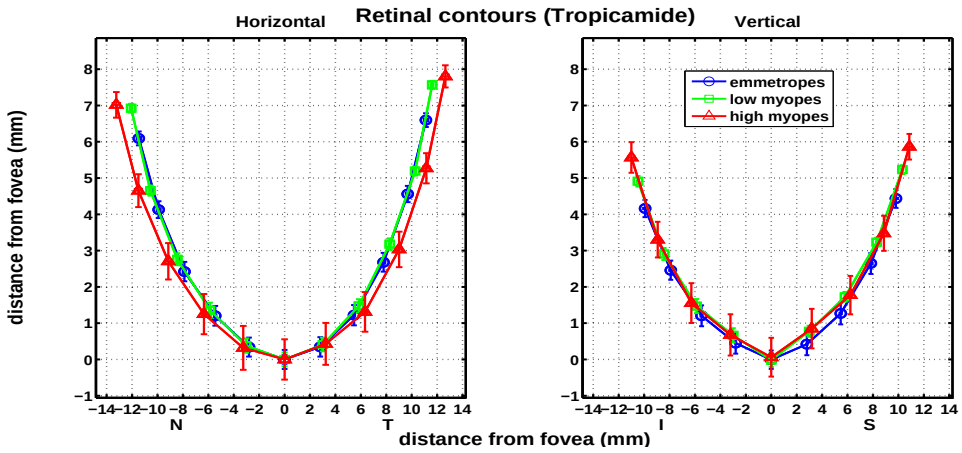

Figure 4.2 Grouped retinal contours plotted in cartesian coordinates as calculated with the Dunne algorithm. Y-axis shows distance from x-y plane tangent to the fovea.

Dunne algorithm, derive retinal contour optically but compensate for the complexities of the optical elements of the eye. Accounting for the complex properties of the optics of the eye allows us to obtain an accurate assessment of the angle of the final ray emerging from the posterior surface of the lens as well as the point on the posterior lens from which it emerges. This information is not available in simplified models and is required for an accurate retinal contour.

It is difficult to assess differences of shape and curvature of the contours in figure 4.2 through visible inspection alone. Because of this, we performed curve fits on all four semi-meridians (nasal, temporal, superior, inferior) in each subject following rough comparison of the retinal contours between the three groups. The results are plotted in figures 4.3 and 4.4, and regression statistics in each semi-meridian are shown in tables 4.1 and 4.2.

Figure 4.3 shows variation in retinal asphericity in terms of the Q coefficient (equations 2.3 and 2.4) in each semi-meridian, plotted as a function of either Spherical Equivalent refractive error (SERx) or subject axial length. As discussed in section 2.4, a negative value of Q corresponds to a prolate curvature while a positive value indicates an oblate curve. Examination of the horizontal meridian reveals that Q becomes more negative in

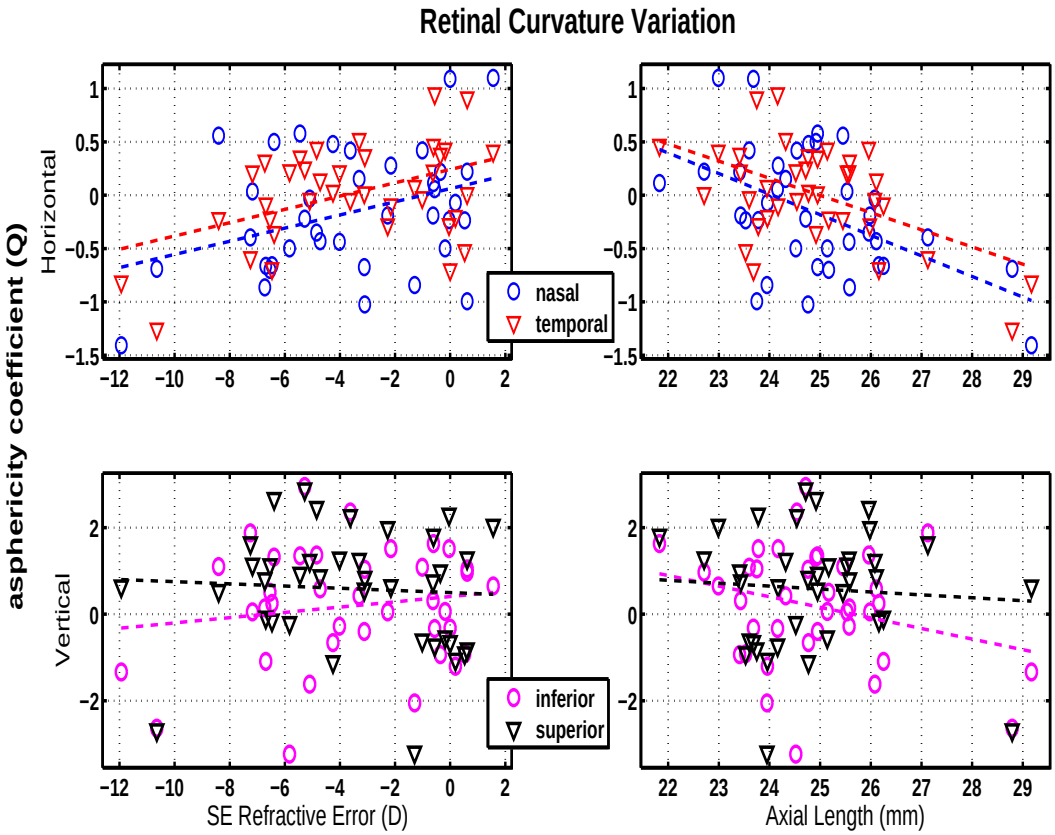

Figure 4.3 Change in the retinal asphericity coefficient (Q) with refractive error and axial length. The variation in Q is plotted as a function of spherical equivalent refractive error and axial length in the horizontal and vertical semi-meridians. Regression details are given in table 4.1

	Spherical Equivalent				Axial Length			
	slope	y_0	r^2	p	slope	y_0	r^2	p
nasal	0.061	0.061	0.128	0.027	-0.193	4.641	0.249	0.001
temporal	0.062	0.241	0.206	0.004	-0.161	4.024	0.272	< 0.001
superior	-0.025	0.499	0.003	0.716	-0.067	2.264	0.005	0.666
inferior	0.061	0.408	0.023	0.365	-0.245	6.277	0.073	0.101

Table 4.1 Regression coefficients and statistical results from linear regressions of the retinal asphericity coefficient (Q) vs spherical equivalent refractive error (column 1) and axial length (column 2) in the four retinal semi-meridians.

both semi-meridians with increasing myopia or axial length. As shown in the table, this trend was significant when analyzed vs SERx, but was much more significant when analyzed vs axial length. Moreover, regression also shows a relative negative offset of the nasal retinal curvature relative to the temporal, suggesting that the nasal retina is slightly more prolate. This was observed in both the SERx and axial length regressions. The slopes of the regression lines were very similar in both the temporal and nasal retina, suggesting that curvature varies similarly with myopia in both semi-meridians.

Examination of the vertical meridian revealed no significant correlation between retinal curvature (Q) and either SERx or axial length in the vertical semi-meridians. The inferior retina did show a slight decreasing trend in Q with increasing myopia that was more pronounced when analyzed vs axial length, it was not significant ($p = 0.101$). This supports our previous observation noted in section 3.1.1 that the low myopes have considerably less relative hyperopia in the vertical meridian than in the horizontal (see figure 3.2).

Central retinal radius of curvature as derived from retinal curve fits is shown in figure 4.4. Analysis of the horizontal meridian shows an increasing central radius of curvature with increasing myopia. This trend was highly significant in both the temporal and nasal retinas when examined vs either SERx or axial length ($p < 0.001$ in all four cases). The vertical meridian in this case yielded only one significant trend: radius of curvature was found to increase significantly with axial length in the inferior retina ($p = 0.048$).

The central radius of curvature is seen to vary much more than expected in both the horizontal and vertical meridians. Curve fits assigned radius of curvature values as high as 25 mm in some cases. Intuitively we might expect the central radius to be about half the axial length, however when dealing with aspheric surfaces this is not always the case. The radius becomes influenced directly by the asphericity and by the coefficients found in the 2nd order polynomial curve fit. This is explained more fully in appendix D.

Our findings in the horizontal meridian are consistent with previous findings that retinal

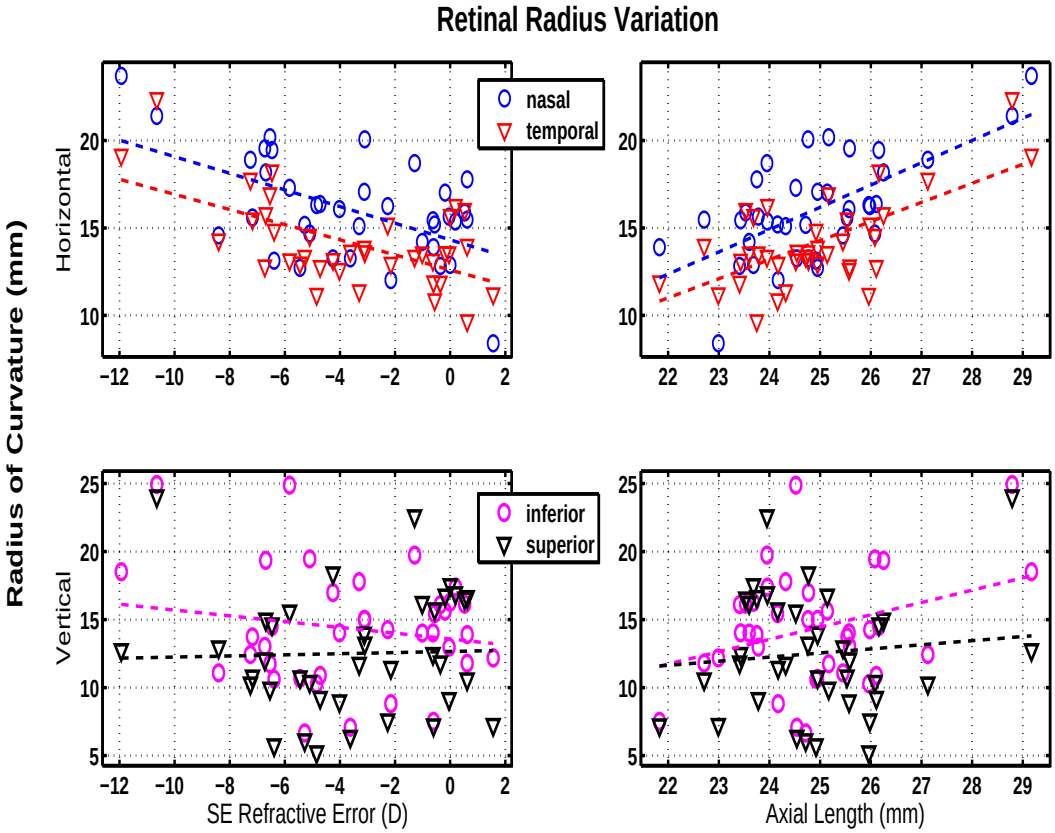

Figure 4.4 Change in the retinal radius of curvature (R) with refractive error and axial length. The variation in R is plotted as a function of spherical equivalent refractive error and axial length in the horizontal and vertical semi-meridians. Regression details are given in table 4.2

	Spherical Equivalent				Axial Length			
	slope	y_0	r^2	p	slope	y_0	r^2	p
nasal	-0.475	14.321	0.295	< 0.001	1.274	-15.661	0.420	< 0.001
temporal	-0.4321	12.596	0.340	< 0.001	1.092	-13.009	0.430	< 0.001
superior	0.041	12.655	< 0.001	0.854	0.302	4.993	0.010	0.546
inferior	-0.213	13.574	0.029	0.306	0.906	-8.203	0.105	0.048

Table 4.2 Regression coefficients and statistical results from linear regressions of the retinal radius of curvature (R) vs spherical equivalent refractive error (column 1) and axial length (column 2) in the four retinal semi-meridians.

contour becomes more prolate with increasing myopia[6,7,15,16]. They also support the model of axial expansion of the retina during myopic growth. Our findings on the vertical meridian are consistent with the data obtained by Atchison et al.[16], in which they found that the vertical meridian showed less of a prolate change with myopia development. However, to the best of our knowledge it has not been noted that curvature or central radius behave differently in the inferior retina than they do in the superior retina, as our data suggest (although the variation in curvature is only a non-significant trend, as previously noted).

The change in retinal radius of curvature with axial length over the inferior retina is also interesting in consideration of the curious behavior of horizontal coma in that region of the retina during accommodation. However, our contours and the asphericity and radii of curvatures fit to them don't provide sufficient detail to fully account for the effect noted in figure 3.19(a). A change in coma could presumably be induced by a slight tilt of the inferior retina along the vertical meridian induced by accommodation, but as our contours only measure retinal position along the meridian, they do not provide sufficient information to determine if such a tilt is induced. To determine this, more data would need to be taken off the vertical meridian. However, our data do show that such an effect isn't outside of consideration, since note here that the shape of the inferior retina shows a much stronger correlation refractive error than the superior retina. The asymmetry as well as the correlation with refractive error would both be required to explain the effect seen in figure 3.19(a).

4.2 Comparison of Retinal Contour Measurement Methods

In the following discussion, a note regarding our sign convention is in order. In our analysis of the effects of ocular parameter variation on calculated retinal contour, we used the retinal

contour from the tropicamide data set as our baseline, as stated above. For each subject, the deviation was measured as the norm of the vector originating at the contour point in the tropicamide data set and terminating on the corresponding point in the data set to be compared. We determined sign by subtracting the distance from the tropicamide point to the cornea from the corresponding distance of the test point from the cornea. Thus if the test point fell farther from the cornea (i.e. the test contour was "behind" the tropicamide contour) it was given a positive sign. If the test contour was closer to the cornea, it was given a negative sign.

4.2.1 Comparison of Dunne and IOL Master Measurement

We compared contours derived from the tropicamide data with contours measured using the IOL Master. The actual contours calculated from the tropicamide data and the IOL Master data are shown in figure 4.5. Note that although the discrepancies for the IOL Master contour were larger than for any other contour calculated, the general shape of the contour suffered no dramatic distortion. This method of retinal contour should therefore not be ruled out, but its use will depend on the precision and accuracy requirements of the specific application to which it is applied.

Note, however, that it is important that the model eye used to calculate the retinal contour be a 3-surface model eye. When this technique was originally presented by Mallen[4], they calculated retinal contour using a 1-surface model eye, pinpointing the retinal location by tracing along a nodal ray at the measured angle. Comparison of the two techniques is shown in figure 4.6. It is immediately apparent that simplification of the eye by using a 1-surface eye results in an exaggeratedly wide retinal contour. This is because tracing the nodal ray through a 1-surface model eye does not take into consideration the separation of the nodal points present in a real eye and instead substitutes a single nodal point. Thus use of a 1-surface model eye doesn't model deviation of the ray due to refraction at the optical

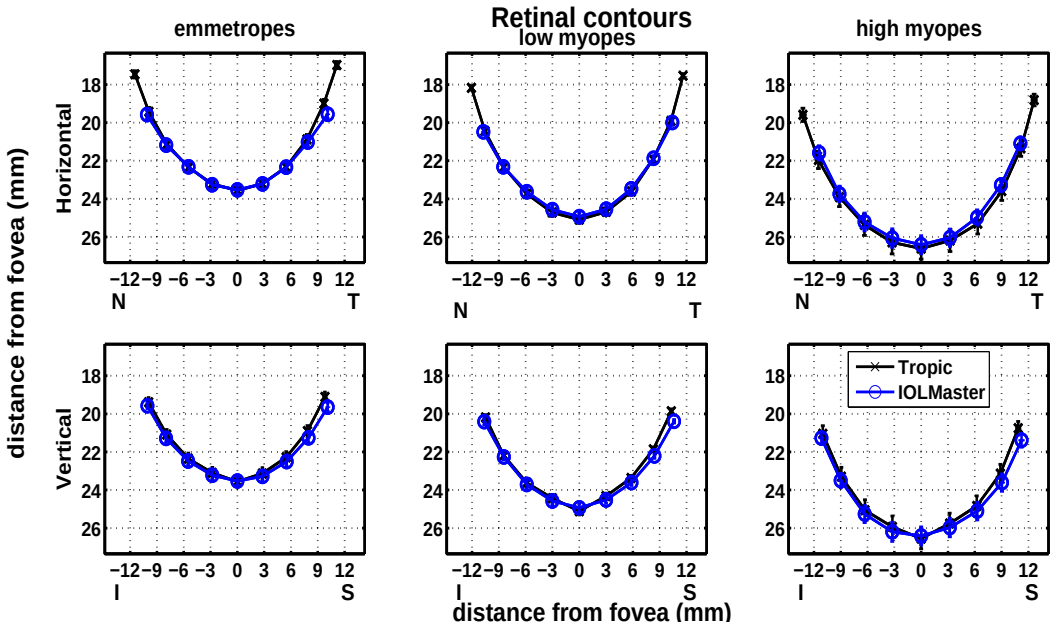

Figure 4.5 Comparison of retinal contours for each group calculated using either tropicamide data sets or IOL Master data. The curves are very similar and discrepancies are more easily noted when plotted as differences, as in figure 4.7.

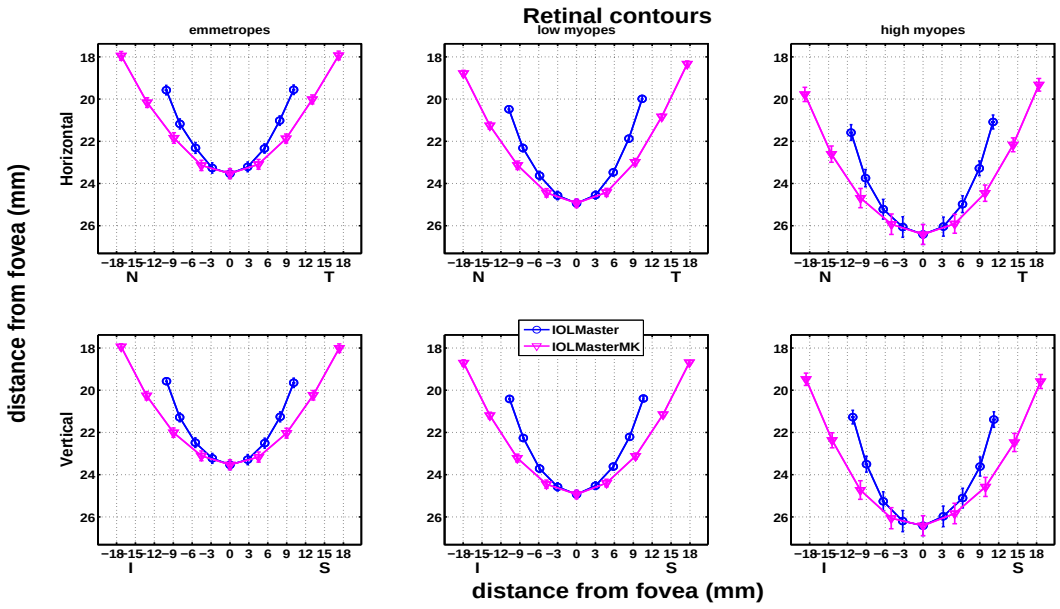

Figure 4.6 Comparison of retinal contours for each group calculated using either our method (3-surface model eye) vs using the method originally presented by Mallen[4] which only incorporates a 1-surface model eye.

surfaces of the eye, which serves to diminish the lateral separation of peripheral contour points..

Pooled and grouped deviations of the IOL Master contour are shown in figures 4.7 and 4.8. It is interesting that the IOL Master contour shows negative discrepancies on the horizontal meridian corresponding to an anterior shift of the retina relative to the tropicamide data, whereas it shows the opposite trend on the vertical meridian. In most locations the contour discrepancy is within ± 0.3 mm, however in some locations the magnitude of the discrepancies for the IOL Master reached above 0.6 mm (far superior and temporal retinas), which was the largest discrepancy of any contour we observed. The range over which those discrepancies spanned likewise was larger than for any contour calculated with the Dunne algorithm.

That there is a pronounced difference between the behavior in the two meridians is very interesting, though not easy to explain. Since these contours were obtained with tropicamide administered similarly to the baseline data, we can reasonably expect that any effect of accommodation on the IOL Master contour should be minimal. The most likely source

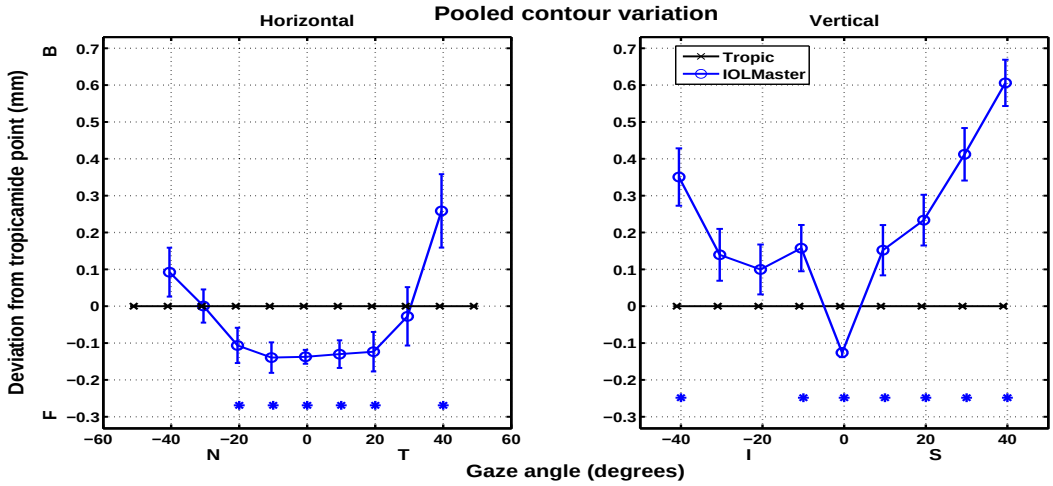

Figure 4.7 Pooled discrepancies in retinal contour are plotted for each refractive group between the Dunne tropicamide data and IOL Master data using a 3-surface eye ray trace.

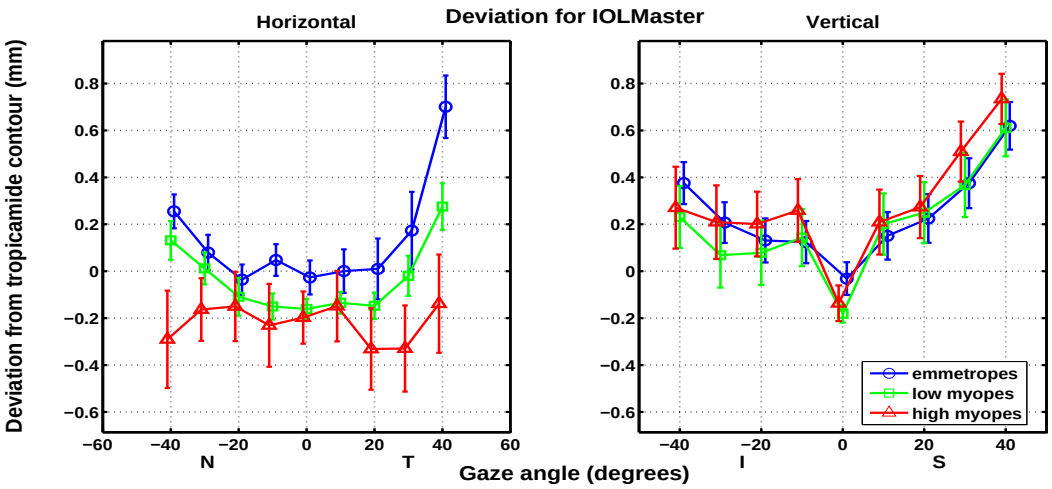

Figure 4.8 Discrepancies in retinal contour are plotted for each refractive group between the Dunne tropicamide data and IOL Master data.

of error would be the process by which contours were derived.

Note that the foveal points between the IOL Master and Dunne contours don't necessarily align – this is because the Dunne algorithm only uses the IOL Master central axial length reading for construction of the initial model eye. The algorithm later adjusts retinal contour based on measured spherocylinder refractions - even at the fovea. That the foveal offset appears fairly constant over the horizontal meridian might suggest that the Dunne contour which we are using as our baseline is actually the one which has been offset. However, the pronounced and rapid changes in contour in the near periphery of the vertical meridian suggest that the IOL Master is probably not ideally suited for accurate measurements of peripheral retinal dimensions unless better adjustments can be made.

We also note in figure 4.8 that the IOL Master contour behaves slightly differently for different refractive groups, particularly on the horizontal meridian. The emmetropes show little shift in contour centrally and a posterior shift in contour in the far horizontal periphery, whereas the myopes show a slight anterior shift in contour relative to the tropicamide Dunne contour. No such separations were visible in the vertical meridian.

4.2.2 The Effect of Accommodation on Retinal Contour Calculation

To analyze the effect of accommodation on retinal contour calculation, we first eliminated the effect of pupil size by correcting Zernike aberrations across all subjects to the minimum pupil diameter (2.28 mm on the horizontal meridian and 2.34 mm on the vertical). Subjects were still excluded based on the accommodative criteria listed in section 2.3.1. Following this, the deviation of the contour from the tropicamide scan was assessed at each gaze position. Data was first observed with subjects pooled together, then divided into refractive groups and observed separately. Results are shown in figures 4.9 and 4.10.

In the plots above, all contours show the smallest discrepancy at the origin (fovea) because each subject's axial length was an inherent parameter used in the construction of the model eye. The algorithm altered the retinal contour based on the refractive error relative to the fovea, and thus very little movement in the foveal retina was necessary for the algorithm to match the model eye with the measured refraction. Despite the curves all having a minimum at the fovea, the pooled deviation plot (figure 4.9) shows an immediate poste-

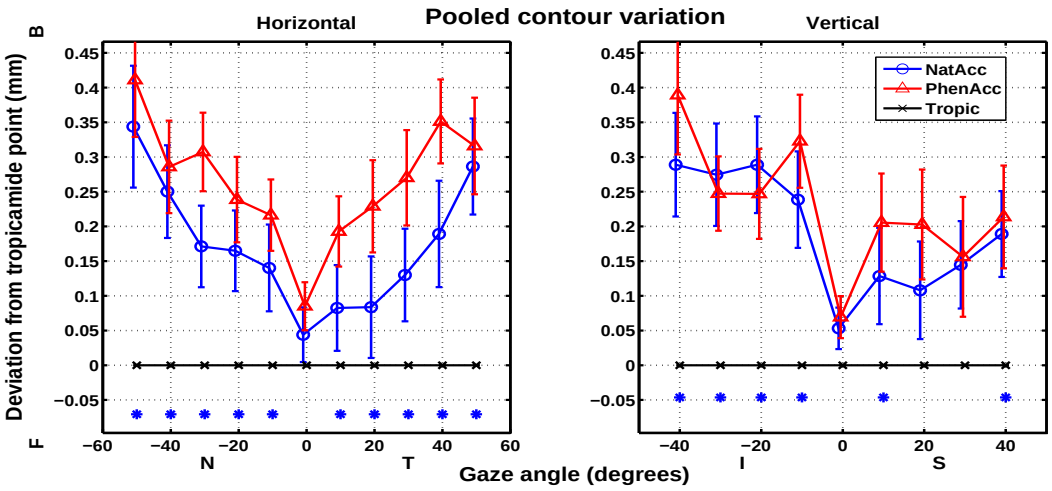

Figure 4.9 Pooled discrepancies between accommodative retinal contours and tropicamide contour pooled at each gaze angle. Negative values correspond to a shift in front (F) of or anterior to the baseline tropicamide scan, whereas positive values correspond to a shift behind (B) or posterior to the baseline tropicamide scan.

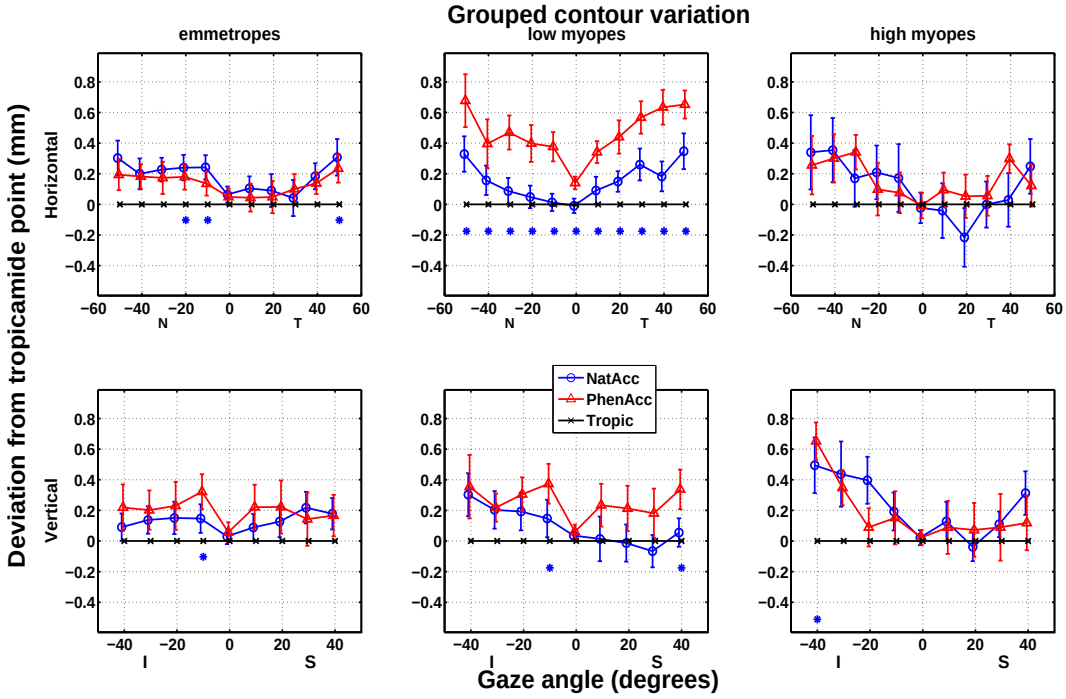

Figure 4.10 Grouped discrepancies between accommodative retinal contours and tropicamide contour pooled at each gaze angle.

rior shift in the retinal contour extending across the entire contour in both the natural and phenylephrine accommodative data. At its largest, this discrepancy reaches the order of 0.4-0.5 mm, which is only slightly larger than the largest error reported by Dunne in the performance of the algorithm itself. In the horizontal meridian it appears that the phenylephrine data produced a retinal contour that was farther behind the tropicamide contour than that produced by the natural accommodative data. Examination of this in the grouped data (figure 4.10) shows a large separation between the two contours for the low myope group only, whereas the two contours for the other groups much less distinguishable. The natural and phenylephrine contours similarly appear much less distinguishable in the vertical meridian, though once again it appears there may be a slight separation for the low myope group (less than in the horizontal meridian).

The difference between the natural and phenylephrine accommodative contours im-

mediately suggests a possible difference in accommodative level between the scans. We therefore took the difference in central SERx between the phenylephrine and natural accommodative scans to assess if such a difference were present. Respective 95% confidence intervals of the difference for the emmetropes, low myopes, and high myopes were: -0.31$\pm$0.22, -0.02$\pm$0.39, and 0.09$\pm$0.34 on the horizontal meridian, and -0.06$\pm$0.40, 0.26$\pm$0.57, and -0.41$\pm$0.56 on the vertical meridian. The only plot shown in figure 4.9 which has a significantly different accommodative level between the two data sets is the emmetropic group on the horizontal meridian, in which they seem to have accommodated slightly less with phenylephrine than with natural pupils ($p = 0.016$). The low myope group shows no difference between accommodative levels on the horizontal meridian ($p = 0.93$).

It is also possible that instillation of the drops themselves might affect the aberration profile in the eye. Carkeet et al. found that instillation of 2.5% phenylephrine produces a smaller change in the central root mean square of aberrations (3rd order and higher) than does instillation of 1.0% cyclopentolate[67]. They did not directly compare aberrations with phenylephrine vs without, nor did they look at peripheral aberrations, but it is conceivable that there could be some direct effect of the drops on the contour. However, this explanation fails to explain why the effect is localized only to the low myopes and only in the horizontal meridian.

The pronounced posterior shift in the accommodative retinal contours for all subjects can be most easily explained due to a relative peripheral myopic shift noted with accommodation, such as that seen in figure 3.6. The Dunne algorithm adjusts corneal asphericity at each gaze position to match the dioptric difference between the measured sagittal and tangential foci. It then adjusts retinal position to match the absolute positions of both foci. A relative peripheral myopia would therefore produce a retinal contour that was shifted back. However, this cannot account for the entire effect, since examination of the peripheral refractive profile shift in figure 3.6 shows temporal-nasal asymmetries which are not present

in the retinal contours, particularly in the high myope group (Since these retinal contours were calculated using spherocylinder refractions computed using 2nd and 4th order Zernike terms, it is more informative to compare them to the power vector terms discussed in sections 3.1.1 and 3.1.2 than to the Zernike terms directly). Moreover, all groups show very little of a relative peripheral myopic shift over the superior retina, and yet these differences are not readily appreciable in the retinal contours.

It is also possible that the subjects' axial length changed slightly in the accommodative state. Mallen et al have noted a slight axial elongation with accommodation on the order of 0.04 mm in emmetropes and 0.06 mm in myopes[26]. Despite that the model eye used in the algorithm was originally specified with a non-accommodative axial length, examination of the plots above shows that in many instances the algorithm shifted the foveal retina back by an amount similar to this. While this may or may not be a small physical shift of the retina, we considered it worthy of investigation. However, our simulations suggest that elimination of this discrepancy by constructing the model eye with an accommodative axial length would not correct the posterior shift we see in figures 4.9 and 4.10, but rather would exacerbate the effect. The details of this simulation are discussed in section 4.2.4.

4.2.3 The Effect of Pupil Size on Retinal Contour Calculation

For examination of pupil size, the pupil and accommodative criteria listed in section 2.3.1 were not applied, since the three scans we compared were all non-accommodative and had pupil sizes well above the limit set for accommodative analysis. Zernikes were not corrected for pupil size across subjects prior to calculation of spherocylinder refraction and retinal contour. Since pupil size is taken into consideration in the calculation of power vectors prior to calculation of spherocylinder refractions and retinal contour (see equations 2.1 and 2.2), it is valid to compare power vectors and spherocylinder refractions taken with different pupil diameters. It is true that different pupil diameters will cause different refrac-

tions, but it is this very effect that we wished to observe. Indeed, we wished to assess the robustness of the Dunne algorithm in calculating retinal contour in the presence of varying peripheral refractions caused by fluctuating pupil diameter. Correction of pupil size across the data would have eliminated the effect which we wished to observe. Instead, Zernikes were only corrected to match pupil diameter for all measurements taken at a given gaze position for each subject individually. The exception to this was one additional data set we made for comparison, which was the tropicamide scan corrected to a 3 mm pupil. This produced three data sets which were compared with our normal tropicamide baseline: natural non-accommodative, phenylephrine non-accommodative, and tropicamide analyzed at 3 mm. The natural and phenylephrine serve as data in which random pupil diameter changes are present, while the 3 mm tropicamide plot served to illustrate the effect when a fixed and more rigidly controlled change in pupil diameter was enforced. Pooled and grouped deviations from the baseline tropicamide are shown in figures 4.11 and 4.12, respectively.

Examination of figure 4.11 shows that pupil size seems to have much less of an effect on retinal contour calculation than accommodative state. The largest deviation from the

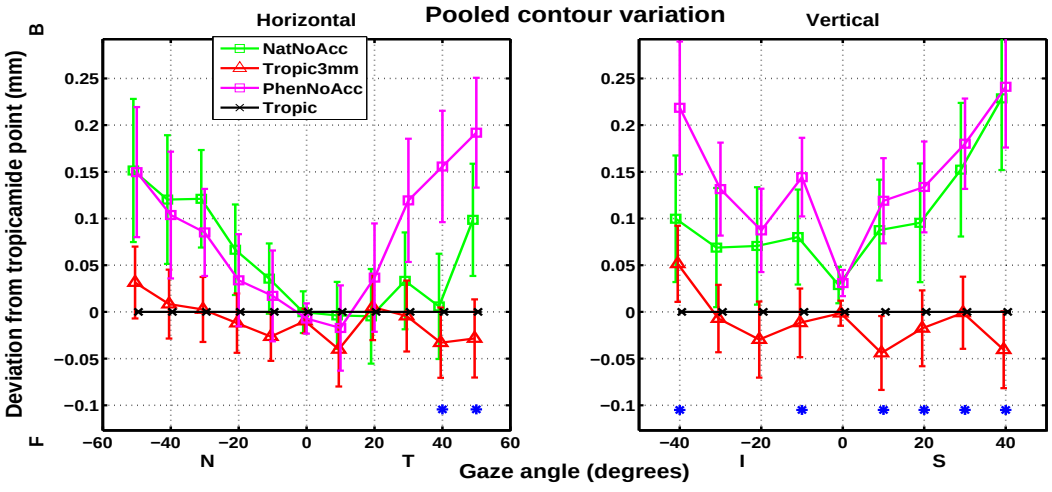

Figure 4.11 Pooled discrepancies for all subjects in retinal contour between the natural non-accommodative pupil, the phenylephrine non-accommodative pupil, the tropicamide data, and the tropicamide data analyzed at a 3mm pupil across all subjects.

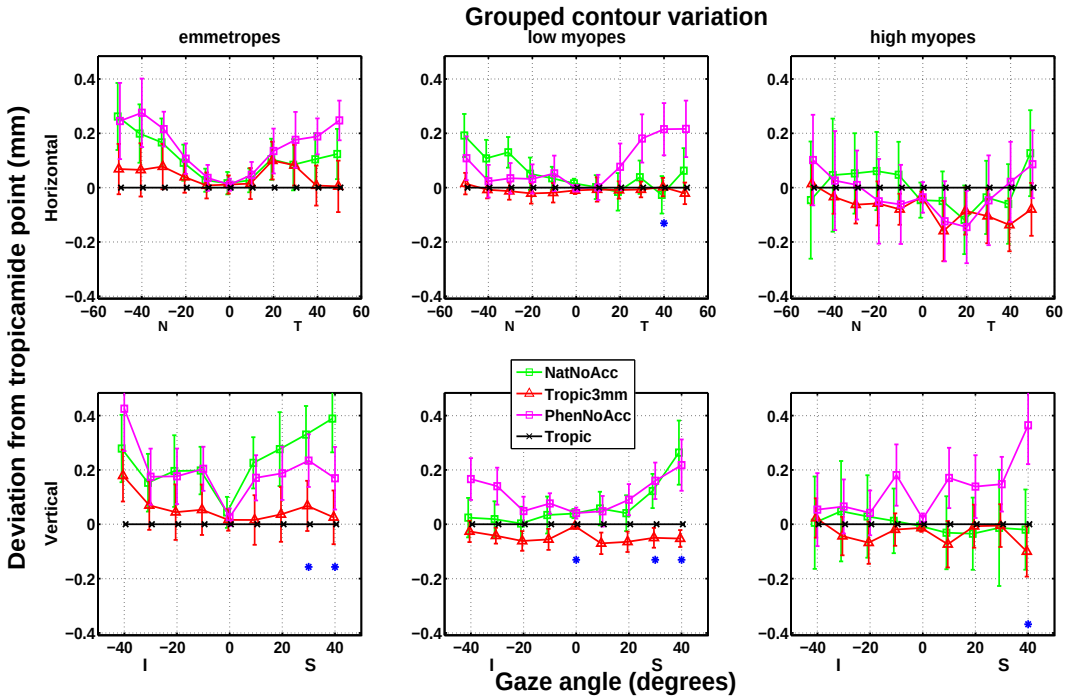

Figure 4.12 Discrepancies in retinal contour are plotted for each refractive group between the non-accommodative data sets of varying pupil diameters.

tropicamide contour is seen in the natural and phenylephrine pupil curves in the far periphery. Even at these points, however, this contour only deviates from the tropicamide contour by about half the magnitude of the accommodative scans. Other than these few points in the far periphery of the natural non-accommodative contour, most of the other contours appear to straddle the tropicamide contour with no immediate pattern. In almost all cases, the deviation is less than the largest error noted by Dunne in his modeling assessment of the algorithm's accuracy. The magnitude of the mean deviations in most cases are small enough compared to their respective spreads that they are non-significant. When examining the grouped data in figure 4.12, the emmetrope and high myope groups seem to show the largest discrepancies in the natural and phenylephrine contours.

Particularly interesting in this case is examination of the tropicamide contour when calculated with the aberrations corrected to a 3mm pupil diameter. Although the same

wavefront is used for both contours, shrinking the pupil is sufficient to alter the retinal contour. To observe this directly, the deviations of this contour are plotted alone for the three groups in figure 4.13. Examination of this suggests a possible separation between the groups on the horizontal meridian. Although the magnitude is small, shrinking the analysis pupil seems to create an anterior shift in retinal contour in high myopes. This discrepancy doesn't appear for low myopes, and becomes a posterior shift for emmetropes. This is also evident in the vertical meridian, though the low and high myope groups show less separation.

To examine this more fully, we looked at the change in the power vector components M and J_{180} between the tropicamide scan analyzed at its full diameter and analyzed at 3 mm. These are shown, respectively, in figures 4.14(a) and 4.14(b). The emmetropic group shows a slightly more hyperopic shift in M than the myopic groups in both meridians. This would not explain the discrepancies in the retinal contour, however, since a hyperopic shift would presumably produce an anterior shift in the retinal contour with the smaller pupil. It might explain why the differences between the groups in contour discrepancies seen in figure

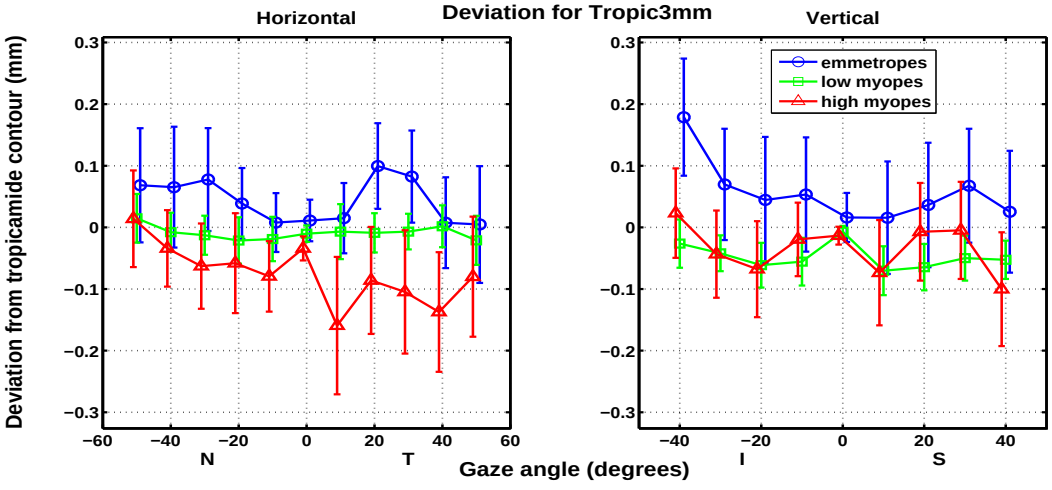

Figure 4.13 Discrepancies in retinal contour are plotted for each refractive group between the normal tropicamide data and the same data analyzed at a 3mm pupil across all subjects.

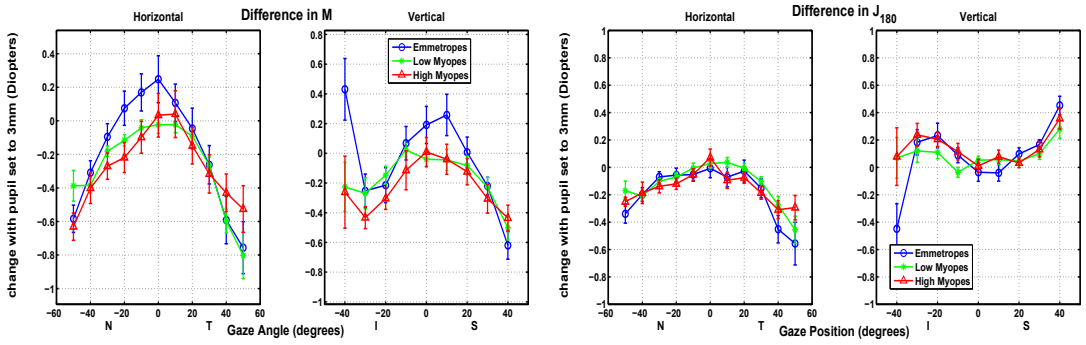

(a) (b)

Figure 4.14 Differences in M (a) and J_{180} (b) between the tropicamide data with normal pupil sizes and tropicamide data with a global 3mm pupil size imposed are plotted for the three groups.

4.13 seem to be minimal in the central regions of both meridians. Surprisingly there was no other notable difference between the groups in either component which could account this effect.

Since we are observing this effect when the analysis pupil diameter is decreased, the simplest explanation is to suggest that it is due to a change in spherical aberration. However, the power vectors contain weighted contributions of 4th order terms, so these terms have already been incorporated into the plots shown. Furthermore, emmetropes have more positive spherical aberration, which would correspond to slightly more myopia with a larger pupil and presumably push the retinal contour with a large pupil posteriorly. Therefore if spherical aberration were responsible for the effect observed in figure 4.13, we would expect the small pupil contour to show an anterior shift rather than a posterior shift (since shrinking the pupil would eliminate the myopic shift caused by the spherical aberration term). However, it is also possible that the algorithm itself compensates for the effect when corneal asphericity is manipulated, and perhaps the effect is due to an overcompensation on the part of the algorithm.

Regardless the source of the effect, figure 4.15 shows the discrepancies in the tropi-

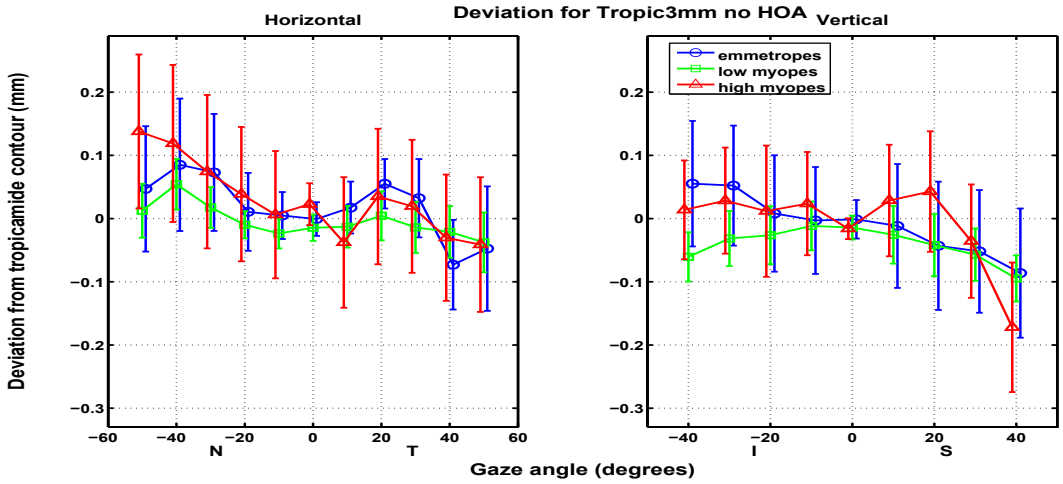

Figure 4.15 Discrepancies in retinal contour are plotted for each refractive group between the normal tropicamide data and the same data analyzed at a 3mm pupil across all subjects.

camide retinal contours calculated at 3mm, but this time with no higher order aberrations included in the calculation of spherocylinder refractions. As can be easily seen, elimination of the 4th order terms completely eliminates the distinct separation between the groups seen in figure 4.13. It does not, however, eliminate the overall discrepancies between the large and small pupil contours, suggesting that the pupil diameter effects the level of 2nd order Zernike terms in the captured wavefront.

4.2.4 The Effect of Anterior Chamber Dimension Variation on Retinal Contour Calculation

When calculating retinal topography using the Dunne algorithm, we used regression data from previous studies[88,89] to declare anterior chamber depth and lens thickness values for subjects in both accommodative and non-accommodative studies. We can naturally assume that the algorithm performs best when the constructed model eye is as faithful of a representation of the original as possible, and as such the use of regression statistics brought to attention the question of how robust the algorithm performed should inaccurate initial

ocular measurements be given as input. Indeed, we originally collected measurements of anterior chamber depth and lens thickness using the Pentacam, but later elected not to use them for modeling due to the distortions these parameters may suffer when obtained by this imaging modality[87]. The values obtained from Pentacam measurements differed from the regression statistics often the by as much as 30% for the anterior chamber depth and 16% for lens thickness (see figure 2.5). We were unable to determine if this was due to distortion from the Pentacam or normal variation in the sample which the regression couldn't predict.

In order to determine how much this could have affected our contours, we calculated contours for the emmetrope group using the original tropicamide data and the original anterior segment parameters as specified. We then intentionally adjusted anterior segment parameters by fixed amounts to see how contours calculated from the original peripheral refractions would be affected by the inaccurate anterior segment parameters. The results of these tests are displayed in figures 4.16, 4.18, and 4.20.

In all of these figures the predominant finding was that alteration of anterior chamber dimensions cause very little effect on calculated retinal contour. In all the simulations we performed, the largest change in calculated retinal contour that was induced was less than 0.1 mm, and in many instances the change was less than 0.02 mm. This was much lower than the spread in our data, and near the inherent error in the algorithm reported by Dunne. It should be noted also that most of the figures display a great deal of symmetry, and often show local minimums. The Dunne algorithm first determines the radii of curvature of the subject's lens using Royston's equations[96] to construct the model eye, using the subject's central refraction, axial length, anterior chamber depth, and lens thickness. Therefore alteration of AC depth and lens thickness will change the radii of curvature of the lens as well, since they still are calculated to match the central refraction. It is our belief that the curves seen in the figures below are produced by a trade-off effect between the altered AC depth and lens thickness and the resulting change in the radii of curvature of the lens. The

precise effects of these changes will be reported separately from this study. It is impressive, nevertheless, that despite so many influencing factors, the algorithm is still able to produce a very consistent retinal contour predominantly by factoring in all these optical changes into a varying local corneal asphericity, calculated at each gaze position.

When we adjusted only the anterior chamber depth in emmetropes, we were impressed by how robust the algorithm performed. As can be seen in figure 4.16, increasing or decreasing the anterior chamber depth by 20% at no time caused the calculated contour to deviate more than 0.1 mm, which was much lower than the deviations seen in the contours calculated from different data sets (compared in sections 4.2.2 and 4.2.3). Indeed, for most positions of gaze in both meridians the deviations were well below 0.04 mm. Generally the deviations showed the same magnitudes on the horizontal and vertical meridians, but there were asymmetries in that the deviations appeared to increase more in the far nasal retina than the far temporal retina. Larger deviations can also be noted in the inferior retina than are present in the superior retina, but the difference is not as pronounced as in the horizontal meridian.

Another interesting finding was that the deviations found showed local minimums. De-

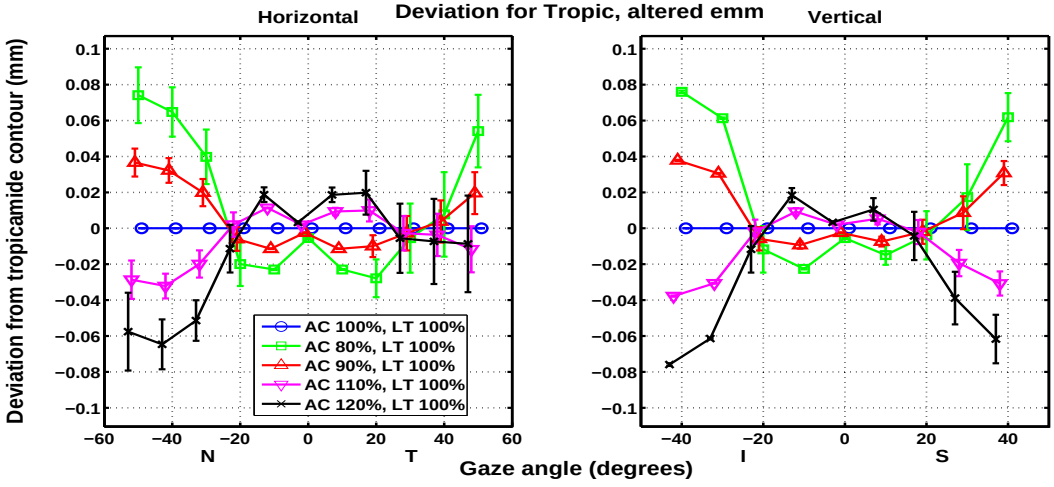

Figure 4.16 Deviation from tropicamide calculated retinal contour of emmetropic group when anterior chamber depth is increased or decreased.

viations reached minimums near 0° and 30° on the horizontal meridian and near 0° and 20° on the vertical meridian. Plotted curves show more or less symmetrical shapes relative to the fovea in each meridian, although this symmetry is more pronounced in the vertical meridian. The curves also increase in amplitude for larger percentage adjustments.

The larger deviation in the nasal retina compared to the temporal retina leads to interesting speculation. This is suggestive of some optical effect which is more pronounced in the nasal retina than in the temporal retina, such that the algorithm is less able to compensate for errors in its input ocular parameters. This could be due to something as simple as lenticular tilt or decentration, or it could be due to something as complex as an asymmetric gradient index distribution within the lens or an asymmetric topography in the temporal cornea.

For completeness, we performed the same alterations on the low and high myope groups. Examination of figures 4.17(a) and (b) show that the magnitude of the deviations in retinal contour caused by anterior chamber depth alterations in these groups is similarly small and comparable to that of the emmetropes in both meridians. Interestingly, however, the asymmetries appear much more pronounced for the myopic subjects. One such differ-

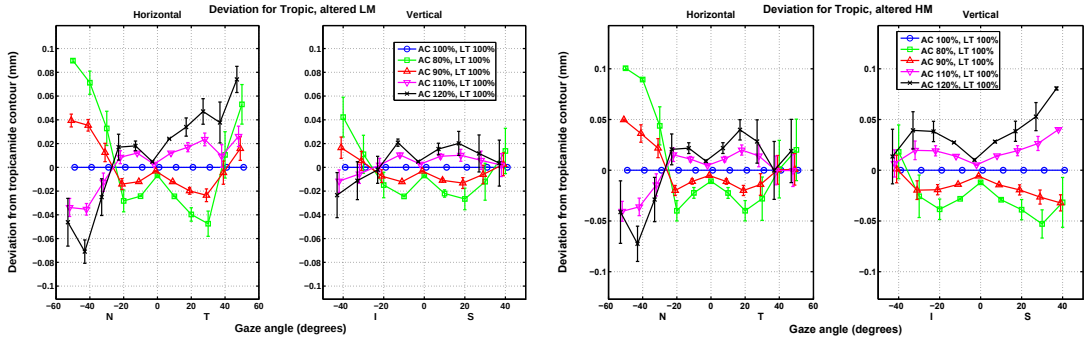

(a) (b)

Figure 4.17 Deviation from tropicamide calculated retinal contour of low myope (a) and high myope (b) groups when anterior chamber depth is increased or decreased.

ence is visible for the low myopes on the temporal retina, where all discrepancies show a posterior shift in the far periphery (may also be notable to a much smaller extent for the emmetrope group in figure 4.16). Another asymmetry is seen in that the high myopes show an increasing separation of the curves on the superior retina, as though the local minimum visible at 20° in emmetropes and 40° in low myopes has completely disappeared.

In general, we found that the algorithm was slightly more sensitive to changes in lens thickness. As figure 4.18 shows, changing lens thickness by as much as 20% caused the calculated retinal contour to deviate by slightly more than 0.1 mm in the far periphery (50° horizontal). Mid-peripheral deviations in both meridians extend as high as 0.075 mm when lens thickness is altered by 20%, which is slightly more than seen when anterior chamber depth was altered. Nevertheless, this is still considerably less deviation than was observed between the contours calculated from different the different accommodative and pupillary states.

Once again, the deviations showed local minimums at 0° and 40° on the horizontal meridian, although the second local minimum appears to have been moved slightly beyond our measurement range on the vertical axis. A slight temporal-nasal asymmetry may be

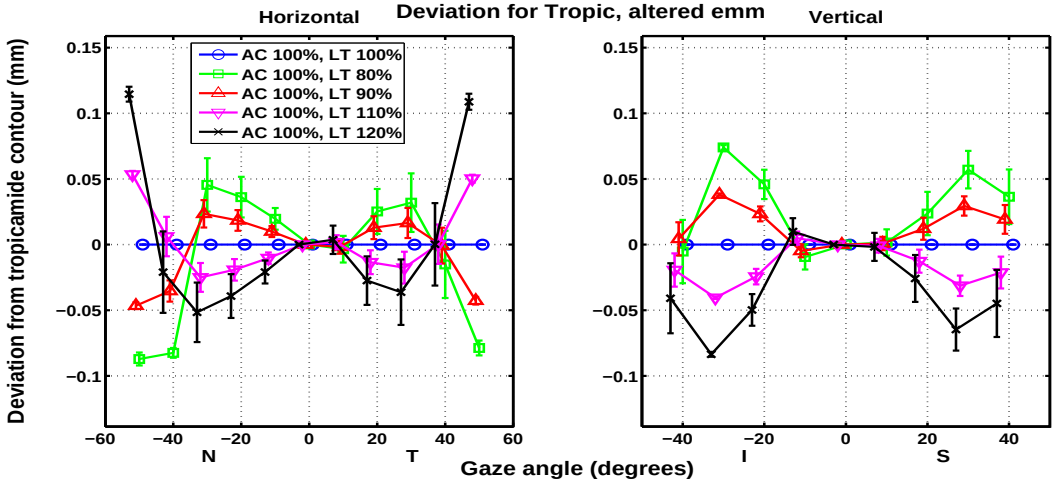

Figure 4.18 Deviation from tropicamide calculated retinal contour of emmetropic group when lens thickness is artificially increased or decreased.

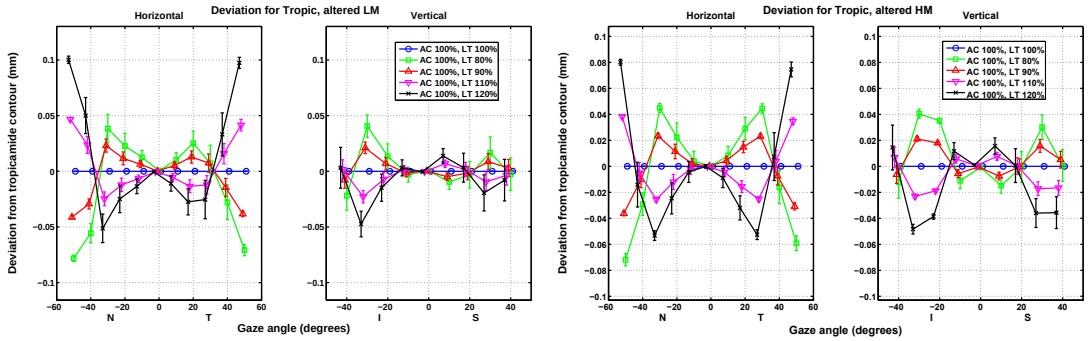

(a) (b)

Figure 4.19 Deviation from tropicamide calculated retinal contour of low myope (a) and high myope (b) groups when lens thickness is increased or decreased.

present, but if so it is much less pronounced than that seen when anterior chamber depth was varied.

Once again, the same adjustments were performed in low and high myope groups. Examination of figures 4.19(a) and (b) shows that once again magnitudes are small and comparable to the emmetrope group. Some minor asymmetries and displacements of local zeros may be evident in both groups, but the differences are much less pronounced than was seen in alteration of anterior chamber depth.

Simultaneous adjustment of anterior chamber depth and lens thickness (figures 4.20 and 4.21) produced differing results depending on how the adjustments were made. In all cases, the effects seemed to cancel and minimize deviations in the central retina, though the degree to which this occurred varied. When the AC depth and lens thickness were simultaneously increased or decreased, large deviations were seen in the periphery of both meridians. An additional local minimum was introduced on the horizontal meridian, producing minimums near 0°, 20°, and 45°. Pronounced asymmetry is seen between the 1st and 2nd minimum, with the nasal retina showing deviations much larger than the temporal retina. Interestingly, this asymmetry doesn't seem apparent at the 50° point. On the vertical meridian, no asymmetry was apparent. Deviations increased in the periphery and were

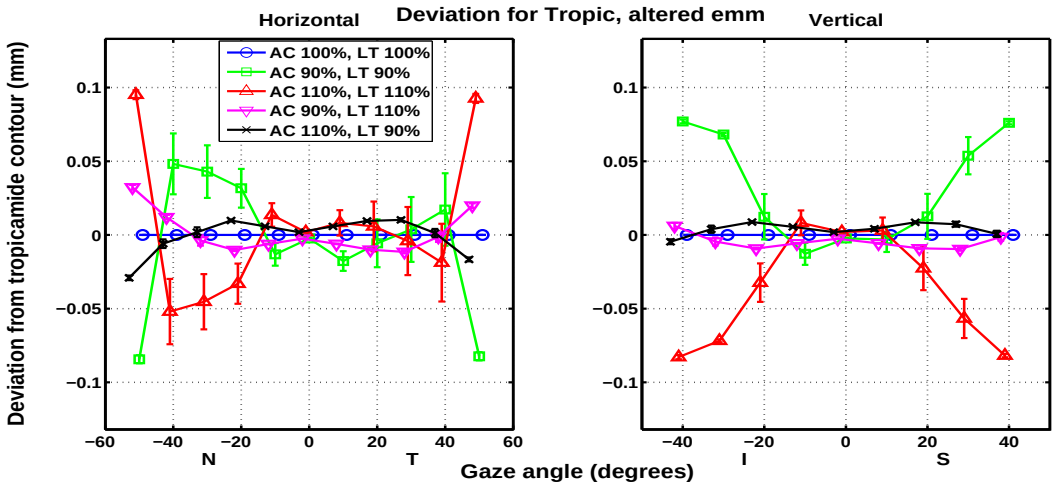

Figure 4.20 Deviation from tropicamide calculated retinal contour of emmetropic group when anterior chamber depth and lens thickness were altered together, either such that the changes opposed one another (AC depth increased and LT decreased, or vice versa) or such that they combined (both parameters increased or decreased simultaneously).

minimized centrally, and a local minimum was observed around 15°.

When AC depth and lens thickness were varied such that they opposed each other, the effect was to minimize deviations throughout the horizontal field. Once again, asymmetry can be seen on the horizontal field in that the first local minimum is pulled farther peripherally in the temporal retina (40°) than in the nasal retina 30°, though there is no appreciable difference in amplitude between the two. Deviations remained small in amplitude – for the most part less than 0.02 mm, except in the far nasal periphery. On the vertical meridian, deviations remained less than 0.01 mm.

These results show that the Dunne algorithm is able to tolerate considerable inaccuracy in the declaration of ocular parameters and still produce a relatively faithful retinal contour. In our case, the Pentacam has been reported to artificially shrink quantitative values for AC depth and lens thickness[87]. This would suggest that were we to use it to calculate our contours, they would be shifted in shape and slightly in amplitude similarly to the green curve shown in figure 4.20.

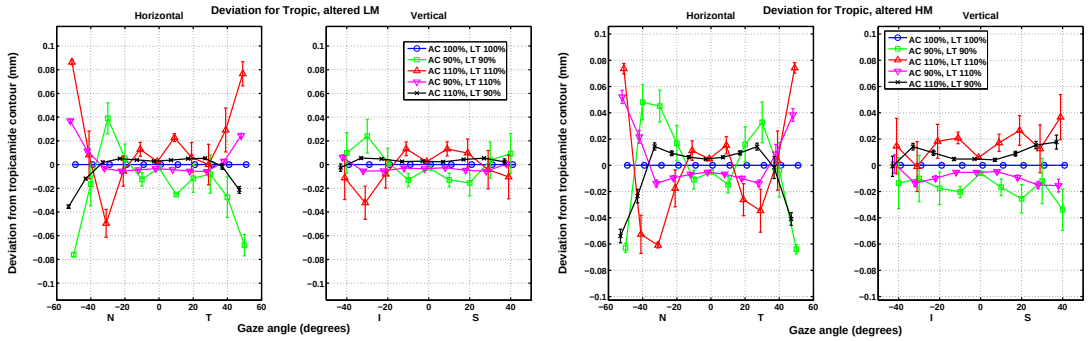

(a) (b)

Figure 4.21 Deviation from tropicamide calculated retinal contour of low myope (a) and high myope (b) groups when AC depth and lens thickness are simultaneously altered.

Once again, examination of the same adjustments performed in low and high myope groups in figures 4.21(a) and (b) shows that once again magnitudes are small and comparable to the emmetrope group. Additional local zeros seem to be present in both groups, but the only large asymmetry appears for the high myope group on the superior retina, where once again a large separation of the curves appears with large eccentricity.

One final consideration that we made was for inaccuracies in axial length declaration. Although the IOL Master has been shown to be very accurate and repeatable in measuring axial length, it has been shown that axial length may increase by as much as 0.06 mm in myopes during accommodation. Our model eyes were constructed with non-accommodative axial lengths, and as such this presented another opportunity to examine the robustness of the algorithm.

Contours were once again computed for the emmetropic subjects using model eyes constructed with their original axial lengths or with artificially altered axial lengths, and retinal contours were calculated from original peripheral refractions. Figure 4.22 shows that in general the algorithm produced retinal contours that shifted in the same direction as the axial length error, meaning that an increase in axial length produced a retinal contour

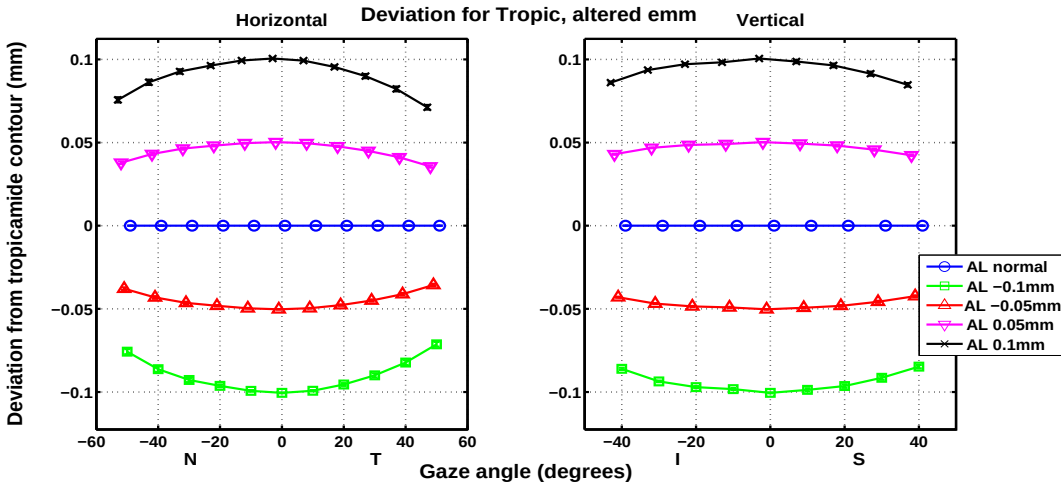

Figure 4.22 Deviation from tropicamide calculated retinal contour of emmetropic group when axial length was increased or decreased by 0.1 mm.

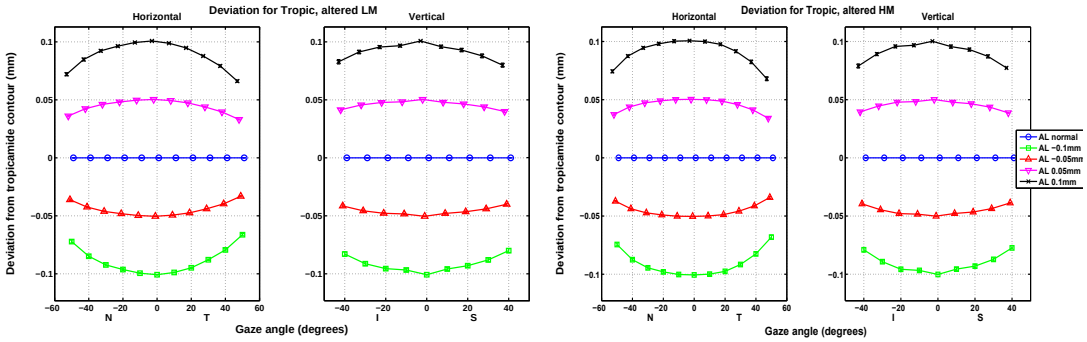

(a) (b)

Figure 4.23 Deviation from tropicamide calculated retinal contour of low myope (a) and high myope (b) groups when axial length is increased or decreased.

that was shifted posteriorly. The magnitude of the discrepancy was equal to the magnitude of the error, save that it decreased slightly in the periphery of both meridians. Discrepancies were symmetric and showed little spread among subjects. Examination of the same changes in low and high myopes, seen in figures 4.23(a) and (b), showed no appreciable difference except that the discrepancies might decrease slightly faster in the periphery of the myopic subjects.

With respect to our accommodative contours discussed in section 4.2.2, this would

suggest that correcting the axial lengths to longer accommodative would cause a small posterior shift in these contours. The amplitude of this shift would be much less than the magnitude of variation seen in these contours (see figures 4.9 and 4.10). Since these contours already showed a posterior discrepancy relative to the non-accommodative tropicamide contour, our modeling suggests that this effect cannot be accounted for by failure to incorporate an accommodative axial length into our initial model eye. Indeed, were we to incorporate a longer axial length, it would case a uniform posterior shift of the accommodative contour, suggesting that our contours are actually slightly underestimating this effect (though once again, the magnitude of the error is small relative to the effect).

Whether the effects of accommodation on retinal contour are due to a true posterior shift of the retina or to optical effects which confound the algorithm is beyond the scope of this study. Without a suitable gold standard for measurement of retinal contour, it is challenging to establish the accuracy of any method. However, we feel that the Dunne algorithm has been shown by modeling to produce very accurate contours and perform robustly to inaccurately determined ocular parameters, and we therefore feel that further study to investigate posterior shifts in retinal contour during accommodation may prove profitable to our understanding of accommodation and possibly myopia development.

Chapter 5

Summary and Conclusion

Our data show that peripheral aberrations change differently with accommodation in myopic and emmetropic eyes. High myopes were seen to show a relative accommodative lag over the temporal meridian. Asymmetric changes in M and J_{180} with accommodation were found in many instances to oppose asymmetries in the non-accommodative profiles for each refractive group.

The three groups appeared to show progressively larger changes in Z_3^1 with increasing eccentricity over the inferior retina. This effect may be associated with differences between the groups in the changes with accommodation in the crystalline lens optics, optical alignment, peripheral retinal contour, or corneal topography.

Myopes in general showed a larger accommodative change in the RMS of Zernike orders than emmetropes, and this change was seen to increase with eccentricity rather than decrease as seen with emmetropes. The RMS change in aberrations with accommodation was asymmetric in both meridians, tending to show more eccentric variation in the nasal and inferior retinas. However, this asymmetry was reversed and greatly diminished in magnitude when 2nd order terms were removed, suggesting that higher order terms slightly counteract the asymmetric effect of 2nd order terms.

Retinal contours are seen to have an exaggerated prolate shape when viewed in terms of gaze angle rather than in true cartesian coordinates. Despite this, the measured contours in high myopia are consistent with a prolate eye shape that has been found in numerous previous studies. Asphericity coefficients were seen to vary significantly with refractive error in both the nasal and temporal retinas, but no such correlation was found in the vertical meridian. Central retinal radius of curvature also showed significant correlations with refractive error and axial length in both horizontal semi-meridians, but only showed a significant correlation with axial length over the inferior retina.

Partial coherence interferometry is a fast method of estimating retinal contour, but it shows more peripheral variation than calculation from peripheral refraction. The Dunne algorithm is fairly robust to computation of retinal contour in the presence of pupil diameter variation and inaccurate measures of anterior segment parameters, but retinal contour may be altered in the presence of accommodation.

Appendix A

Consent form

THE NEW ENGLAND COLLEGE OF OPTOMETRY
424 Beacon Street
Boston, MA 02115
Tel: 617.266.2030 ext 5275
Fax: 617.424.9202

STATEMENT OF INFORMED CONSENT

Measurements of retinal contour:
The effects of pupil size and accommodation

Overview
You are being asked to participate in a research project to study the effect of pupil size and the focusing power of the eye (accommodation) on the measurement of eye shape. The following measurements will be taken in this study: visual acuity, pressure inside the eye, depth and angle of the anterior chamber of the eye, optical quality of the eye, pupil size, and length of the eye along different angles of gaze. All of these tests are non-invasive and are described below. All measurements are taken using commercially available clinical instruments.

The testing will take place at New England College of Optometry and is expected to take approximately 5 hours, to be completed in three 1.5-2 hour visits. Up to 40 subjects are being recruited for this study.

Description of Tests & Procedures
The same tests and procedures will be performed on all subjects. After an initial refraction and acuity assessment and screening tests on both eyes, subsequent measurements will be taken on only the left eye.

Visual acuity (1st visit): You will be asked to read a letter chart. We will initially test both the right eye and the left eye. Both eyes must have a best corrected vision of at least 20/25 for you to be eligible to participate in the study.

Intraocular Pressure (pressure inside the eye; 2nd and 3rd visits): Pressure measurements will be taken using a non-contact air-puff device. You will be seated at a chin rest and asked to fixate a target while the machine takes this reading on each eye.

Anterior Chamber Angle Measurement (2nd and 3rd visits): The depth of the eye's anterior chamber (the area between the cornea and iris) will be measured at the margin of the cornea using a conventional clinical instrument, a slit lamp. You will be seated at the slit lamp and asked to fixate a target while the measurement is taken.

Aberrometry (Optical Quality and Refraction; all visits):
The optical quality of your eye will be measured using an instrument that records images of light passing through the eye. You will be seated at a chinrest and forehead restraint in front of the device and asked to fixate a target of letters. The target will be moved to take multiple measurements at various positions of gaze. Several images will be taken of your eye, from which the optical quality of the entire eye will be determined. The process will be repeated with the target adjusted to relax the focus of the eye.

This set of measurements will be taken five times: twice during the first visit, twice during the second visit, and once during the third and final visit. During the first visit, the measurements will be taken under normal viewing conditions. During the second visit, the measures will be made with drops administered to dilate your pupils (phenlyephrine). During the third visit, the measurements will be repeated with drops administered that relax your eye's focusing power and dilate your pupils (tropicamide). Both these types of drops will cause your pupil to dilate, and as a result, you may experience sensitivity to light. The drops that relax focus will also eliminate your ability to focus on near targets, so you may experience blurry vision when attempting to read or look at close objects. The effect will take a few hours to wear off completely. The exact amount of time these effects take to wear off varies between individuals, but is usually around 6-8 hours. You will be asked to wait 30-40

minutes during each visit while the drops take their full effect. At the end of testing in each session, we will recheck the pressure within your eye and dispense a pair of non-prescription sunglasses for you to wear while the dilating drops wear off.

Corneal Topography (1st visit):
During the first visit, corneal shape will be measured with a clinical instrument known as a Humphrey Atlas 995 corneal topographer. These measurements will be used to measure the corneal power and overall corneal shape. You will look into the device and fixate a red light. Four images of the front of the eye will be recorded.

Anterior chamber measurements (2nd and 3rd visits): Anterior measurements will be taken with a rotating camera called a Pentacam. The Pentacam will take a cross-sectional image of the anterior (front) portion of your eye. For these images you will be seated at a chinrest and asked to fixate a target while the device acquires images of your left eye. One measurement will be taken during the second visit after you have been administered phenylephrine (the dilating drop). During this visit, you will be asked to look at a near target through a mirror with your right eye while measurements are taken on the left eye. Another measurement will be taken during the third visit, after you have been administered tropicamide (the drop that will relax your eye's focusing power). You will be asked to look at the target in the machine while the measurements are taken.

Ocular dimension measurements (3rd visit): These measurements will be taken during the third visit. Prior to administration of drops that dilate and relax the focusing ability of the eye (tropicamide), two measurements will be taken using an ultrasound probe. This probe will measure the length of your eye and the distance between various components of it. You will be asked to close your left eye and the probe will be placed over your left eyelid. With your right eye, you will be asked to view a target. Measurements will be taken first with you viewing a distant target, and then with you viewing a near target.

Following administration of the drops to relax the focusing ability of the eye (tropicamide), measurements will be taken of eye shape. An instrument called a Zeiss IOL Master will be used to take these measurements which are made by scanning the eye with a red beam of light. You will be seated at a chinrest and asked to fixate a target while the instrument measures the length of your eye. You will be instructed to fixate different targets so that measurements can be taken in various positions of gaze.

Possible Discomforts or Risks
These experimental sessions involve the application of anesthetic and dilating/cycloplegic drops to the tested eye. The anesthetic drops (1 drop 0.5% proparacaine) will cause a numbing of the cornea lasting about 1 hour. The anesthetic drops also cause a temporary softening of the outer corneal layer (corneal epithelium), so I should avoid rubbing my eyes for up to 1 hour after this procedure. The dilating drops (either 1 drop of 2.5% phenylephrine in visit 1 or 2 drops of 1% Tropicamide in visit 2) cause pupil dilation lasting up to 8 hours. I will experience increased sensitivity to bright light while my pupils are dilated. The dilating drops in visit 2 (Tropicamide 1%) are also cycloplegic in that they result in substantially blurred near vision lasting for about 1 hour followed by a milder blurring of near vision for up to 8 hours.

Dilation presents a very small risk of increased pressure inside the eye due to angle closure. This means that there is a slight risk that the dilating pupil might block the flow of fluid in your eye, causing an increase in the pressure of the fluid in your eye. To minimize the possibility of this occurring, we will measure the angle between your cornea and iris at the edge of your cornea in order to ensure that it is large enough so that the dilating iris will not block the flow of fluid in the eye. We will also measure the pressure in your eye to ensure that you are not at risk for angle closure. Studies show that if the angle of your eye is wide or your pressure is normal, there is less risk of angle closure. If your chamber angles are narrow or pressure is elevated, you will not be allowed to participate in the study.

In the unlikely event that any adverse reaction does occur during regular examination hours (9 am - 5 pm weekdays), you will be referred to the New England Eye Institute at 617 262 -2020. If an adverse reaction should occur outside of regular office hours, you should seek emergency medical care. You will be financially responsible for the medical care for an adverse reaction.

Benefits
Your participation in this study will contribute to our understanding of the effect that pupil size and accommodation have on the eye's peripheral refraction and measurements of retinal contour. This will allow researchers and clinicians to take more accurate measurements of retinal contour when conducting studies or treating diseases, and to understand the relationship between peripheral refraction and accommodation. In appreciation for your efforts, you will be given $60 after you complete the third visit of the study; full compensation will not be available if only the first and second visits are completed.

Confidentiality
Your medical records will be kept as confidential as possible within the limitations of state and federal law.

If you decide to be a subject in this study, both demographic and technical information about you will be collected. Demographic information will include, but will not be limited to such things as, your name, date of birth, address, gender, ethnicity, etc. Technical information will include elements of your personal health history and results of all the tests and measurements related to the study. This information is collected in order to determine whether you are eligible to be a subject in the study; that is, to meet the inclusion/exclusion criteria and, if so, to allow the study investigators to gather the data from you that is necessary to support the study's purpose. The results from all of the subjects in the study can then be analyzed to develop the study's conclusion.

All study-related information will remain confidential with the study investigators or administrative staff. However, any regulatory authority or the Institutional Review Board may inspect the investigator's records pertaining to you as a subject. But they too should maintain confidentiality.

The results of the study may be used in health care education or in scientific publications. Neither your name nor any information that specifically could identify you will be used in any such presentation or publication.

Personal Health Information
Your personal health information (PHI), as related to this study, is described in the "Confidentiality" section above. If you sign this informed consent form, it grants permission to use your PHI as specifically discussed. This permission does not have an expiration date, but you can cancel in at any time by writing to the principal investigator(s) at the address below.

If you cancel your permission to use your PHI after you have started the study but before your study participation would normally be concluded, you will not be allowed to continue in the study and the investigators will stop collecting data. However, they retain the right to use the information they have already collected to evaluate the study's results.

Privacy Practices and Your Rights
Health care providers are required by law to keep private any health information that identifies people. Federal Privacy Regulations require that you authorize the release of any health information that may reveal your identity. The persons and entities that you are authorizing to use or inspect all of the health information generated or collected about you during this study includes the study doctor(s), the study staff, the Institution, any study Sponsor (or the authorized agents of the sponsor), the Food and Drug Administration (FDA), the Department of Health and Human Services (DHHS) agencies, and the Institutional Review Board. Because of the need to release information to these parties absolute confidentiality cannot be guaranteed. Once your personal health information is released it may be redisclosed, at which point your health information may no longer be protected by federal privacy regulations.

You may ask the study investigator to see a copy of your PHI related to the study. You may also request the study investigator to correct any information that you feel is incorrect. However, you may have to wait until the end of the study to see your records so that the study can be organized and conducted scientifically.

You must be given notice of your investigator's privacy policies. The Confidentiality, Personal Health Information, and Privacy Practices and Your Rights sections of this form fulfill this requirement.

Unless you authorize the use and disclosure of your personal health information, you cannot participate in this research study. If you refuse to give your authorization, your medical care will not be affected.

Voluntary Participation/Withdrawal from the Study

Participation in this study is voluntary and you may withdraw at any time. Refusal to participate or withdrawal from the study will not involve any penalty or loss of benefits to which you are otherwise entitled. We will disclose to you in a timely manner any significant new findings that may influence your willingness to participate in the study. The investigators or the Institutional Review Board may terminate your participation in the study (with or without your consent) if it is believed to be in your best interest.

Questions

Any questions you may have about this study or about your rights as a study participant may be directed to the investigator, Drs. Nancy J. Coletta**.** If you experience any study-related illness or injury during or after the study, you should contact the investigator, Dr. Nancy J. Coletta at 617 266 2030 ext 5275 or 617 620 8673 or Dr. Frank Thorn at 617 266 2030 ext 5271. You may also contact Dr. Paul White (617-266-2030 ext 5251), Chairman of the Institutional Review Board of the New England College of Optometry, 424 Beacon Street, Boston MA 02115.

Voluntary Consent

I have read this consent form and I understand it. Any questions concerning this study have been answered to my satisfaction and I have been offered a copy of this consent form. By signing this form, I voluntarily agree to participate in this study.

I understand the potential risks and benefits involved in this study and that I may withdraw at any time without penalty in general; if I am a member of the student or staff community at NECO, withdrawal from the study will not affect my status at NECO. I understand that I must notify the study investigator immediately if I notice any medical problems that may be related to my participation in the study. I also understand that my participation in the study may be terminated at any time if the investigators or the Institutional Review Board feel that it is in my best interest or if I fail to keep the required study appointment(s) or follow the study instructions.

I understand that the study records may be inspected by the Institutional Review Board.

_____

Subject's Name (PRINT)

_____ _____

Signature of Subject Date

_____ _____

Signature of Witness Date

_____ _____

Signature of Investigator or Desginee Date

Appendix B

Questionnaire

Questionnaire for Potential Subjects

Name _____ **Date of Birth**_____ **Gender** ____ **M** ____ **F**

Please check below if you have knowledge of any of the following conditions, regarding your eyes or vision:

- ☐ visual acuity not correctable to at least 20/25 in each eye
- ☐ cataract or other media opacity
- ☐ fixational instability (e.g., nystagmus) or restricted movement of either eye
- ☐ narrow anterior chamber angles (angle less than 1:3 by von Herrick method)
- ☐ intraocular pressure above 18mm Hg
- ☐ any history of acute angle closure
- ☐ other history of ocular disease, surgery, or orthokeratology
- ☐ any present ocular medications
- ☐ central astigmatism greater than 1.50 diopters

Eye History:

1. Do you have any current or past eye pathology? ____ yes ____ no

   If yes, please describe: _____

   _____

   _____

2. Have you had any eye surgery (including refractive surgery) or refractive procedures such as ortho-keratology? ____ yes ____ no

   If yes, please describe: _____

   _____

   _____

3. Have you had any eye injuries? ____ yes ____ no

   If yes, please describe: _____

   _____

   _____

4. Have you ever experienced any complication with eye dilation? ____ yes ____ no

   If yes, please describe: _____

   _____

   _____

If you do not wear contact lenses, please skip to question #11. If you do wear contact lenses, please answer questions #5 - 10:

Contact Lens Wear:

5. What type of lenses do you wear?

   ____ soft ____ rigid gas permeable*

   ____ daily wear ____ extended wear*

   ____ single vision ____ multifocal*

   *If you wear rigid lenses, extended wear lenses or multifocal lenses, you may not participate in the study. (Monovision is OK.)

6. How long have you worn the type of lenses you are currently wearing? ____ years

7. Did you wear a different type of lenses prior to your current lenses? ____ yes ____ no

   If yes, what type of lenses did you previously wear? _____ For how long? ____ years

8. How many days per week do you typically wear your lenses? ____ days

9. How many hours per day do you typically wear your lenses? ____ hours

10. Have you had any problems with your lenses? ____ yes ____ no

    If yes, please describe: _____

    _____

    _____

Most Recent Eye Exam:

11. When was your most recent eye exam? _____

12. Who performed the exam and where? _____

_____

13. If you were examined at New England Eye Institute, may we have permission to examine your clinical file?

____ yes ____ no

Signature_____ Date_____

Appendix C

Bootstrap Method for Analysis of Significance

To examine the significance of trends spanning multiple positions of gaze, we developed a method with the help of our statistician. Analysis of individual p-values at each gaze position yielded limited results because often the groups failed to show sufficient separation at any one specific point of gaze to be marked as significant. The number of tests made data difficult to interpret on such a large scale and made adjustments for significance excessively restrictive; Bonferroni correction would have imposed a corrected p-value of $p < 0.05/700$ to reach significance, which was unlikely given our moderate number of subjects. However, we were not interested in investigating the separation of group aberration values at individual points of gaze. Rather we wanted to asess whether the groups showed a level of separation which was consistent over a range of consecutive positions of gaze, and if the aberration values for each group generally maintained the same relative relationship with respect to one another. In this case we wanted a means to quantify how significant such a separation over that entire range of values would be.

We therefore defined a "trend" as an aberration (or change in aberration, during ac-

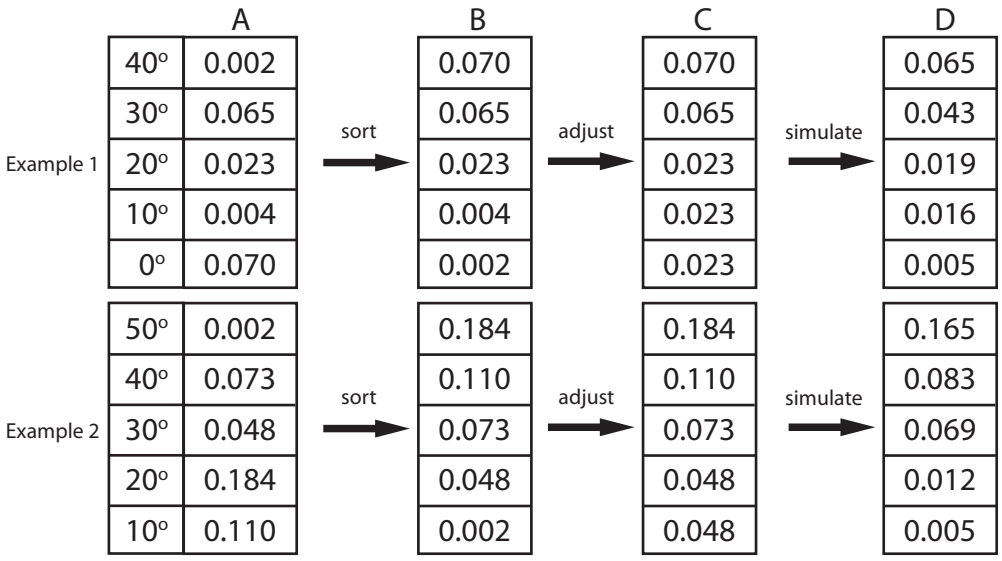

Figure C.1 Illustration of our to analyze significance of trends. Suspected trends over consecutive gaze angles were found in the test array and separated for analysis (A). The trend in question was first sorted (B). It was then adjusted depending on its median value (C, example 1 vs example 2), to prevent excessive restriction on matching in simulated conditions. Simulations were then run ($\times n$ iterations) to find the likelihood of random generation of equivalent trends (D).

commodation) behaving differently for one of the refractive groups over a certain range of gaze positions. We made the assumption that if a particular aberration behaved differently between refractive groups, then that behavior should hold over some extended area of the retina, and not be limited to one gaze position. We then analyzed the significance of the spread in any such trend arising through chance using a numerical Bootstrap method[78,79].

We wrote an algorithm to progress through our array of p-values to search for possible trends. In our algorithm we defined a suspected trend as successive ANOVA p-values lower than 0.25 in a single coefficient across various consecutive gaze positions. When progressing through a trend to determine its length, a p-value as high as 0.35 was permitted inclusion in the suspected trend providing that the successive p-value fell below the original cutoff. When a suspected trend was found, its significance was analyzed numerically as outlined below. The process is illustrated in figure C.1.

The trend in question was first sorted in ascending order (figure C.1B), which permitted a better overall view of the combined significance of the p-values in the trend and made numerical analysis simpler. The median p-value in the trend was queried, and the trend was adjusted in preparation for analysis of significance. If the median was lower than 0.05, then all lower p-values were considered equivalent and set at that value (figure C.1C, example 1). If the median value in the trend was greater than 0.05, then only those values in the trend which were lower than 0.05 were adjusted so that they matched the largest p-value below 0.05 (figure C.1C, example 2). This adjustment was performed at the advice of our statistician to eliminate extremely small p-values which might provide too stringent of requirements for matching in our numerical simulation when analyzing the trend for significance.

We then tested the null hypothesis that the low p-values appeared next to each other randomly through use of a computational bootstrap method. A simulation was run in which arrays of the same size (11×35 for horizontal vs 9×35 for vertical) were generated with random numbers between 0 and 1, which would be the distribution of p-values in the case where no significant difference existed between the groups. We chose to perform $n = 10,000$ iterations, so we would have a good chance of picking up at least 1 match for even the most unlikely trends. Each simulated array was progressed through systematically and consecutive blocks of elements the same size as the trend in question were removed for analysis. The block was tallied as a match if, after sorting, each element fell below the corresponding element of the trend in question (figure C.1D). After the simulation was complete, the number of iterations and the number of matches found were used to calculate the probability that the trend in question arose from chance alone:

$$p = \frac{(\text{\# of tallied matches})}{(\text{\# of iterations})} \tag{C.1}$$

This provided an estimate of the probability of the trend in question arising through

chance in an array of randomly arranged numbers, and thus provide a p-value for that trend.

This analysis was adequate for flagging possible trends in our data, but it does have several shortcomings. Perhaps the most notable flaw in this method is that calculation of significance relied primarily on the ANOVA test, which is not directionally sensitive. This means that information regarding the relative position of the three groups throughout the trend is lost. The significance reported is only a measurement of the significance of the spread at each point falling together, not incorporating position the relative values of each group across position, and therefore resulting in the reported significance being overly conservative.

This is illustrated in figure C.2. In figure C.2A, the three groups show some separation at various points on the graph, but numerous points where the group values are inconsistent

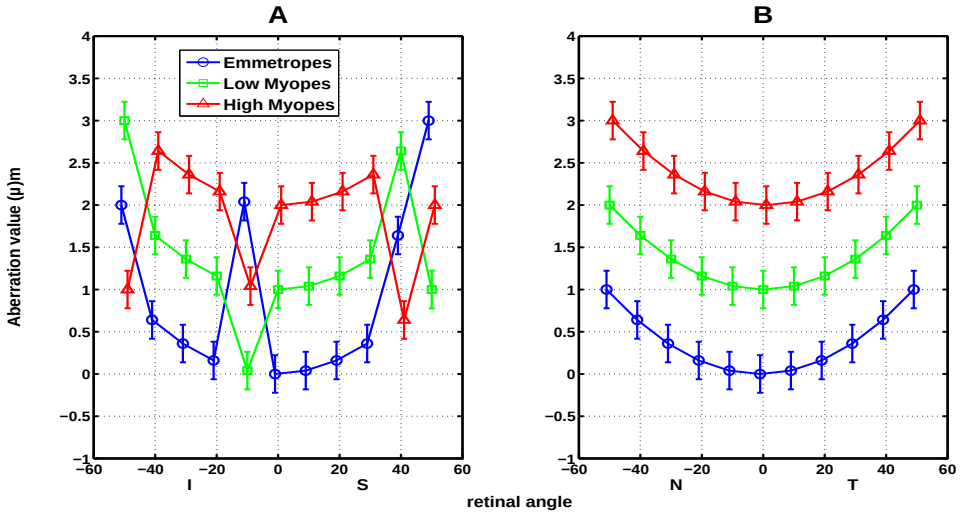

Figure C.2 Illustration depicting the inherent error in our method due to the fact that it relies only on the spread at each point, and doesn't retain information about the relative positions of the three groups. Figures A and B would be calculated to have the same significance because they have the same spread at each point, despite the fact that an obvious trend is visible in B while A appears much less notable. If position could be retained in the method, B would have a much higher significance.

in their relative positions. Note however that the spread is consistent at each point across the plot. Because ANOVA is not sensitive to the relative positions of the three groups, the points at which the groups change position (-40°, -10°, and 40–50°) will be marked at the same significance level as the rest, since the groups maintain the same relative spread. When put into our numerical method this trend may or may not reach significance.

In figure C.2B, the three groups maintain the same consistent spread at each point across the plot, but this time also maintain the same relative position. However, since our method is not sensitive to position, this calculation for this trend will yield the same significance as that in plot C.2A, since the spreads are identical throughout the two plots. Were it possible to incorporate the relative position of the groups into the ANOVA test used in our method, the trend in C.2B would be marked as much more significant, thus indicating that our method is conservative in marking significance. Because of this, a notable trend may fail to be marked as significant if adequate separation is not seen to be flagged by our test.

The converse situation is also true – a trend similar to one in figure C.2A could be marked as significant despite having little consistency in the groups' relative positions, as long as there is a large spread between the groups at each point. Because of the possibility of missing some notable trends or including noisy plots with high spreads, after possible trends were analyzed for significance, plots of aberrations were observed directly to examine the nature of the trends which were found. We were thus able to assess if a trend marked as significant was truly notable and to look for any possible trends which might not have been flagged by our method.

Appendix D

Retinal Curve Fitting Process

In his paper describing his algorithm, Dunne uses a conic section fit to discuss the asphericity of the cornea when raytracing through the eye:

$$y^2 = 2\mathrm{r}_0 x - px^2. \tag{D.1}$$

Similar to our notation described in section 2.4, p refers to the asphericity of the curve and r_0 refers to the central radius of curvature. However observation of figure 6 in Dunne's paper shows that his convention for naming axes differs from ours. This equation refers to y as the lateral separation from the visual axis, which is x in figure 2.6. It also refers to separation along the visual axis as x, which we refer to as z in our model. To adapt this equation we first will replace the variables with those in our model. We also want to translate the curve along the z-axis by the axial length. This is done by replacing the variables and introducing a translation factor:

$$x^2 = 2\mathrm{r}_0 (z - a) - p (z - a)^2 . \tag{D.2}$$

Algebraic manipulation of this yields

$$\frac{-x^2}{p} = (z-a)^2 - \frac{2\mathrm{r}_0}{p}(z-a) + \left(\frac{\mathrm{r}_0}{p}\right)^2 - \left(\frac{\mathrm{r}_0}{p}\right)^2, \tag{D.3}$$

which factors to

$$\frac{\mathrm{r}_0^2 - px^2}{p^2} = \left[(z-a) - \left(\frac{\mathrm{r}_0}{p}\right)\right]^2. \tag{D.4}$$

Taking the root and manipulating algebraically yields

$$z = \frac{\left(\pm\sqrt{\mathrm{r}_0^2 - px^2}\right)}{p} + a + \frac{\mathrm{r}_0}{p},$$

which is equation 2.3.

The 2nd order polynomial curve fits of retinal contours yielded coefficient solutions to the equation

$$x^2 = Az^2 + Bz + C. \tag{D.5}$$

Note that the x-coordinate (distance from fovea in the plane tangent to the retina) had to be squared prior to curve fitting. The coefficients obtained from the curve fit were used to calculate the conic section coefficients in equation 2.3. Rearrangement of equation 2.3 yields

$$x^2 = -pz^2 + 2(\mathrm{r}_0 + ap)z - \left(2a\mathrm{r}_0 + pa^2\right). \tag{D.6}$$

The coefficients found in the 2nd order polynomial curve fit can then related to the coefficients for the conic section as

$$
\begin{aligned}
A &= -p \\
B &= 2\left(\mathrm{r}_0 + ap\right) = 2\mathrm{r}_0 - 2aA \\
C &= -2a\mathrm{r}_0 - pa^2 = -Ba - Aa^2.
\end{aligned} \tag{D.7}
$$

The asphericity coefficient p, central radius of curvature r_0, and axial length (a) are easily solved from the above equations as

$$
\begin{aligned}
p &= -A \\
\mathrm{r}_0 &= \frac{B}{2} + aA \\
0 &= Aa^2 + Ba + C,
\end{aligned} \tag{D.8}
$$

where the axial length is found as the zero of the third function. In our algorithm, a was found in the curve fitting process using Matlab's fzero function, which finds a local zero of a continuous function numerically using the secant method. If in any case this function returned an error or was unable to find a solution to the above equation, then the subject's measured axial length was used to compute the central radius of curvature r_0 in the above equation.

Appendix E

Supplemental Plots

E.1 Non-accommodative Zernike Supplemental Plots

E.1.1 Foveally normalized non-accommodative Zernike plots

Figure E.1 shows non-accommodative 2nd order Zernike terms in the three refractive groups plotted relative to their foveal values. Compare to figure 3.10, which plots absolute values for these same coefficients.

Figure E.2 shows non-accommodative 3rd order vertical and horizontal coma terms in the three refractive groups plotted relative to their foveal values. Compare to figure 3.12, which plots absolute values for these same coefficients.

E.1.2 Low Significance non-accommodative Zernike Plots

Figure E.3 shows Zernike coefficeints Z_7^1 and Z_7^3. flagged for trends. A trend was flagged in Z_7^1 between 0° and 20° nasal ($p = 0.02$), however it is not readily appreciable even when the data is magnified as in figure E.3(a). The trend is of very low magnitude and likely due to very small relative spreads between the groups. Another trend was flagged in Z_7^3 from

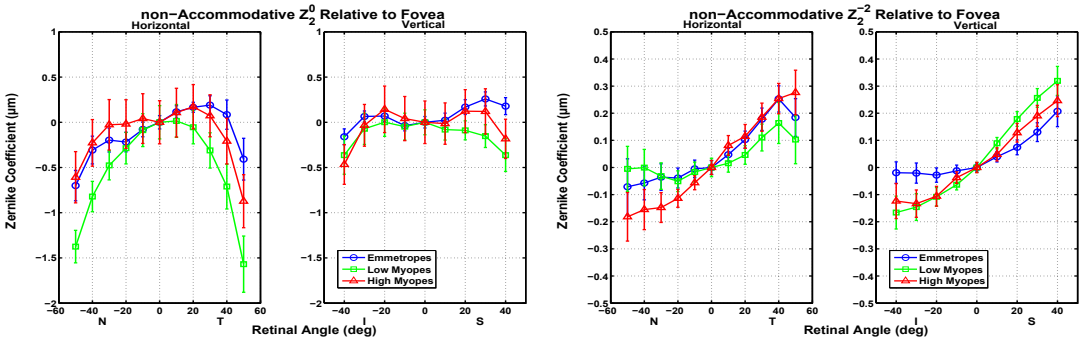

(a) Z_2^0

(b) Z_2^{-2}

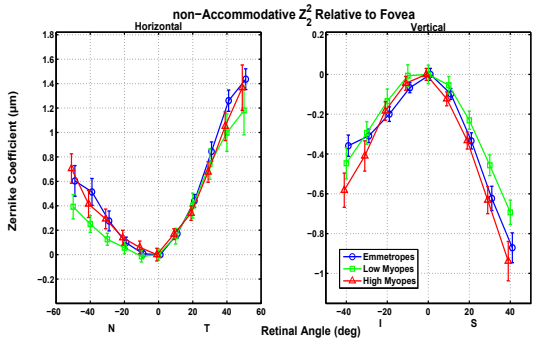

(c) Z_2^2

Figure E.1 Plots of non-accommodative 2nd order Zernike coefficients Z_2^0 (a), Z_2^{-2} (b), and Z_2^2 (c).

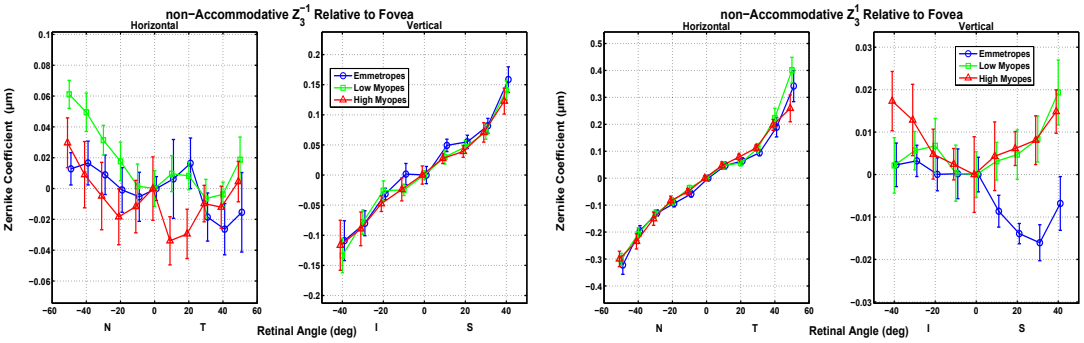

(a) Z_3^{-1}: -0.0179, 0.0067, 0.0192

(b) Z_3^1: 0.0099, -0.0070, -0.0047

Figure E.2 Non-accommodative 3rd order vertical (a) and horizontal (a) coma terms, Z_3^{-1} and Z_3^1, relative to fovea. Respective foveal values for emmetropes, low myopes, and high myopes are shown in subcaptions.

0° to 40° temporally. Magnification of the plot reveals a slightly lower value of Z_7^3 for the high myope group in this region.

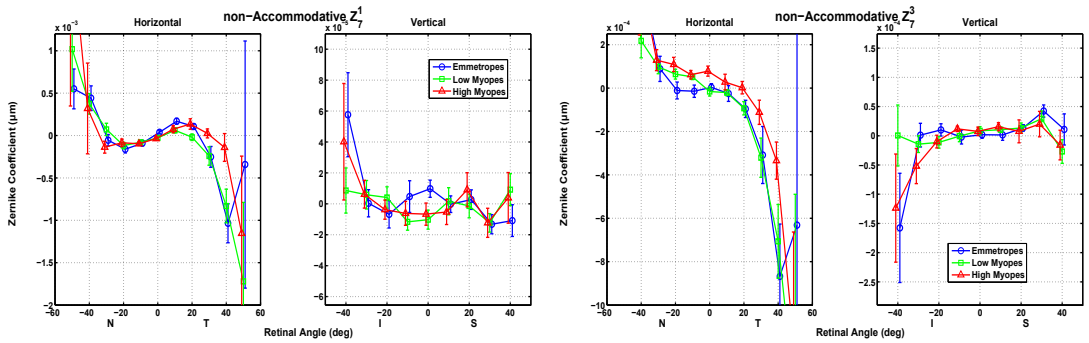

(a) Z_7^1 (b) Z_7^7

Figure E.3 Non-accommodative Z_7^1 and Z_7^3 plots.

E.2 Low Significance Accommodative Difference Zernike Plots

Accommodative changes in 3rd order trefoil (Z_3^{-3} and Z_3^3) and vertical coma (Z_3^{-1}) terms were small in magnitude and showed little systematic behavior across gaze angle or refractive error. A significant trend was found in Z_3^{-1} ($p = 0.001$, figure E.4(c)), manifesting as a central separation of the low myope and emmetropic groups, from $10°$ nasal to $10°$ temporal. A systematic trend was present in Z_3^{-3} the nasal retina ($p = 0.09$, figure E.4(a)). No systematic trends were observed in Z_3^3 (figure E.4(b)).

Significant trends were found in the inferior retinas of both Z_4^{-4} and Z_6^{-4} terms ($p = 0.007$ and $p < 0.001$ respectively, shown in figure E.5). The trends are small in magnitude but do show a consistent appearance in both 4th and 6th order terms of the plots for the emmetropic and high myope groups appearing separated across the horizontal axis, while the plot for the low myope group is intermediary between the two and progresses closer to

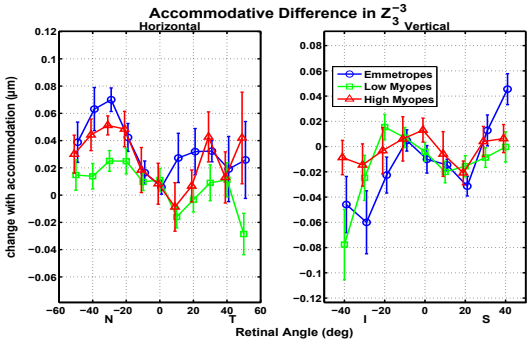

(a) Z_3^{-3}

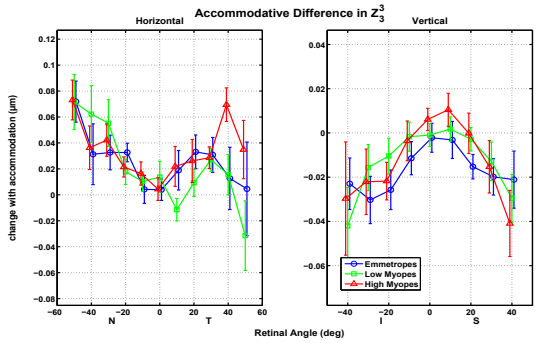

(b) Z_3^{3}

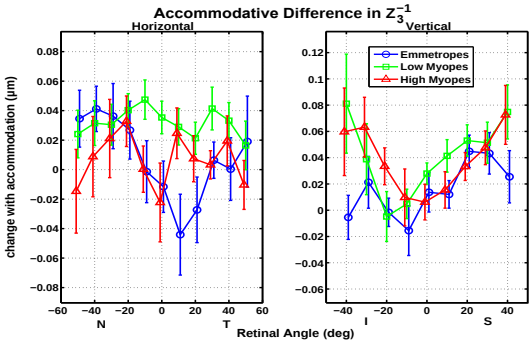

(c) Z_3^{-1}

Figure E.4 Changes in trefoil (a) and vertical coma (c) with accommodation (Z_3^{-3} and Z_3^{-1}).

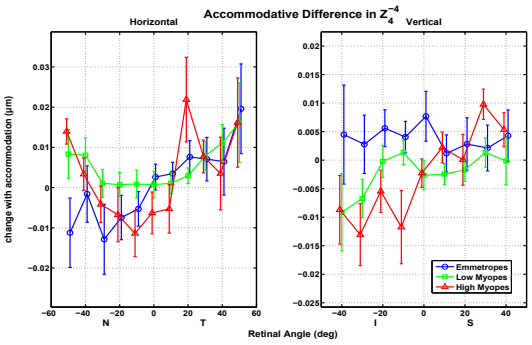

(a) Z_4^{-4}

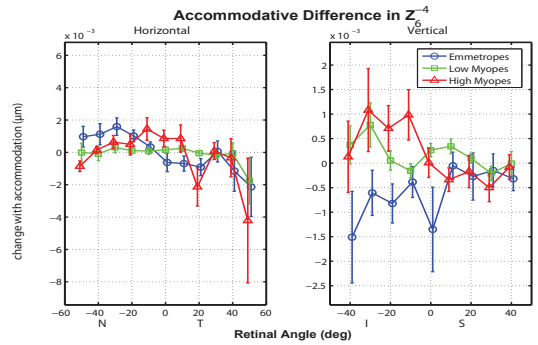

(b) Z_6^{-4}

Figure E.5 Changes in Z_4^{-4} (a) and Z_6^{-4} (b) with accommodation.

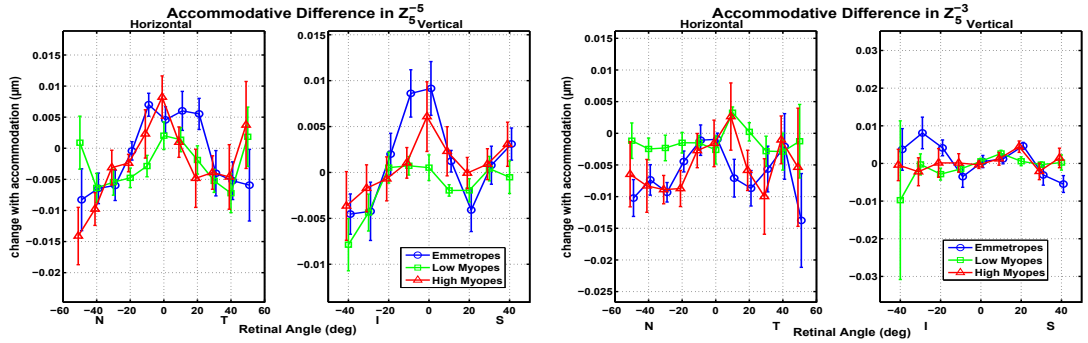

(a) Z_5^{-5}

(b) Z_5^{-3}

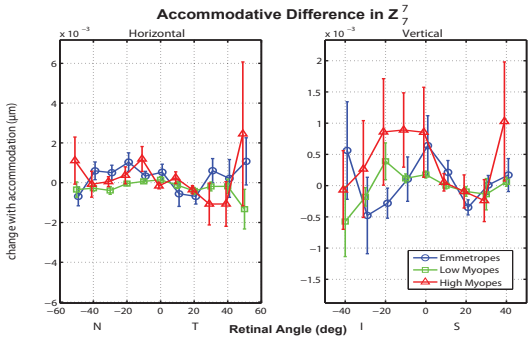

(c) Z_7^7

Figure E.6 Changes in Z_5^{-5} (a), Z_5^{-3} (b), and Z_7^7 (c) with accommodation.

the high myope curve with increasing eccentricity. Our algorithm also flagged significant trends in the horizontal meridian for both the terms (p$=0.02$ and p$=10^{-4}$), but they showed no consistent pattern of separation and don't lend themselves to interpretation.

Changes in Zernike coefficients Z_5^{-5}, Z_5^{-3}, and Z_7^7 are displayed in figure E.6. Z_5^{-5} (figure E.6(a)) showed separation trends between the three groups on the central horizontal (p$=0.056$) and central vertical meridians (p$=0.045$). While this is easier to see on the vertical meridian, both are of small magnitude. Z_5^{-3} (figure E.6(b)) showed a separation trend on the nasal retina, manifesting as the low myope group having a less negative Z_5^{-3} than the emmetropic or high myope groups. Z_7^7 was found to have a significant separation between the groups between the fovea (0°) and 50° on the nasal retina (p$=0.013$), but it

is of very small magnitude and only shows a consistent pattern of separation between the three groups between 20° and 40° nasal.

E.3 Retinal Contour plots for Refractive Groups

Figures E.7 and E.8 plot the averaged retinal contours for each group for tropicamide and accommodative data as a function of retinal distance from fovea (mm; E.7) or retinal gaze angle (deg; E.8). Subtle differences between the contours are visible, but are better appreciated in figure 4.10.

Figures E.9 and E.10 plot the averaged retinal contours for each group for non-accommodative data of varying pupillary conditions as a function of retinal distance from fovea (mm; E.9) or retinal gaze angle (deg; E.10). Subtle differences between the contours are visible in some instances, but are better appreciated in figure 4.12.

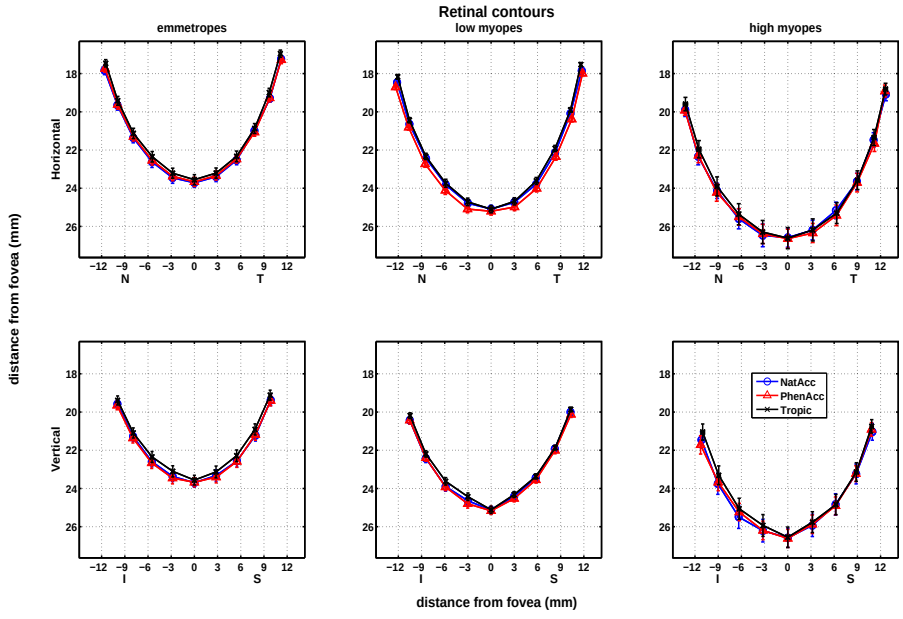

Figure E.7 Comparison of retinal contours for each group, with and without accommodation.

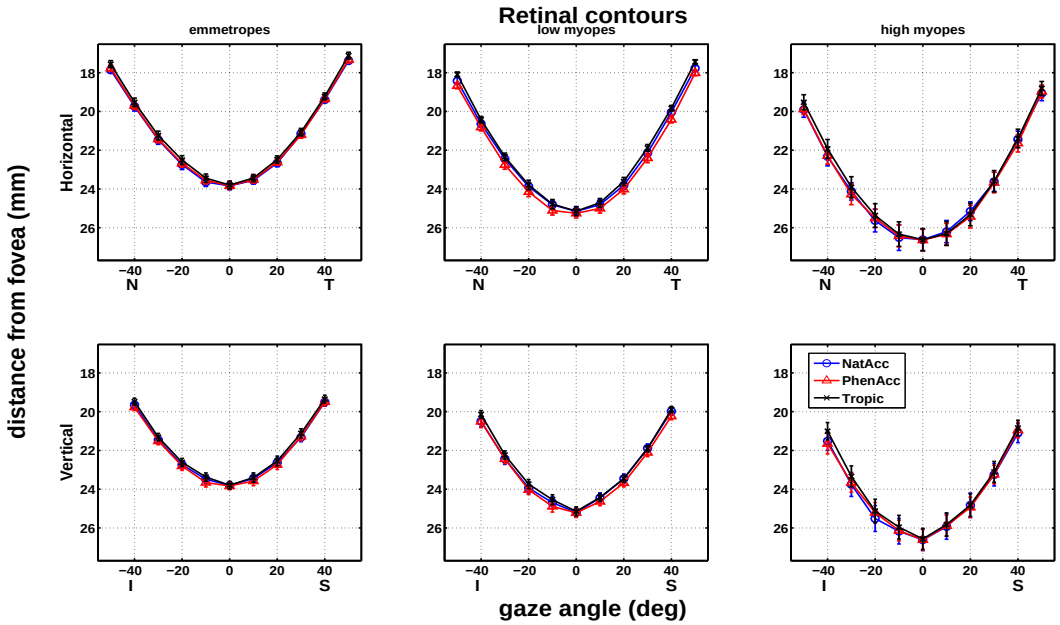

Figure E.8 Comparison of retinal contours for each group, with and without accommodation.

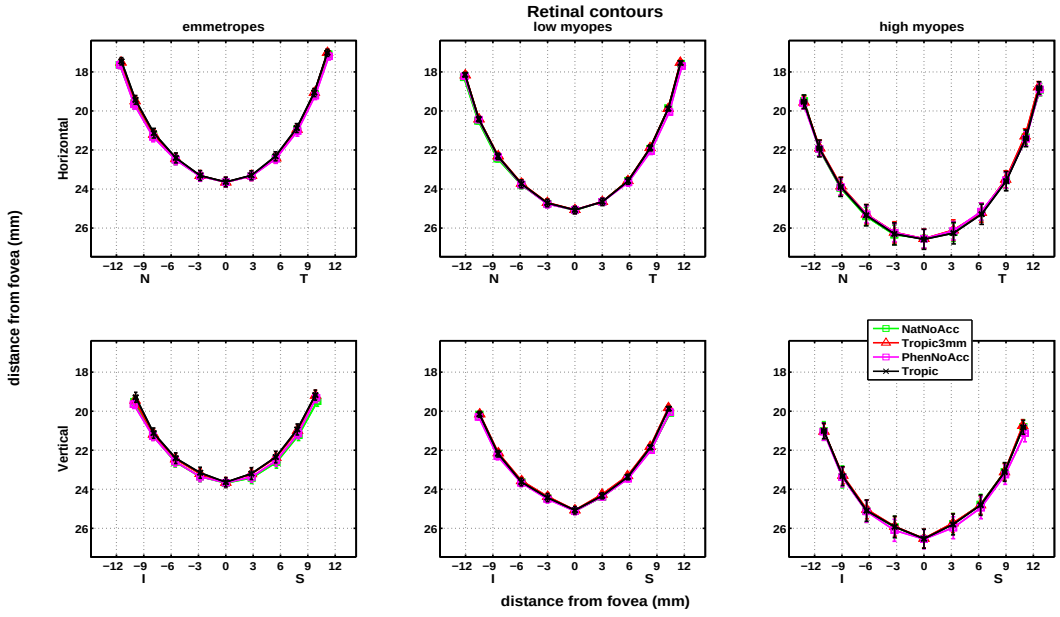

Figure E.9 Comparison of retinal contours for each group calculated using non-accommodative data sets of varying pupil diameter.

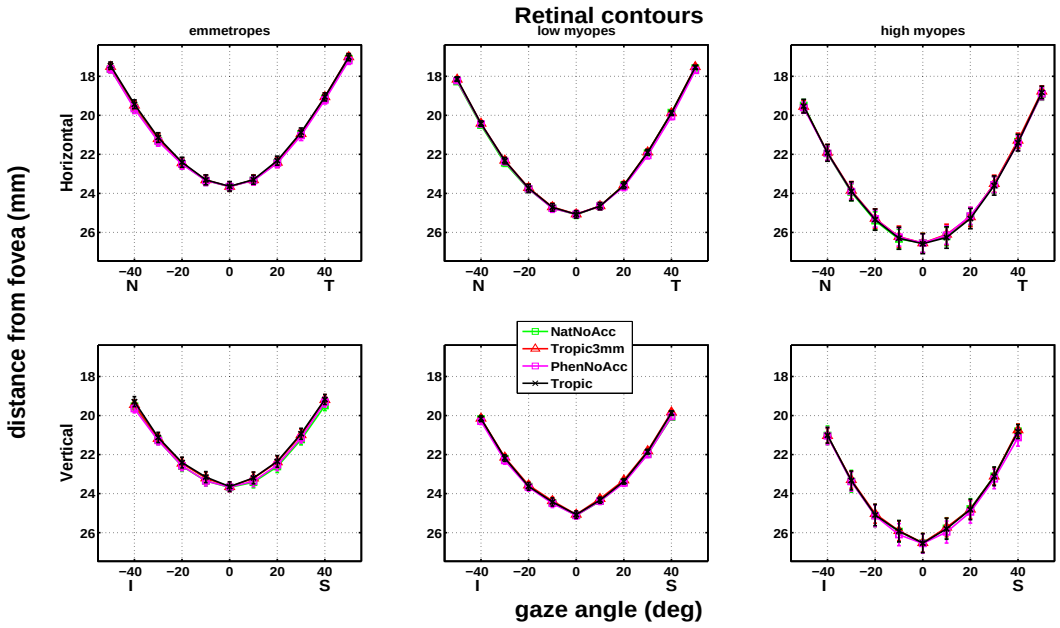

Figure E.10 Comparison of retinal contours for each group calculated using non-accommodative data sets of varying pupil diameter.

Bibliography

[1] L. Lundström, A. Mira-Agudelo, and P. Artal, (2009)"Peripheral optical errors and their change with accommodation differ between emmetropic and myopic eyes," Journal of Vision **9,** 17:1–11 , [PubMed ID: 19761308].

[2] A. Mathur, D. A. Atchison, and W. N. Charman, (2009)"Effect of accommodation on peripheral ocular aberrations," Journal of Vision **9,** 20:1–11 , [PubMed ID: 20053111].

[3] M. C. M. Dunne, (1995)"A computing scheme for determination of retinal contour from peripheral refraction, keratometry and A-scan ultrasonography," Ophthal Physiol Opt. **15,** 133–143 , [PubMed ID: 7659409].

[4] E. A. H. Mallen and P. Kashyap, (2007)"Technical Note: Measurement of retinal contour and supine axial length using the Zeiss IOLMaster," Ophthal. Physiol. Opt. **27,** 404–411 , [PubMed ID: 17584293].

[5] J. Hoogerheide, F. Rempt, and W. P. Hoogenboom, (1971)"Acquired myopia in young pilots.," Ophthalmologica **163,** 209–215 , [PubMed ID: 5127164].

[6] D. O. Mutti, R. I. Sholtz, N. E. Friedman, and K. Zadnik, (2000)"Peripheral Refraction and Ocular Shape in Children," Invest Ophthalmol Vis Sci. **41,** 1022–1030 , [PubMed ID: 10752937].

[7] G. F. Schmid, (2003)"Variability of retinal steepness at the posterior pole in children 7-15 years of age," Curr Eye Res. **27,** 61–68 , [PubMed ID: 12868010].

[8] J. Wallman and J. Winawer, (2004)"Homeostasis of eye growth and the question of myopia," Neuron **43,** 447–468 , [PubMed ID: 15312645].

[9] D. O. Mutti, J. R. Hayes, G. L. Mitchell, L. A. Jones, M. L. Moeschberger, S. A. Cotter, R. N. Kleinstein, R. E. Manny, J. D. Twelker, and K. Zadnik, (2007)"Refractive Error, Axial Length, and Relative Peripheral Refractive Error before and after the Onset of Myopia," Invest Ophthalmol Vis Sci. **48,** 2510–2519 , [PubMed ID: 17525178].

[10] J. Wallman, M. D. Gottlieb, V. Rajaram, and L. Fugate-Wentzek, (1987)"Local retinal regions control local eye growth and myopia," Science **235,** 73–77 , [PubMed ID: 3603011].

[11] S. Diether and F. Schaeffel, (1997)"Local Changes in Eye Growth induced by Imposed Local Refractive Error despite Active Accommodation," Vision Res. **37,** 659–668 , [PubMed ID: 9156210].

[12] E. L. Smith III, C. Kee, R. Ramamirtham, Y. Qiao-Grider, and L. Hung, (2005)"Peripheral Vision Can Influence Eye Growth and Refractive Development in Infant Monkeys," Invest Ophthalmol Vis Sci. **46,** 3965–3972 , [PubMed ID: 16249469].

[13] E. L. Smith III, C. Kee, R. Ramamirtham, Y. Qiao-Grider, L. Hung, J. Huang, C. Kee, D. Coats, and E. Paysse, (2007)"Effects of Foveal Ablation on Emmetropization and Form-Deprivation Myopia," Invest Ophthalmol Vis Sci. **48,** 3914–3922 , [PubMed ID: 17724167].

[14] N. C. Strang, B. Winn, and A. Bradley, (1998)"The role of neural and optical factors in limiting visual resolution in myopia," Vision Res. **38,** 1713–21 , [PubMed ID: 9747504].

[15] D. A. Atchison, C. E. Jones, K. L. Schmid, N. Pritchard, J. M. Pope, W. E. Strugnell, and R. A. Riley, (2004)"Eye Shape in Emmetropia and Myopia," Invest Ophthalmol Vis Sci. **45,** 3380–3386 , [PubMed ID: 15452039].

[16] D. A. Atchison, N. Pritchard, K. L. Schmid, D. J. Scott, C. E. Jones, and J. M. Pope, (2005)"Shape of the Retinal Surface in Emmetropia and Myopia," Invest Ophthalmol Vis Sci. **46,** 2698–2707 , [PubMed ID: 16043841].

[17] N. J. Coletta and T. Watson, (2006)"Effect of myopia on visual acuity measured with laser interference fringes," Vision Res. **46,** 636–51 , [PubMed ID: 16045959].

[18] D. A. Atchison, K. L. Schmid, and N. Pritchard, (2006)"Neural and optical limits to visual performance in myopia," Vision Res. **46,** 3707–22 , [PubMed ID: 16806392].

[19] N. A. McBrien and M. Millodot, (1986)"The effect of refractive error on the accommodative response gradient," Ophthal Physiol Opt. **6,** 145–149 , [PubMed ID: 3748560].

[20] J. Gwiazda, F. Thorn, J. Bauer, and R. Held, (1993)"Myopic Children Show Insufficient Accommodative Response to Blur," Invest Ophthalmol Vis Sci. **34,** 690–694 , [PubMed ID: 8449687].

[21] M. L. Abbott, K. L. Schmid, and N. C. Strang, (1998)"Differences in the accommodation stimulus response curves of adult myopes and emmetropes," Ophthal Physiol Opt. **18,** 13–20 , [PubMed ID: 9666906].

[22] P. M. Allen and D. J. O'Leary, (2006)"Accommodation functions: co-dependency and relationship to refractive error," Vision Res. **46,** 491–505 , [PubMed ID: 16009391].

[23] G. W. Fulk, L. A. Cyert, and D. E. Parker, (2000)"A randomized trial of the effect

of single-vision vs. bifocal lenses on myopia progression in children with esophoria," Invest Ophthalmol Vis Sci. **77,** 395–401 , [PubMed ID: 10966065].

[24] J. T. Leung and B. Brown, (1999)"Progression of myopia in Hong Kong Chinese schoolchildren is slowed by wearing progressive lenses," Optom Vis Sci. **76,** 346–354 , [PubMed ID: 10416928].

[25] J. Gwiazda *et al.*, (2003)"A Randomized Clinical Trial of Progressive Addition Lenses versus Single Vision Lenses on the Progression of Myopia in Children," Invest Ophthalmol Vis Sci. **44,** 1492–1500 , [PubMed ID: 12657584].

[26] E. A. H. Mallen, P. Kashyap, and K. M. Hampson, (2006)"Transient Axial Length Change during the Accommodation Response in Young Adults," Invest Ophthalmol Vis Sci. **47,** 1251–1254 , [PubMed ID: 16505066].

[27] T. W. Walker and D. O. Mutti, (2002)"The Effect of Accommodation on Ocular Shape," Optom Vis Sci. **79,** 424–430 , [PubMed ID: 12137396].

[28] M. Dubbelman, G. L. V. der Heijde, H. A. Weeber, and G. F. Vrensen, (2003)"Changes in the internal structure of the human crystalline lens with age and accommodation," Vision Res. **43,** 2363–75 , [PubMed ID: 12962993].

[29] J. C. He, J. Gwiazda, F. Thorn, R. Held, and W. Huang, (2003)"Change in corneal shape and corneal wave-front aberrations with accommodation," Journal of Vision **3,** 456–463 , [PubMed ID: 14507252].

[30] S. B. Vohra and P. A. Good, (2000)"Altered globe dimensions of axial myopia as risk factors for penetrating ocular injury during peribulbar anaesthesia," Br J Anaesth **85,** 242–5 , [PubMed ID: 10992832].

[31] J. F. P. Deller, A. D. O'Connor, and A. Sorsby, (1947)"X-ray measurements of the diameters of the living eye," Proc Roy Soc Biol Lond **134,** 453–457 , [PubMed ID: not indexed].

[32] F. R. Wang, X. D. Zhou, and S. Z. Zhou, (1994)"A CT Study of the Relation Between Ocular Axial Biometry and Refraction," Zhonghua Yan Ke Za Zhi **30,** 39–40 , [PubMed ID: 8082473].

[33] X. D. Zhou, F. R. Wang, and S. Z. Zhou, (New York: Springer; 1998)"A Computed Tomographic Study of the Relation Between Ocular Axial Biometry and Refraction," Myopia Updates: Proceedings of the 6th International Conference on Myopia pp. 112–115 , [ISBN: 4431701990].

[34] J. F. Chen, A. E. Elsner, S. A. Burns, R. M. Hansen, P. L. Lou, K. K. Kwong, and A. B. Fulton, (1992)"The Effect of Eye Shape on Retinal Responses," Clin. Vision Sci. **7,** 521–530 , [VisionNet ID: b1099295].

[35] H. M. Cheng, O. S. Singh, K. K. Kwong, J. Xiong, B. T. Woods, and T. J. Brady, (1992)"Shape of the myopic eye as seen with high-resolution magnetic resonance imaging," Optom Vis Sci. **69,** 698–701 , [PubMed ID: 1437010].

[36] A. Chau, K. Fung, K. Pak, and M. Yap, (2004)"Is eye size related to orbit size in human subjects?," Ophthal. Physiol. Opt. **24,** 35–40 , [PubMed ID: 14687199].

[37] J. M. Miller, C. F. Wildsoet, H. Guan, M. Limbo, and J. L. Demer, (2004)"Refractive Error and Eye Shape by MRI," Invest Ophthalmol Vis Sci. **45,** E–Abstract 2388 , [ARVO Abstract].

[38] K. D. Singh, N. S. Logan, and B. Gilmartin, (2006)"Three-Dimensional Modeling of the Human Eye Based on Magnetic Resonance Imaging," Invest Ophthalmol Vis Sci. **47,** 272–2279 , [PubMed ID: 16723434].

[39] F. A. Vera-Diaz, P. V. McGraw, N. C. Strang, and D. Whitaker, (2005)"A Psychophysical Investigation of Ocular Expansion in Human Eyes," Invest Ophthalmol Vis Sci. **46,** 758–763 , [PubMed ID: 15671310].

[40] R. A. Stone and D. I. Flitcroft, (2004)"Ocular Shape and Myopia," Ann Acad Med Singapore **33,** 7–15 , [PubMed ID: 15008555].

[41] N. S. Logan, B. Gilmartin, and M. C. M. Dunne, (1995)"Computation of retinal contour in anisomyopia," Ophthalmic Physiol Opt. **15,** 363–366 , [PubMed ID: 8524555].

[42] N. S. Logan, B. Gilmartin, C. F. Wildsoet, and M. C. M. Dunne, (2004)"Posterior Retinal Contour in Adult Human Anisomyopia," Invest Ophthalmol Vis Sci. **45,** 2152–2162 , [PubMed ID: 15223789].

[43] G. F. Schmid, B. L. Petrig, C. E. Riva, E. Logean, and R. Wlti, (2001)"Measurement of eye length and eye shape by optical low coherence reflectometry," Int Ophthalmol. **23,** 317–20 , [PubMed ID: 11944856].

[44] G. F. Schmid, (2003)"Axial and peripheral eye length measured with optical low coherence reflectometry," J Biomed Opt. **8,** 655–62 , [PubMed ID: 14563204].

[45] L. A. Macfadden, L. S. Gray, N. C. Strang, and D. Seidel, (2007)"The Effect of Eye Rotation on Measurements of Peripheral Retinal Shape Using the IOLMaster," Invest Ophthalmol Vis Sci. **48,** E–Abstract 4002 , [ARVO Abstract].

[46] M. Millodot and A. Lamont, (1974)"Refraction of the periphery of the eye," Invest Ophthalmol Vis Sci. **64,** 110–111 , [PubMed ID: 4813433].

[47] R. Navarro, P. Artal, and D. R. Williams, (1993)"Modulation transfer of the human eye as a function of retinal eccentricity," J Opt Soc Am A **10,** 201–212 , [PubMed ID: 8478746].

[48] D. R. Williams, P. Artal, R. Navarro, M. J. McMahon, and D. H. Brainard, (1996)"Off-axis optical quality and retinal sampling in the human eye," Vision Res. **36,** 1103–1114 , [PubMed ID: 8762715].

[49] A. Guirao and P. Artal, (1999)"Off-axis monochromatic aberrations estimated from double pass measurements in the human eye," Vision Res. **39,** 207–217 , [PubMed ID: 10326131].

[50] V. Choh and J. G. Sivak, (2005)"Lenticular accommodation in relation to ametropia: the chick model," J Vis. **5,** 165–176 , [PubMed ID: 15929643].

[51] T. I. Ronkina, L. S. Chabrova, L. M. Borisova, V. I. Vasin, and S. N. Bagrova, (1989)"[The biomechanical properties of the crystalline lens capsule in emmetropia and myopia]," Oftalmol Zh. **7,** 420–425 , [PubMed ID: 2633095].

[52] D. O. Mutti, (2010)"Hereditary and environmental contributions to emmetropization and myopia," Optom Vis Sci. **87,** 255–9 , [PubMed ID: 20019643].

[53] L. N. Thibos and D. Horner, (2001)"Power vector analysis of the optical outcome of refractive surgery," J Cataract Refract Surg. **27,** 80–5 , [PubMed ID: 11165859].

[54] T. O. Salmon, R. W. West, W. Gasser, and T. Kenmore, (2003)"Measurement of Refractive Errors in Young Myopes Using the COAS Shack-Hartmann Aberrometer," Optom Vis Sci. **80,** 6–14 , [PubMed ID: 12553539].

[55] M. Millodot, (1981)"Effect of ametropia on peripheral refraction," Am J Optom & Physiol Optics **58,** 691–695 , [PubMed ID: 7294139].

[56] A. Seidemann, F. Schaeffel, A. Guirao, N. Lopez-Gil, and P. Artal, (2002)"Peripheral refractive errors in myopic, emmetropic, and hyperopic young subjects," J Opt Soc Am A Opt Image Sci Vis. **19,** 2363–2373 , [PubMed ID: 12469730].

[57] D. A. Atchison, N. Pritchard, and K. L. Schmid, (2006)"Peripheral refraction along the horizontal and vertical visual fields in myopia," Vision Res. **46,** 1450–1458 , [PubMed ID: 16356528].

[58] L. N. Davies and E. A. H. Mallen, (2009)"Influence of accommodation and refractive status on the peripheral refractive profile," Br J Ophthalmol **93,** 1186–1190 , [PubMed ID: 19525242].

[59] W. N. Charman and J. A. M. Jennings, (2006)"Longitudinal changes in peripheral refraction with age," Ophthalmic Physiol Optics **26,** 447–55 , [PubMed ID: 16918768].

[60] D. A. Atchison, N. Pritchard, S. D. White, and A. M. Griffiths, (2005)"Influence of age on peripheral refraction," Vision Res. **45,** 715–720 , [PubMed ID: 15639498].

[61] R. Calver, H. Radhakrishnan, E. Osuobeni, and D. O'Leary, (2007)"Peripheral refraction for distance and near vision in emmetropes and myopes," Ophthal Physiol Opt. **27,** 584–593 , [PubMed ID: 17956364].

[62] D. A. Berntsen, D. O. Mutti, and K. Zadnik, (2008)"Validation of aberrometry-based relative peripheral refraction measurements," Ophthalmic Physiol Opt. **28,** 83–90 , [PubMed ID: 18201339].

[63] J. Huang, L. F. Hung, R. Ramamirtham, T. L. Blasdel, T. L. Humbird, K. H. Bockhorst, and E. L. S. III, (2001)"Effects of form deprivation on peripheral refractions and ocular shape in infant rhesus monkeys (Macaca mulatta)," Invest Ophthalmol Vis Sci. **41,** 2511–2520 , [PubMed ID: 19420338].

[64] R. Schippert and F. Schaeffel, (2006)"Peripheral defocus does not necessarily affect central refractive development," Vision Res. **46,** 3935–3940 , [PubMed ID: 16806391].

[65] G. Smith, M. Millodot, and N. McBrien, (1988)"The effect of accommodation on oblique astigmatism and field curvature of the human eye," Clin Exp Optom **71,** 119–125 , [Pubmed ID: not indexed].

[66] A. Whatham, F. Zimmerman, A. Martinez, S. Delgado, P. L. de la Jara, P. Sankaridurg, and A. Ho, (2009)"Influence of accommodation on off-axis refractive errors in myopic eyes," Journal of Vision **9,** 14:1–3 , [PubMed ID: 19757953].

[67] A. Carkeet, S. Veladan, Y. K. Tan, D. Y. Lee, and D. T. Tan, (2003)"Higher order ocular aberrations after cycloplegic and non-cycloplegic pupil dilation," J Refract Surg. **19,** 316–322 , [PubMed ID: 12777027].

[68] A. Mathur, D. A. Atchison, and W. N. Charman, (2009)"Myopia and peripheral ocular aberrations," Journal of Vision **9,** 15:1–12 , [PubMed ID: 19810796].

[69] L. S. Harris, (1968)"Cycloplegic-induced intraocular pressure elevations a study of normal and open-angle glaucomatous eyes," Arch Ophthalmol **79,** 242–246 , [PubMed ID: 5640848].

[70] J. Hancox, I. Murdoch, and D. Parmar, (2002)"Changes in intraocular pressure following diagnostic mydriasis with cyclopentolate 1562–566 , [PubMed ID: 12194069].

[71] C. E. Ferree, G. Rand, and C. Hardy, (1931)"Refraction for the Peripheral Field of Vision," Arch Ophthal. **5,** 717–731 , [PubMed ID: not indexed].

[72] C. E. Ferree and G. Rand, (1933)"Interpretation of Refractive conditions in the Peripheral Field of Vision," Arch Ophthal. **9,** 925–938 , [PubMed ID: not indexed].

[73] H. Radhakrishnan and W. N. Charman, (2008)"Peripheral refraction measurement: does it matter if one turns the eye or the head?," Ophthalmic Physiol Opt. **28,** 73–82 , [PubMed ID: 18201338].

[74] P. Prado, J. Arines, S. Bar, S. Manzanera, A. Mira-Agudelo, and P. Artal, (2009)"Changes of ocular aberrations with gaze," Ophthalmic Physiol Opt. **29,** 264–271 , [PubMed ID: 19422557].

[75] A. Mathur, D. A. Atchison, S. Kasthurirangan, N. A. Dietz, S. Luong, S. P. Chin, W. L. Lin, and S. W. Hoo, (2009)"The influence of oblique viewing on axial and peripheral refraction for emmetropes and myopes," Ophthalmic Physiol Opt. **29,** 155–161 , [PubMed ID: 19236585].

[76] L. Lundström and P. Unsbo, (2007)"Transformation of Zernike coefficients: scaled, translated, and rotated wavefronts with circular and elliptical pupils," J Opt Soc Am A Opt Image Sci Vis **24,** 569–577 , [PubMed ID: 17301846].

[77] L. Lundström, J. Gustaffson, and P. Unsbo, (2009)"Population distribution of wavefront aberrations in the peripheral human eye," J Opt Soc Am A **26,** 2192–2198 , [PubMed ID: 19798398].

[78] B. Efron, *Introduction to Quantum Mechanics*, 2nd ed. (Society for Industrial and Applied Mathematics, Philadelphia, PA, 1987), [ISBN - 0898711797].

[79] B. Efron and R. Tibshirani, (1986)"Bootstrap Methods for Standard Errors, Confidence Intervals, and Other Measures of Statistical Accuracy," Statistical Science **1,** 54–75 , [JSTOR ID: 2245500].

[80] A. K. Lam, R. Chan, and P. C. Pang, (2001)"The repeatability and accuracy of axial length and anterior chamber depth measurements from the IOLMaster," Ophthal Physiol Opt. **21,** 477–483 , [PubMed ID: 11727876].

[81] R. C. III, P. B. III, and R. J. Olson, (2002)"Accuracy and reproducibility of biometry using partial coherence interferometry," J Cataract Refract Surg. **28,** 235–238 , [PubMed ID: 11821202].

[82] C. J. Heatley, L. A. Whitefield, and C. E. Hugkulstone, (2002)"Effect of pupil dilation on the accuracy of the IOLMaster," J Cataract Refract Surg. **28,** 1993–1996 , [PubMed ID: 12457675].

[83] L. T. Rose and C. N. Moshegov, (2003)"Comparison of the Zeiss IOLMaster and applanation A-scan ultrasound: biometry for intraocular lens calculation," Clin Experiment Ophthalmol. **31,** 121–124 , [PubMed ID: 12648044].

[84] G. Nemeth, A. Vajas, B. Kolozsvari, A. Berta, and L. Modis Jr., (2006)"Anterior chamber depth measurements in phakic and pseudophakic eyes: Pentacam versus ultrasound device," J Cataract Refract Surg. **32,** 1331–1335 , [PubMed ID: 16863970].

[85] M. S. Reuland, A. J. Reuland, Y. Nishi, and G. U. Auffarth, (2007)"Corneal Radii and Anterior Chamber Depth Measurements Using the IOLMaster Versus the Pentacam," J Refract Surg. **23,** 368–373 , [PubMed ID: 17455832].

[86] U. Elbaz, Y. Barkana, Y. Gerber, I. Avni, and D. Zadok, (2007)"Comparison of Different Techniques of Anterior Chamber Depth and Keratometric Measurements," Am J Ophthalmol **143,** 48–53 , [PubMed ID: 17101110].

[87] P. Rosales and S. Marcos, (2009)"Pentacam Scheimpflug quantitative imaging of the crystalline lens and intraocular lens," J Refract Surg. **25,** 421–8 , [PubMed ID: 19507794].

[88] M. Dubbelman, G. L. V. der Heijde, and H. A. Weeber, (2005)"Change in shape of the aging human crystalline lens with accommodation," Vision Res. **45,** 117–32 , [PubMed ID: 15571742].

[89] D. A. Atchison, (2006)"Optical models for human myopic eyes," Vision Res. **46,** 2236–50 , [PubMed ID: 16494919].

[90] D. R. Iskander, B. A. Davis, M. J. Collins, and R. Franklin, (2007)"Objective refraction from monochromatic wavefront aberrations via Zernike power polynomials," Ophthalmic Physiol Opt. **27,** 245–55 , [PubMed ID: 17470237].

[91] L. Lundström, (2007)"Wavefront aberrations and peripheral vision," PhD thesis, Royal Institute of Technology Stockholm, Sweden , [Published on institution website].

[92] X. Cheng, N. L. Himebaugh, P. S. Kollbaum, L. N. Thibos, and A. Bradley, (2003)"Validation of a clinical Shack-Hartmann aberrometer," Optom Vis Sci. **80,** 587–595 , [PubMed ID: 12917578].

[93] D. A. Atchison, (2003)"Comparison of Peripheral Refractions Determined by Different Instruments," Optom Vis Sci. **80,** 655–660 , [PubMed ID: 14502047].

[94] D. A. Atchison, N. Pritchard, D. H. Scott, and W. N. Charman, (2007)"Measuring ocular aberrations in the peripheral visual field using HartmannShack aberrometry," J Opt Soc Am A **24,** 2963–2973 , [PubMed ID: 17767268].

[95] W. N. Charman and D. A. Atchison, (2009)"Decentred optical axes and aberrations along principal visual field meridians," Vision Res. **49,** 1869–76 , [PubMed ID: 19426752].

[96] J. M. Royston, M. C. Dunne, and D. A. Barnes, (1989)"Calculation of crystalline lens radii without resort to phakometry," Ophthalmic Physiol Opt. **9,** 412–4 , [PubMed ID: 2631008].

Index

Bootstrap Method, 112

Conclusion, 101
Consent form, 103

Initial Measurements, 15

Methods, 15

Peripheral Aberrations, 8
Peripheral Aberrations - Myopia, 8
Peripheral Aberrations, effect of Accommodation on, 11
Peripheral Aberrations, Measurements of, 17
Peripheral Aberrations, Method of Comparison, 25
Peripheral Aberrations, Results and Discussion, 38
Peripheral Retinal contour, 1
Power Vectors, analysis of, 39
Power Vectors, calculation of, 34
Power Vectors, differences with accommodation, 44
Power Vectors, non-accommodative, 39
Pupil correction, 25

Questionnaire, 108

Retinal contour and myopia, theories regarding, 2
Retinal Contour Calculation, the effect of anterior segment parameter variation on, 91
Retinal Contour Measurement, the effect of accommodation on, 83
Retinal Contour Measurement, the effect of pupil size on, 86
Retinal Contour, analysis of, 73
Retinal Contour, Calculation of, 31
Retinal Contour, comparison of Dunne and IOL Master, 79
Retinal Contour, comparison of measurement methods, 78
Retinal Contour, curve fitting, 117
Retinal contour, methods of measuring, 3, 5
Retinal Contour, Results and Discussion, 72

Statistical Analysis, 27
Subject Grouping, 27
Subjects, 15
Summary, 101
Supplemental plots, 120

Zernike Coefficients RMS, differences with accommodation, 69
Zernike Coefficients RMS, non-accommodative, 57
Zernike Coefficients, analysis of, 48
Zernike Coefficients, differences with accommodation, 61
Zernike Coefficients, non-accommodative, 49
Zernike plots, foveally normalized, 120
Zernike plots, low significance accommodative difference trends, 122
Zernike plots, low significance non-accommodative trends, 120
Zernike plots, low significance trends, 125